AXIAL FLUX BLDC MOTOR & GENERATOR WITH EMBEDDED TORQUE SENSING FOR PERFORMANCE AND EFFICIENCY EVALUATION

Graduation Project II

2025 - 2026

An-Najah National University

Faculty of Engineering and Information Technology

Department of Electrical Engineering

Graduation Project II

Axial Flux BLDC Motor & Generator with Embedded Torque Sensing for Performance and Efficiency Evaluation

Team members

1. **Mohammad Ja'afrah** 2. **Tala Sharif** 3. **Anas Hammad**

Supervisor

Dr. Omar Tamimi

Presented in partial fulfillment of the requirements for Bachelor degree in Electrical Engineering

2025 – 2026

Acknowledgments

Acknowledgments

I would like to take this opportunity to express my sincere gratitude to all those who contributed, directly or indirectly, to the successful completion of this graduation project titled "Axial Flux BLDC Motor & Generator with Embedded Torque Sensing for Performance and Efficiency Evaluation."

First and foremost, I would like to express my deepest appreciation and thanks to my project supervisor, Dr. Omar Tamimi, for his continuous guidance, valuable feedback, and unwavering support throughout all stages of this project. His expertise, insightful suggestions, and encouragement played a vital role in shaping the direction of this work and ensuring its academic and technical quality.

I would also like to extend my sincere thanks and appreciation to the Head of the Department for his support, encouragement, and dedication to providing a productive academic environment that enables students to achieve their academic and professional goals.

Furthermore, I would like to express my gratitude to the faculty members of the Department of Electrical Engineering at An-Najah National University for the knowledge, skills, and practical experience they have provided throughout our academic journey, which greatly contributed to the successful completion of this project.

Finally, I would like to thank our families and friends for their continuous encouragement, patience, and moral support. Their belief in us has been a constant source of motivation and inspiration throughout the preparation and completion of this project.

Dedication

Dedication

This project is dedicated to our parents and families, whose unconditional love, patience, and sacrifices have been the foundation of our journey. They taught us to trust in Allah, to persevere in the face of challenges, and to believe in ourselves even when the path was unclear. Their continuous support and encouragement have been a constant source of strength, without which this achievement would not have been possible.

We also dedicate this work to our homeland, Palestine, where resilience, hope, and determination are part of everyday life. Despite the challenges and circumstances, we carry the belief that knowledge is a form of resistance and that education is a path toward a better future. This project reflects our commitment to learning, growth, and contributing positively to society through the development of engineering solutions that enhance performance, efficiency, and technological advancement.

Finally, this dedication extends to everyone who believes in the power of education, perseverance, and faith. May this work represent a meaningful step toward personal development and collective progress, guided by knowledge, patience, and hope.

Abstract

Abstract

The development of high-efficiency electric machines has become increasingly important in modern energy systems, particularly in applications involving renewable energy and electric mobility. Axial Flux Brushless (BLDC) machines offer several advantages over conventional radial flux machines, including higher power density, compact structure, and improved efficiency. However, accurately evaluating their performance requires precise measurement of key parameters, especially torque, which plays a critical role in determining system efficiency.

This project presents the design and implementation of an Axial Flux Motor and Generator integrated with an embedded torque sensing mechanism for performance and efficiency evaluation. The system is designed to operate in both motor and generator modes, enabling comprehensive analysis under different operating conditions. The embedded torque sensing unit allows real-time measurement of torque, providing accurate data for efficiency calculations.

The project follows a systematic engineering approach, including electromagnetic design, mechanical construction, and system integration. Simulation tools and analytical methods were used to optimize the machine design, while experimental testing was conducted to validate the results. The system incorporates appropriate control techniques, data acquisition methods, and measurement instruments to ensure reliable and precise evaluation.

Overall, this work provides a practical and efficient platform for analyzing axial flux machines and contributes to improving their design and application in energy conversion systems. The integration of embedded torque sensing enhances the accuracy of performance evaluation, making the system a valuable tool for research and development in electrical machine engineering.

Keywords

Keywords

The following keywords represent the main concepts and technologies addressed in this project. They highlight the core topics related to the Axial Flux BLDC Motor and Generator system and facilitate the identification of the project's research domain.

Axial Flux Machine	BLDC Motor	Electric Generator
Torque Sensing	Performance Evaluation	Efficiency Analysis
Electromagnetic Design	Energy Conversion	Data Acquisition
Embedded Systems	Mechanical Design	Experimental Testing

Table of Contents
TOC

Contents

List of Figures
LOF

List of Tables
LOT

Chapter One

Chapter One

Introduction

Chapter 1: Introduction

Electric machines play a vital role in modern industry, energy systems, and transportation. Their widespread use in manufacturing processes, renewable energy applications, and electric vehicles makes their performance and efficiency a key factor in overall system effectiveness. Improving motor efficiency not only reduces energy consumption but also enhances reliability, lowers operational costs, and contributes to sustainable technological development.

Among the various types of electric machines, Brushless DC (BLDC) motors have gained significant attention due to their high efficiency, reliability, and reduced maintenance requirements. In recent years, Axial Flux BLDC machines have emerged as a promising alternative to conventional radial flux machines. Their unique structure, characterized by a shorter magnetic path and a larger effective air-gap area, enables higher torque density, compact size, and improved power-to-weight ratio. These advantages make axial flux machines particularly suitable for applications such as electric vehicles, renewable energy systems, and compact electromechanical devices.

The growing interest in axial flux technology is evident in both academic research and industrial applications. Advanced designs have demonstrated exceptional performance capabilities, with some prototypes achieving remarkably high-power densities compared to traditional machines. Companies such as YASA (Yokeless and Segmented Armature) have contributed significantly to the development of this technology, enabling the production of lightweight, high-performance electric machines used in modern electric and hybrid vehicles.

Despite these advantages, the design and evaluation of axial flux BLDC machines present several technical challenges. The electromagnetic behavior of these machines is more complex due to non-uniform flux distribution, sensitivity to air-gap variations, and the strong interaction between magnetic and mechanical parameters. Additionally, accurate performance evaluation requires precise measurement of key quantities such as torque and efficiency, which are essential for validating design assumptions and ensuring optimal operation.

This project focuses on the design and implementation of an axial flux BLDC motor and generator integrated with an embedded torque sensing system for performance and efficiency evaluation. The system is designed to operate under different conditions, allowing comprehensive analysis in both motor and generator modes. By incorporating real-time torque measurement, the project aims to enhance the accuracy of efficiency calculations and provide a reliable platform for experimental validation.

The remainder of this report is organized as follows: Chapter Two presents a literature review and background on axial flux machines and BLDC technology. Chapter Three discusses the system design and specifications. Chapter Four focuses on the mechanical design aspects. Chapter Five covers the detailed electromagnetic design and optimization. Chapter Six presents simulation and experimental results, followed by conclusions and recommendations in the final chapter.

Chapter Two

Chapter Two

Overview

Chapter 2: Overview of Axial Flux BLDC Machines and Torque Sensing Technologies

Following the general introduction presented in Chapter One, which highlighted the importance of electric machines and the growing relevance of axial flux technology in modern applications, this chapter provides a comprehensive overview of the fundamental concepts and previous research related to axial flux BLDC machines. The aim is to establish a solid theoretical and technical background that supports the design and implementation of the proposed system in the subsequent chapters.

This chapter focuses on reviewing the evolution of axial flux machines, their main topologies, and the key differences compared to conventional radial flux machines. In addition, it explores control methods used in BLDC motors, including both sensor less and sensor zed techniques, with emphasis on their impact on performance and torque control. Furthermore, the chapter introduces embedded torque sensing technologies, which represent a critical component in this project for accurate performance evaluation.

The discussion also extends to efficiency considerations and loss mechanisms in axial flux permanent magnet machines, highlighting the factors that influence overall system performance. Finally, various methods for performance evaluation are presented, including analytical, simulation-based, and experimental approaches.

Unlike the detailed design approach presented in later chapters, this chapter serves as a knowledge foundation that bridges theoretical concepts with practical implementation. It provides the necessary understanding required to justify design decisions and to interpret the results obtained from simulation and experimental validation.

Axial flux BLDC machines have attracted increasing attention in recent years due to their superior torque density, compact structure, and high efficiency compared to conventional radial flux machines. These characteristics make them particularly suitable for modern engineering applications such as electric vehicles, renewable energy systems, and aerospace technologies. However, understanding their operation and performance requires a comprehensive study of their electromagnetic behavior, structural configurations, and control strategies.

From a historical perspective, the concept of axial flux machines dates back to early developments in electromagnetic energy conversion. Although initial designs were not widely adopted, advancements in permanent magnet materials and power electronics have significantly improved their practicality and performance. As a result, axial flux machines have evolved into a promising solution for high-performance applications.

At the system level, the performance of BLDC machines depends not only on their electromagnetic design but also on the effectiveness of control strategies and the accuracy of parameter measurement. In particular, torque plays a crucial role as a primary indicator of machine performance and efficiency. Therefore, integrating reliable torque sensing mechanisms is essential for achieving accurate evaluation and control.

This chapter adopts a structured review approach, where each section addresses a key aspect of axial flux BLDC systems. The objective is to provide a clear and connected understanding of machine topology, control methods, sensing technologies, and performance evaluation techniques. This foundation is essential for supporting the detailed design, optimization, and experimental validation presented in the following chapters.

Furthermore, practical considerations such as system integration, measurement accuracy, and implementation constraints are also discussed. These factors are critical in ensuring that theoretical concepts can be effectively translated into a functional and reliable engineering system.

Subsections:
2.1: Axial Flux Machine Topologies
2.2: BLDC Control Methods and Torque Estimation Approaches
2.3: Embedded Torque Sensing Technologies
2.4: Efficiency and Loss Mechanisms in Axial Flux Machines
2.5: Methods for Performance Evaluation

2.1: Axial Flux Machine Topologies

Axial flux machines represent an advanced class of electrical machines in which the magnetic flux flows parallel to the axis of rotation. This configuration differs significantly from conventional radial flux machines, where the magnetic flux flows radially from the rotor to the stator. Due to this structural difference, axial flux machines offer several advantages, including higher torque density, compact design, and improved efficiency.

The fundamental difference between radial and axial flux machines is illustrated in the following figure. The torque production capability of electrical machines is strongly related to the effective air-gap surface area and the radius at which the electromagnetic force is applied. In axial flux machines, the larger effective radius and flat disc structure allow for increased torque generation compared to radial flux machines of similar size. This makes axial flux machines particularly suitable for applications requiring high torque in limited space.

In addition, axial flux machines exhibit a shorter magnetic path and reduced core losses, which contribute to higher efficiency. Their compact and lightweight structure also makes them highly attractive for modern applications such as electric vehicles and aerospace systems.

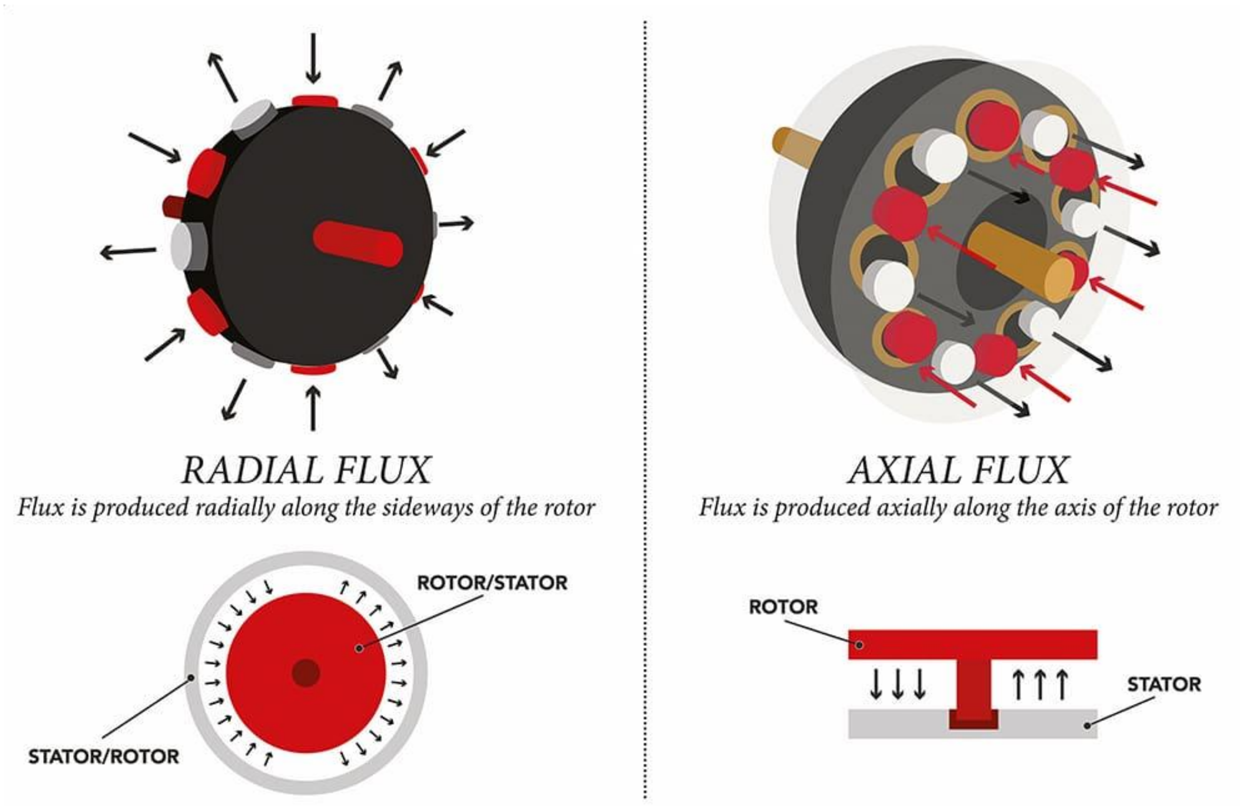

Figure 1: Radial vs Axial Flux Comparison

A comparison between radial flux and axial flux machines is presented in the following table.

Table 1: Comparison Between Radial and Axial Flux Machines

Feature	Radial Flux Machine	Axial Flux Machine
Flux Direction	Radial	Axial
Structure	Cylindrical	Disc-shaped
Torque Density	Moderate	High
Size	Larger	Compact
Efficiency	Moderate	Higher
Cooling Capability	Limited	Improved

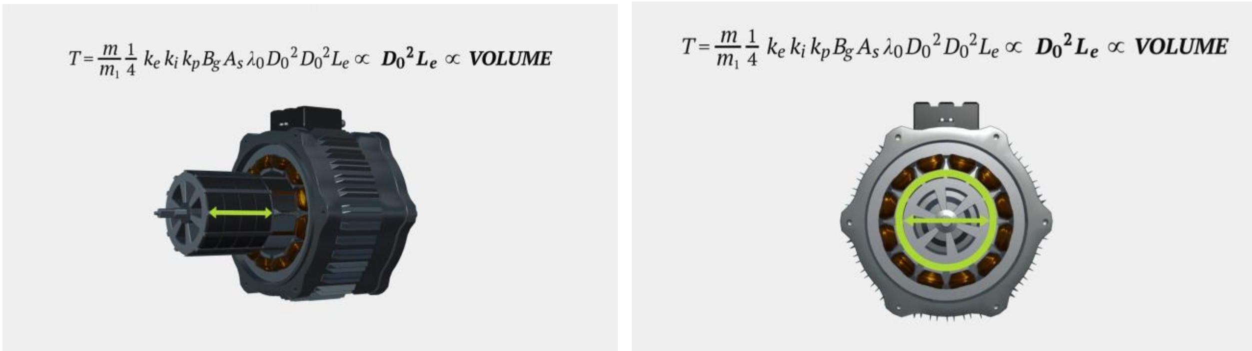

Figure 2: Traditional Radial Flux Machine (RFM)

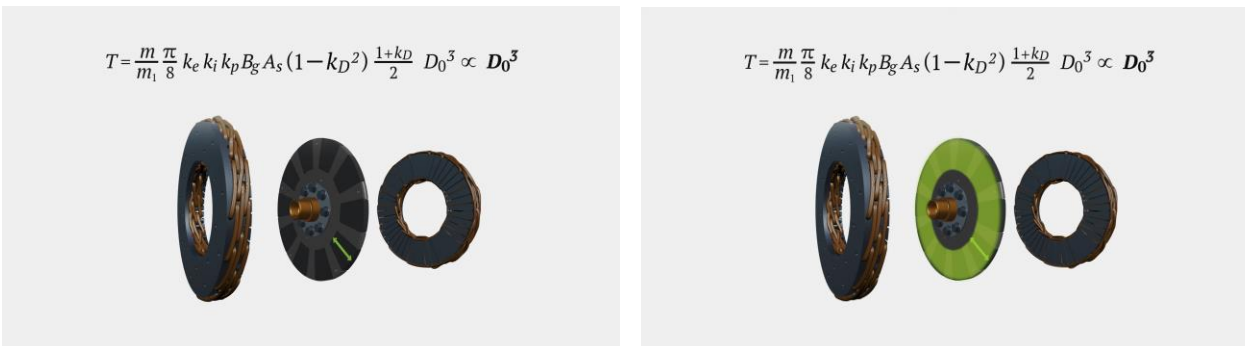

Figure 3: Axial Flux Direct Current brushless machine

The torque produced in both axial flux and radial flux machines is strongly influenced by two main factors: the effective air-gap surface area and the average radius at which the electromagnetic force acts on the rotor. As illustrated in the figures above, axial flux machines typically have a larger air-gap surface area and a greater effective radius compared to radial flux machines of similar size.

Consequently, for two motors with the same outer dimensions, the axial flux machine is capable of generating higher torque. This advantage is mainly attributed to the three-dimensional (3D) magnetic field distribution in axial flux machines, whereas radial flux machines rely on a simpler two-dimensional (2D) magnetic field configuration.

In addition to their superior torque density, axial flux machines feature a simpler structural design, reduced size, and more compact packaging. These characteristics result in lower weight and make them highly suitable for applications such as electric vehicles (EVs), where space optimization and weight reduction are critical design considerations.

Furthermore, the straightforward design of axial flux machines leads to lower manufacturing and operational costs. This contributes not only to improved efficiency but also to environmental benefits, including reduced carbon dioxide emissions and minimized long-term environmental impact.

This comparison highlights the superior torque density and compactness of axial flux machines, which are key factors in their increasing adoption in modern engineering systems.

Types of Axial Flux Machines

Axial flux machines can be classified into several topologies based on the arrangement of stators and rotors. The most common configurations include single stator single rotor, double stator single rotor, and multi-rotor structures such as YASA topology.

1. Single Stator Single Rotor (SSSR)

The single stator single rotor configuration is the simplest form of axial flux machine. It consists of one stator and one rotor, where the stator contains windings and the rotor carries permanent magnets.

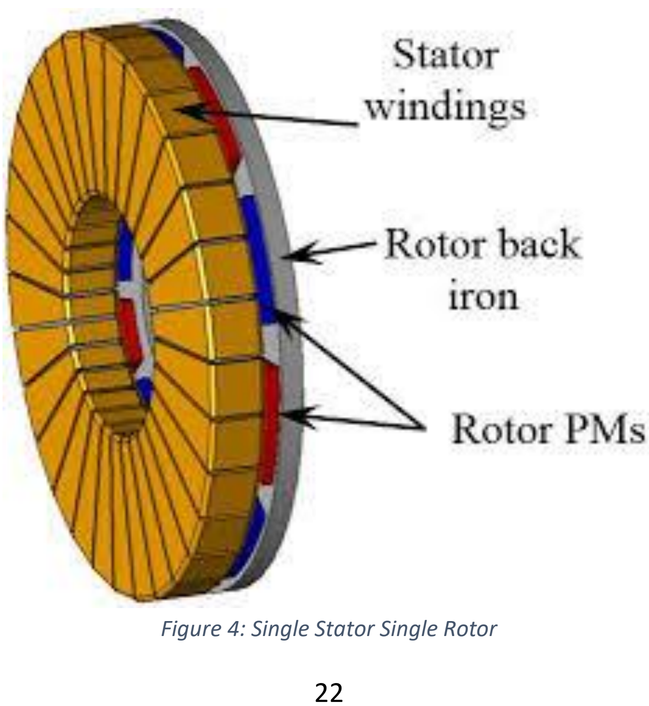

Figure 4: Single Stator Single Rotor

In this configuration, the magnetic flux passes axially between the stator and rotor through a single air gap. Although this design is simple and cost-effective, it suffers from unbalanced magnetic forces and relatively lower torque density compared to more advanced topologies. Additionally, part of the magnetic flux may not be effectively utilized, reducing overall efficiency.

2. Double Stator Single Rotor (DSSR)

The double stator single rotor configuration includes two stators positioned on both sides of a single rotor. The rotor is typically placed in the middle, with permanent magnets mounted on both sides.

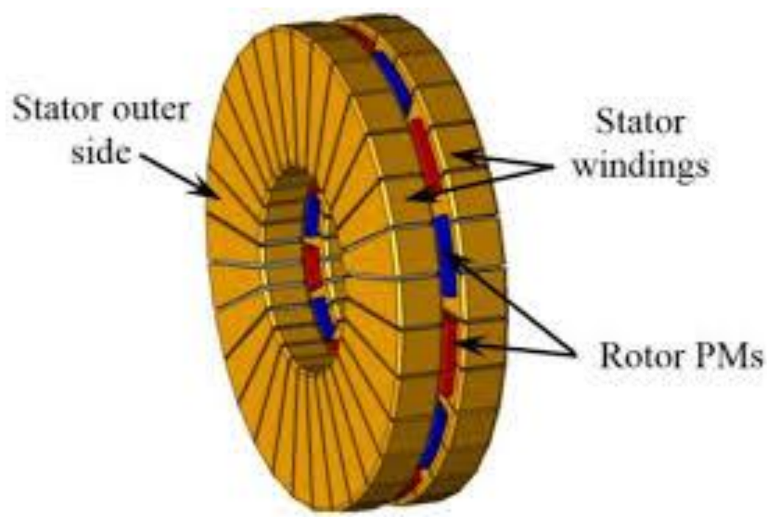

Figure 5: Double Stator Single Rotor

This structure improves the magnetic flux distribution and balances the magnetic forces acting on the rotor. As a result, torque production is significantly increased, and the machine achieves higher efficiency compared to the single stator configuration. However, the design becomes more complex and requires additional materials, which increases manufacturing cost.

3. YASA (Yokeless and Segmented Armature)

The YASA topology is an advanced axial flux machine design that eliminates the stator yoke and uses segmented armature windings.

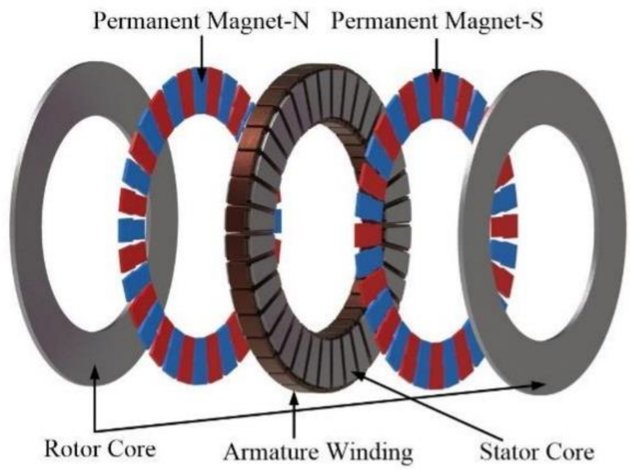

Figure 6: YASA Topology

This configuration reduces core losses and weight while improving thermal performance and efficiency. The absence of a stator yoke allows for better utilization of magnetic flux and enhances power density. YASA machines are widely used in high-performance applications such as electric vehicles due to their superior efficiency and compact design.

In summary, axial flux machines offer significant advantages over radial flux machines in terms of torque density, compact design, and overall efficiency. These characteristics make them particularly suitable for modern applications such as electric vehicles, where performance, weight reduction, and space utilization are critical factors.

Having established the fundamental differences and advantages of axial flux machines, the next section will focus on the different types of axial flux machine configurations, highlighting their structures, operating principles, and key features.

2.2: BLDC Control Methods and Torque Estimation Approaches

Brushless DC (BLDC) motors are widely used in modern applications due to their high efficiency, reliability, and superior torque characteristics. To achieve optimal performance, appropriate control methods and accurate torque estimation techniques are essential. This section presents the main BLDC control strategies along with commonly used torque estimation approaches.

BLDC Control Methods (Sensorized Control Methods)

BLDC motors require electronic commutation, which is achieved through different control techniques depending on the application requirements.

1. Trapezoidal Control (Six-Step Commutation)

This is the simplest and most commonly used control method. It relies on six-step commutation based on rotor position, typically obtained from Hall sensors. The back electromotive force (Back-EMF) has a trapezoidal shape, and the phase currents are applied accordingly.

- Simple implementation
- Low cost
- Produces torque ripple and noise

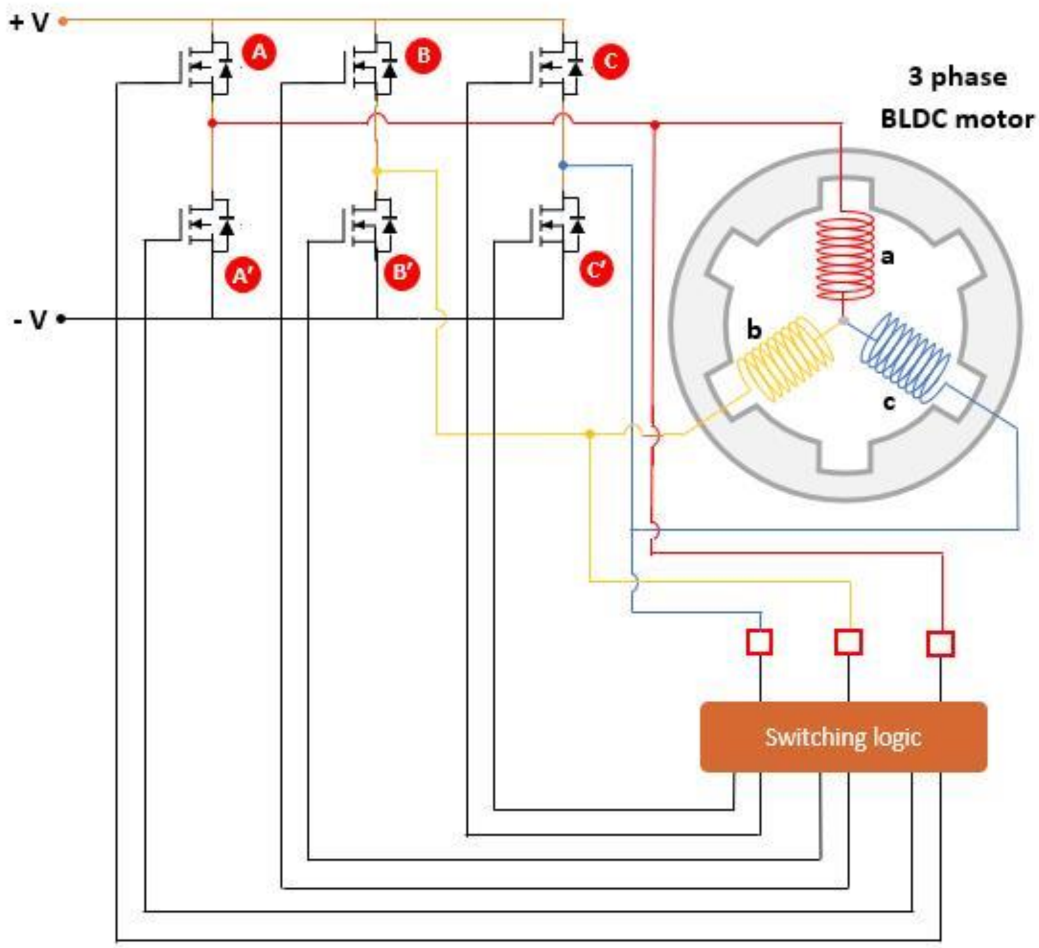

Figure 7: Trapezoidal Control (Six-Step Commutation)

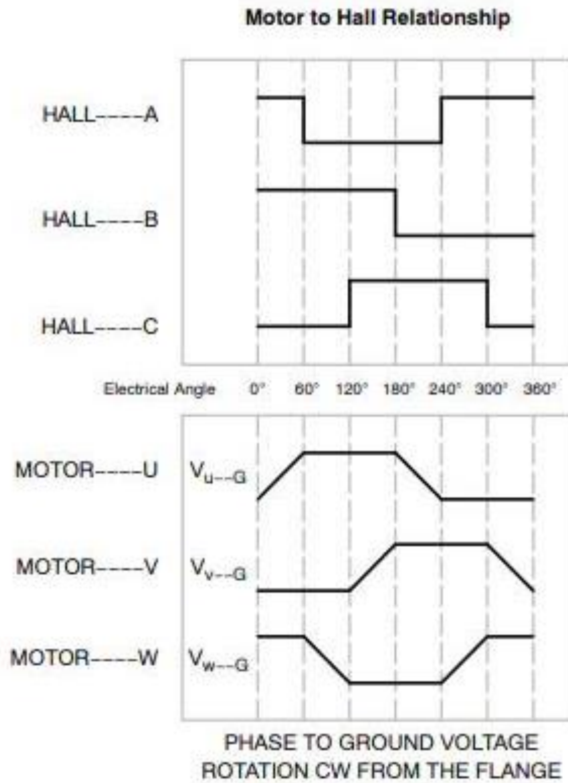

Figure 8: Hall Sensor Commutation Timing Diagram

2. Sinusoidal Control

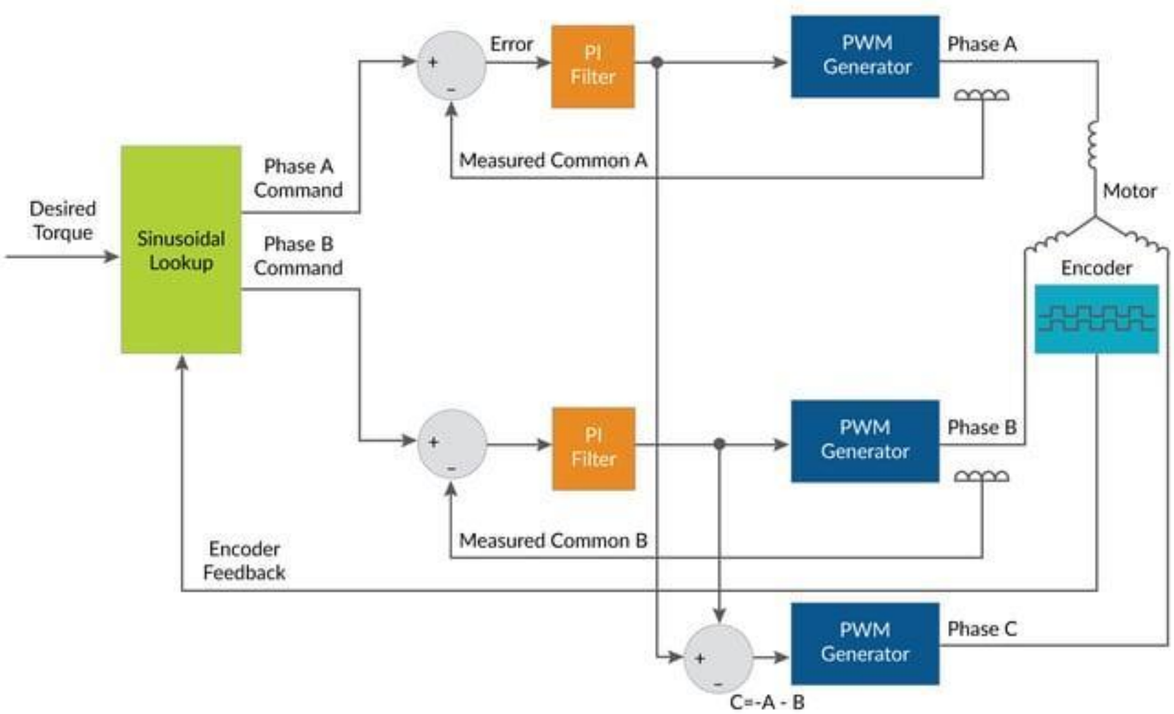

Figure 9: Sinusoidal Control

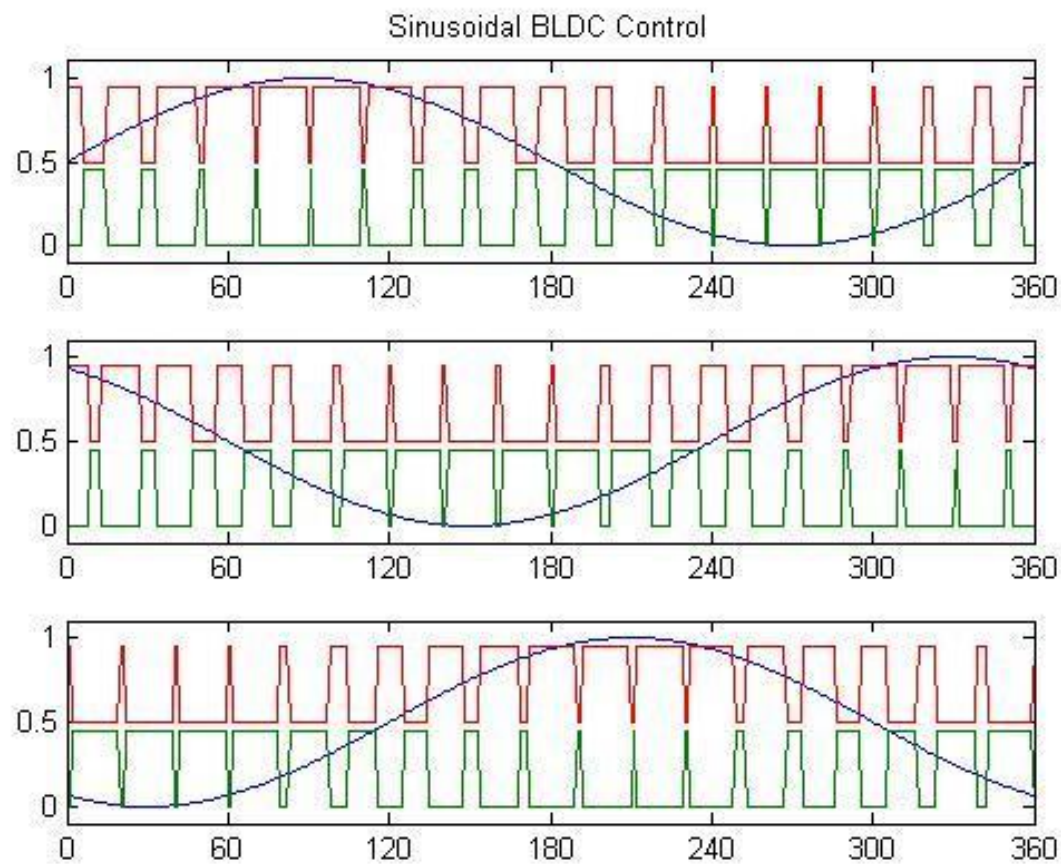

Figure 10: Sinusoidal Control

In this method, the phase currents follow a sinusoidal waveform, resulting in smoother torque production compared to trapezoidal control.

- Reduced torque ripple
- Lower acoustic noise
- More complex control and sensing

3. Field-Oriented Control (FOC)

Field-Oriented Control (also known as vector control) is the most advanced technique. It decouples torque and flux components using mathematical transformations (d-q axis control), enabling precise and efficient motor operation.

- High efficiency and dynamic performance
- Very low torque ripple
- Requires complex computation and controllers

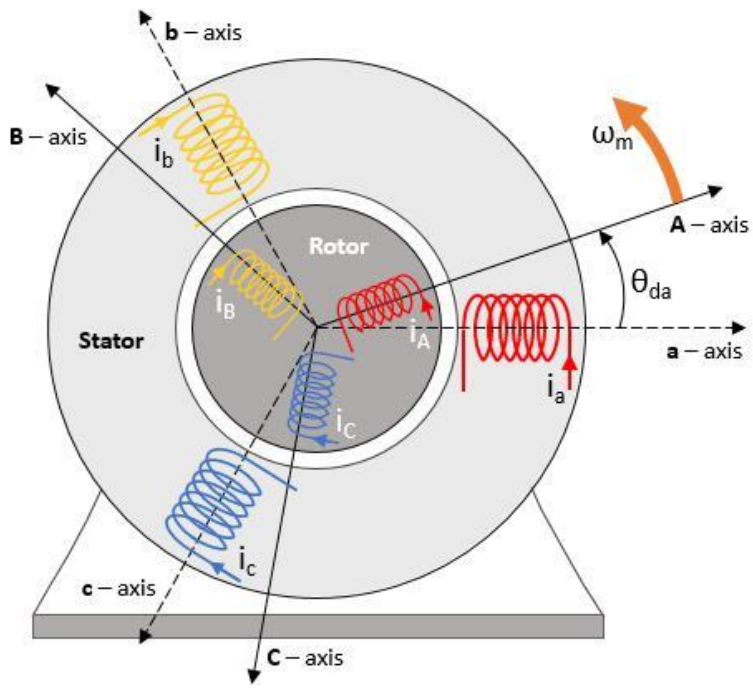

Figure 11: Field-Oriented Control (FOC)

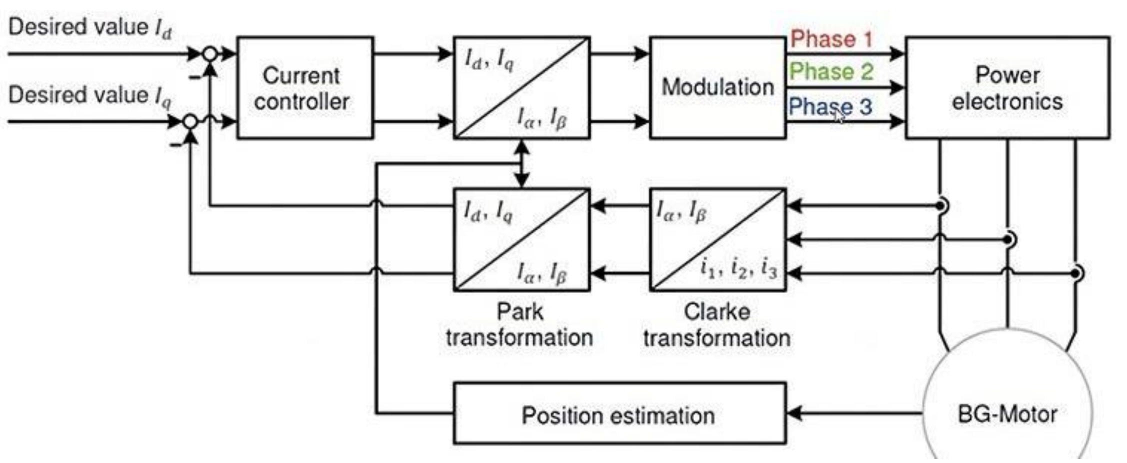

Figure 12: Draft of the FOC principle

The figures presented for BLDC control methods illustrate the fundamental differences between trapezoidal control, sinusoidal control, and field-oriented control (FOC) in terms of current waveforms, switching strategies, and overall performance.

In the trapezoidal control figures, the phase currents appear in a quasi-square waveform, synchronized with the rotor position through discrete commutation steps. These figures highlight the simplicity of the switching mechanism, where only two phases are energized at a time. However, the sharp transitions in current clearly explain the presence of torque ripple and increased acoustic noise.

The sinusoidal control figures, on the other hand, show smooth and continuous current waveforms distributed across all three motor phases. This visual representation emphasizes how gradual transitions in current reduce torque pulsations and improve motor smoothness. The figures also indicate the need for more precise rotor position information compared to trapezoidal control.

In the FOC-related figures, the diagrams typically include coordinate transformations and control loops in the d-q reference frame. These visuals demonstrate how the stator current is decomposed into two orthogonal components: one controlling flux and the other controlling torque. The figures clearly reflect the advanced nature of this method, showing multiple control blocks and feedback loops that enable high-performance and efficient motor operation.

Torque Estimation Approaches (Sensorless Control Methods)

Accurate torque estimation is crucial for control, monitoring, and protection of BLDC motors, especially in applications like electric vehicles.

1. Current-Based Estimation

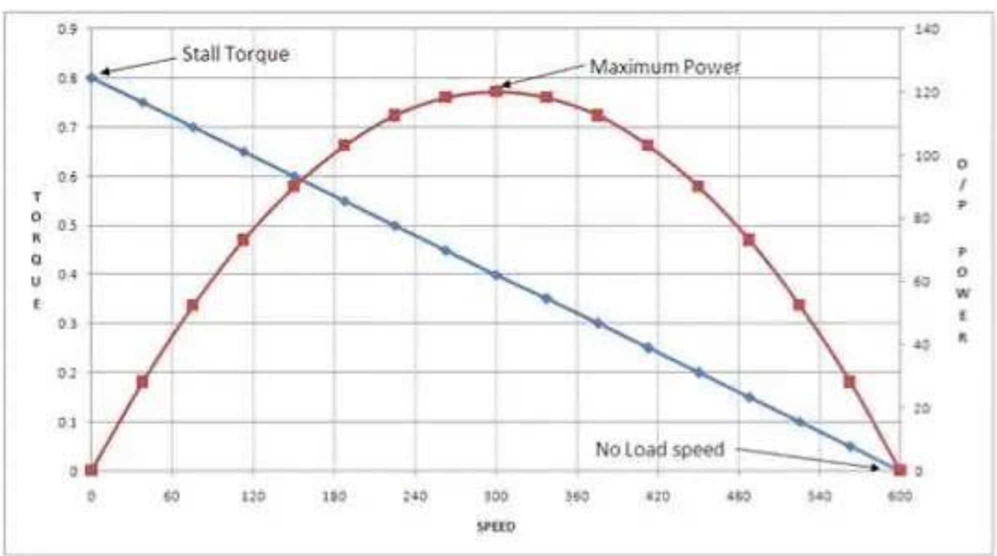

Figure 13: Speed-Torque-Power Curve

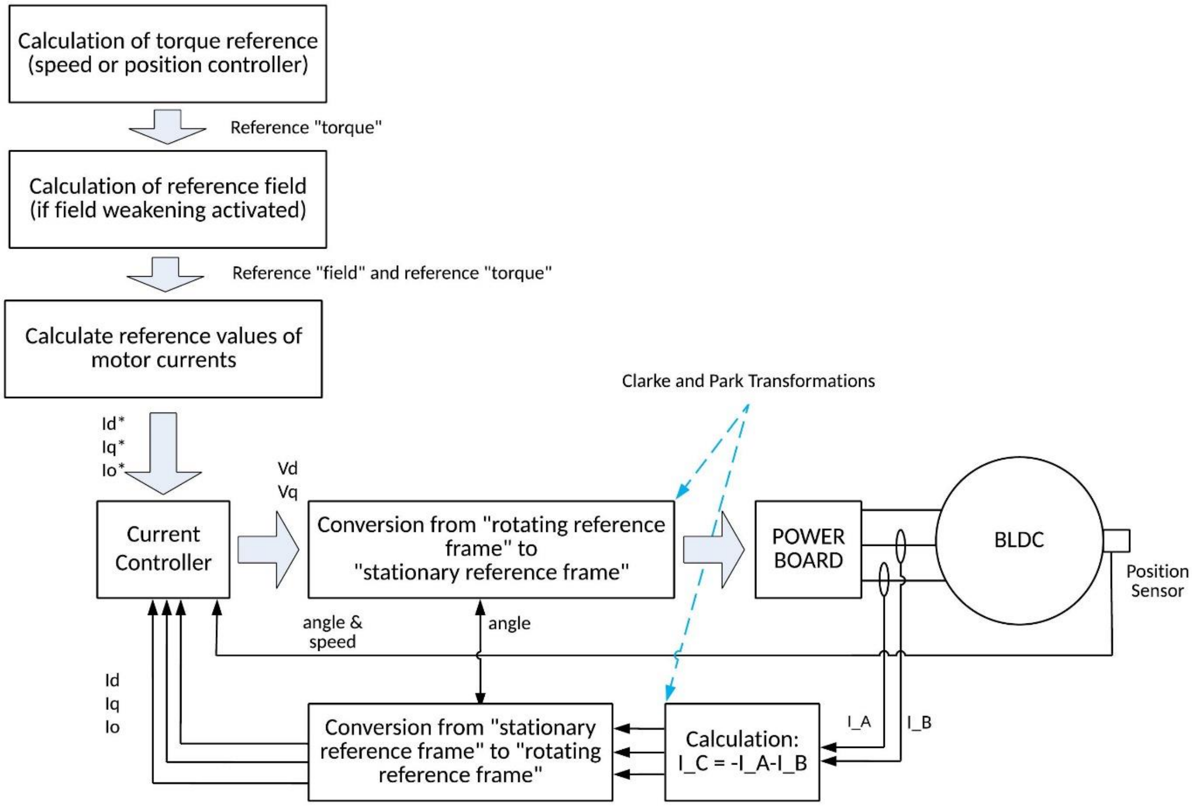

Figure 14: Current-Based Estimation

Torque is estimated using the relationship between stator current and torque: **T∝I** This method is simple and widely used but may be affected by parameter variations.

2. Back-EMF Based Estimation

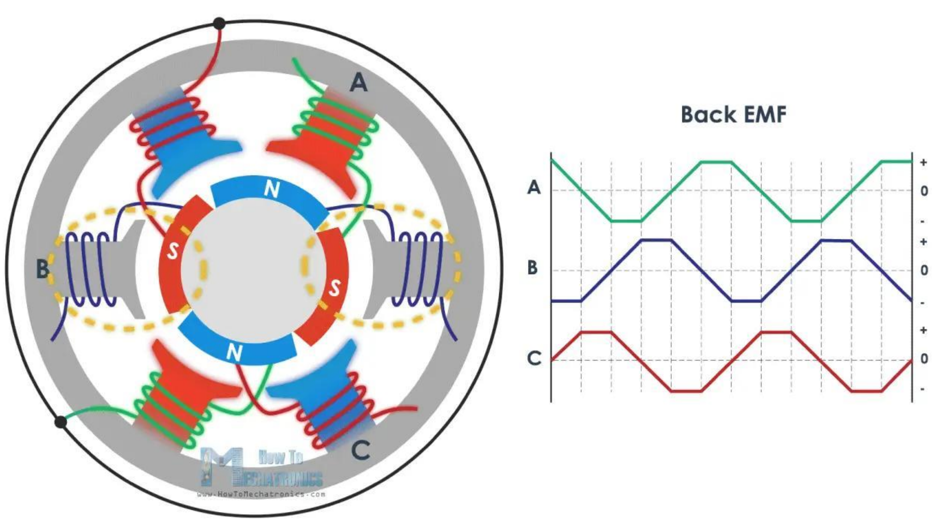

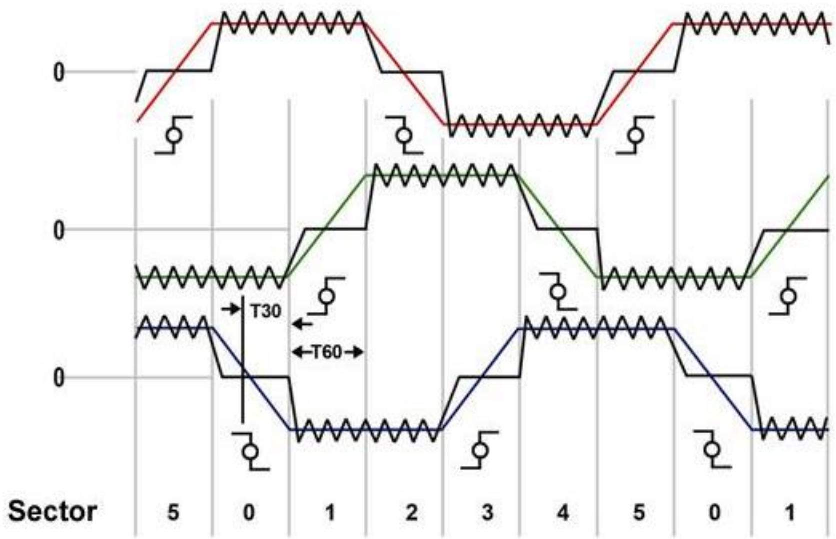

Figure 15: Back-EMF Based Estimation

This method estimates torque based on the back-EMF signal, which is proportional to rotor speed and magnetic flux.

- ➢ No need for torque sensors
- ➢ Suitable for sensorless control
- ➢ Less accurate at low speeds

3. Observer-Based Estimation

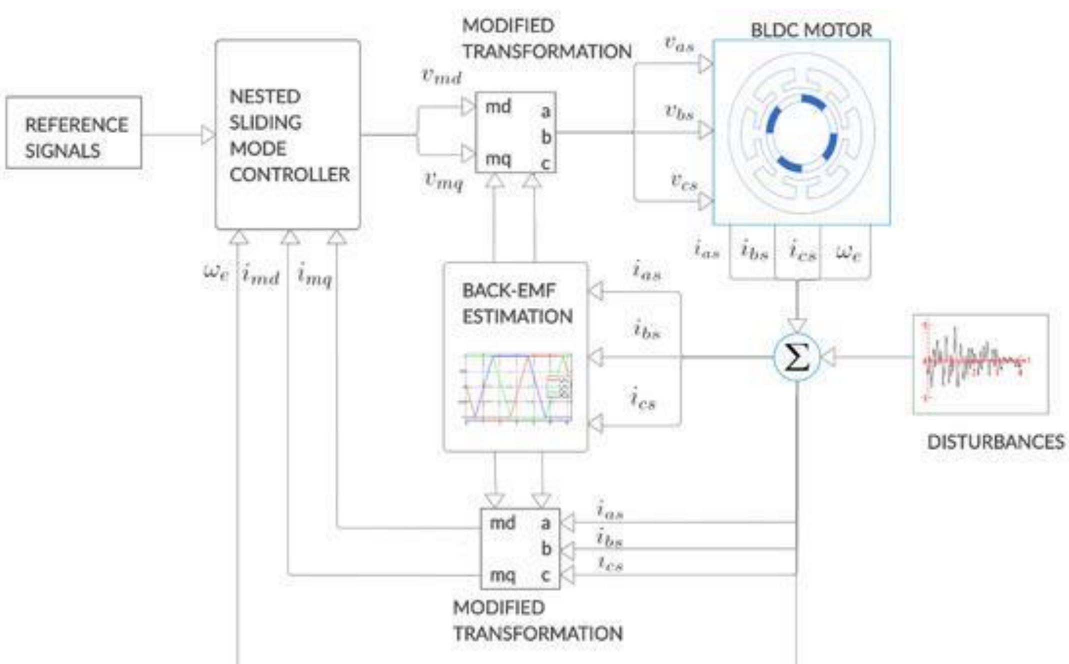

Figure 16: Observer-Based Estimation

Advanced techniques such as observers (e.g., Kalman filter, sliding mode observer) estimate torque using system models and measured signals.

- High accuracy
- Robust against noise and disturbances
- Computationally intensive

The figures associated with torque estimation approaches illustrate different techniques used to estimate the electromagnetic torque of a BLDC motor without relying on direct mechanical sensors.

In the current-based estimation figures, the relationship between stator current and torque is directly visualized. These figures typically show proportional behavior, indicating that torque can be approximated from current measurements. However, they also imply sensitivity to parameter variations, such as resistance changes and temperature effects.

The back-EMF-based estimation figures present the waveform of the induced voltage in the motor windings. These visuals demonstrate how back-EMF varies with rotor speed and position, providing an indirect method for estimating torque. The figures often highlight zero-crossing points or waveform shapes, which are essential for sensorless control, but also reveal limitations at low speeds where the signal becomes weak.

In observer-based estimation figures, block diagrams are used to represent mathematical models combined with real-time measurements. These figures show how estimated states (such as torque) are derived using observers like Kalman filters or sliding mode observers. The complexity of these diagrams reflects the higher accuracy and robustness of these methods, as they compensate for noise and system uncertainties.

BLDC motor performance depends heavily on the selected control method and the accuracy of torque estimation. While simple methods like trapezoidal control are suitable for low-cost applications, advanced techniques such as FOC and observer-based estimation provide superior performance for high-precision and high-efficiency systems.

2.3: Embedded Torque Sensing Technologies

In this section, we discuss the most important embedded torque sensing technologies used in electric drive systems, especially in BLDC motor applications. These technologies differ in working principle, cost, accuracy, and suitability for different environments.

Strain Gauge (Strain Meter) Technology

Strain gauge technology is considered the most traditional and widely used method for torque measurement. It works by measuring the torsional deformation (strain) on the shaft surface. When torque is applied, the shaft slightly twists, causing a change in electrical resistance in the strain gauges attached to it.

Typically, strain gauges are connected in a Wheatstone bridge configuration, which improves sensitivity and reduces temperature effects. This method can achieve very high accuracy (often less than 1% error), which is why it is commonly used as a reference in calibration systems.

However, this method requires physical contact with the rotating shaft. To transfer signals from the rotating part, slip rings or wireless telemetry systems are used, which may reduce reliability over long-term operation, especially in harsh environments.

Fiber Bragg Grating (FBG) Torque Sensors

Fiber Bragg Grating (FBG) sensors are optical-based torque sensing technologies. They work by reflecting a specific wavelength of light that changes when strain or temperature is applied to the fiber.

When the optical fiber is wrapped helically around a shaft, it can detect torsional strain very accurately. One of the biggest advantages of FBG sensors is that they are immune to electromagnetic interference, making them ideal for use inside electric motors or noisy environments.

On the downside, these sensors are expensive due to the need for optical interrogators. They are also fragile and sensitive to temperature changes, which requires compensation techniques during implementation.

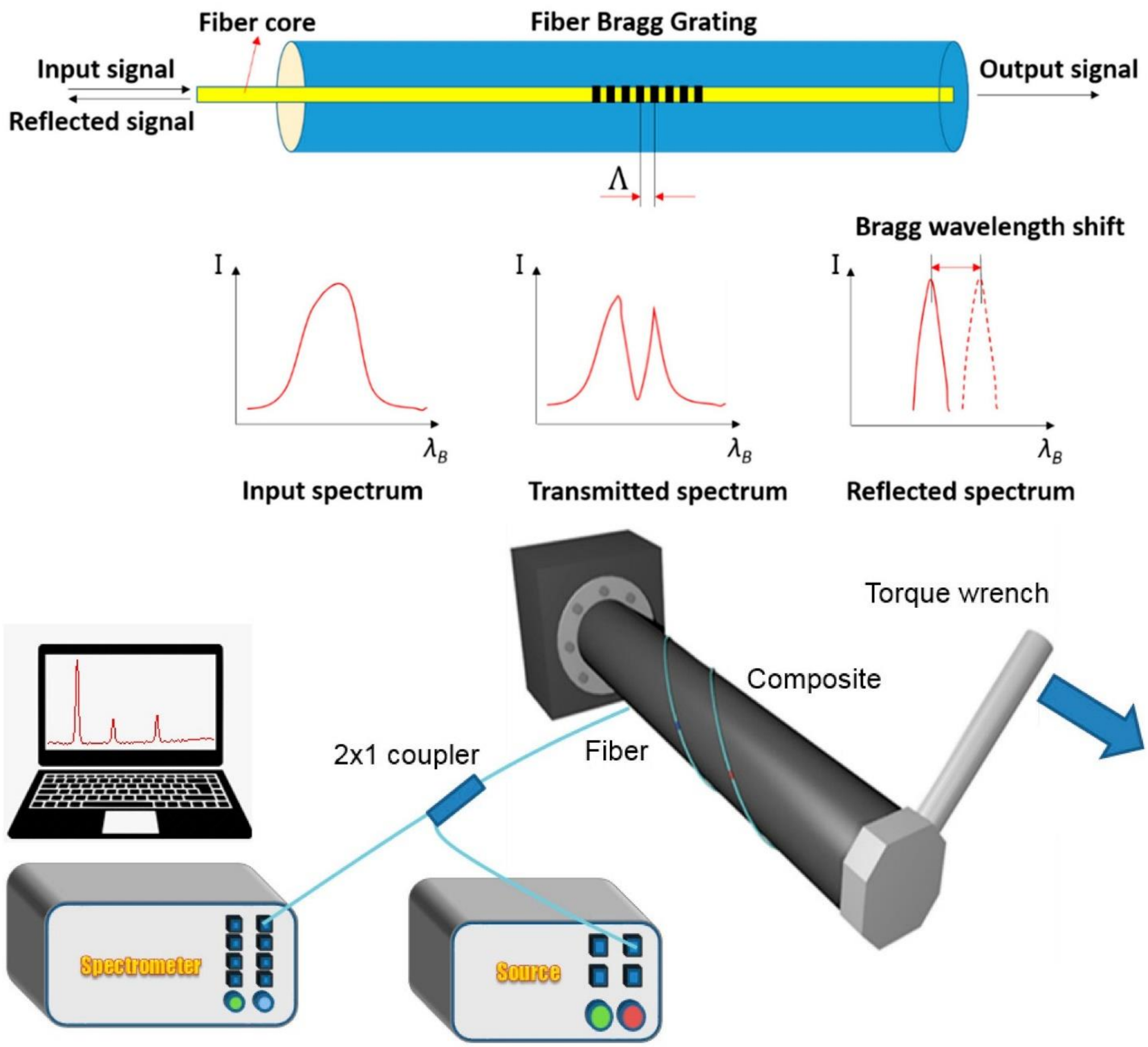

Figure 17: Fiber Bragg Grating (FBG) Torque Sensors

Hall-Based and Inductive Torque Sensors (Magnetic Method)

Magnetic torque sensing is a non-contact method that depends on changes in magnetic properties of materials under stress. When torque is applied to a ferromagnetic shaft, its internal magnetic field changes slightly. This variation can be detected using Hall-effect sensors or inductive coils placed near the shaft.

This method is highly suitable for harsh environments because there is no physical contact with the rotating shaft. It also reduces maintenance requirements and improves system durability.

However, this technique is sensitive to external magnetic fields and temperature variations. Also, proper calibration and material selection are very important to achieve accurate results.

Piezoelectric Torque Sensors

Piezoelectric sensors use materials that generate an electric charge when subjected to mechanical stress. When torque is applied, the shear stress produces a proportional electrical signal.

These sensors are known for their fast response and high sensitivity, making them very useful for detecting dynamic or rapidly changing torque. They are commonly used in applications where transient torque measurement is required.

The main limitation is that they cannot measure static torque accurately due to charge leakage over time. Additionally, they require special signal conditioning circuits and protection from vibrations and temperature variations.

MEMS-Based Torque Sensors

MEMS (Micro-Electro-Mechanical Systems) torque sensors are a modern solution that uses microfabricated structures to detect very small deformations. These sensors can be capacitive, resonant, or piezoresistive.

They are very small in size, consume low power, and can be easily integrated into compact systems such as BLDC motors or robotic joints. This makes them very attractive for embedded applications.

Despite these advantages, MEMS sensors currently have limitations in handling high torque values. They are also sensitive to mechanical damage and environmental conditions. However, ongoing research is improving their performance and durability.

Comparison of Torque Sensing Technologies

Before selecting a suitable torque sensing method, it is important to compare the main characteristics of each technology.

Table 2: Comparison of Torque Sensing Technologies

Technology	Accuracy	Type	Cost	Advantages	Limitations
Strain Gauge	Very High	Contact	Medium	High accuracy, widely used, reliable reference	Requires mechanical coupling and signal transfer
FBG Optical	Very High	Non-contact	High	Immune to electromagnetic interference	Expensive, fragile, temperature sensitive
Magnetic (Hall-based)	Medium	Non-contact	Low–Medium	Suitable for harsh environments, no contact	Sensitive to external magnetic fields
Piezoelectric	High (Dynamic)	Contact	Medium	Fast response, high sensitivity	Cannot measure static torque
MEMS	Medium	Contact	Low	Small size, low power, easy integration	Limited torque range, fragile structure

This table summarizes the key differences between the major embedded torque sensing technologies. Based on the application requirements (accuracy, cost, environment), the appropriate method can be selected.

2.4: Efficiency and Loss Mechanisms in Axial Flux Machines

The efficiency of axial flux permanent magnet (AFPM) machines depends on the balance between electromagnetic design, material selection, and mechanical configuration. Compared to radial flux machines, AFMs provide a shorter magnetic path and higher torque density.

However, several types of losses affect the overall efficiency, including core losses, copper losses, permanent magnet losses, and mechanical losses.

Core Losses

Core losses occur in the stator and rotor due to alternating magnetic fields. These losses consist of hysteresis losses and eddy current losses.

$$\text{Eddy Current Loss } (P_e) = K_e\, B_m^2\, f^2 t^2 V$$

Where,

P_e = Eddy curret loss (Watt)

B_m = Maximum Flux density(W_b/m^2)

f = Frequency of supply (f)

t = Thickness of lamination(meter)

V = Volume of the material (M^3)

K_e = Eddy current Constant

Figure 18: Core Losses Equation

This equation shows that core losses increase with frequency and magnetic flux density. Therefore, selecting proper magnetic materials and reducing flux variations can improve efficiency.

Copper Losses

Copper losses are caused by the resistance of stator windings when current flows through them.

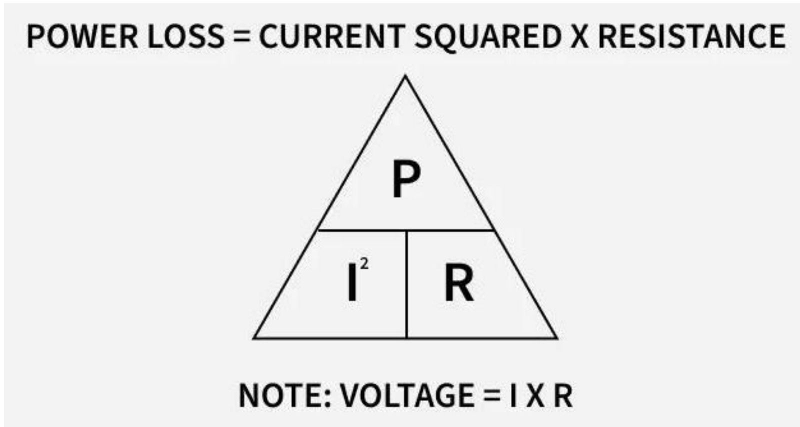

Figure 19: Copper Losses Equation

Where:
I = phase current
R = winding resistance

Copper losses increase with the square of the current, which means high current significantly increases heating. These losses can be reduced by using high conductivity materials, optimizing winding design, and improving cooling.

Permanent Magnet (PM) Eddy Current Losses

Permanent magnets in AFM machines, especially Neodymium magnets, are exposed to time-varying magnetic fields, which induce eddy currents inside the magnets.

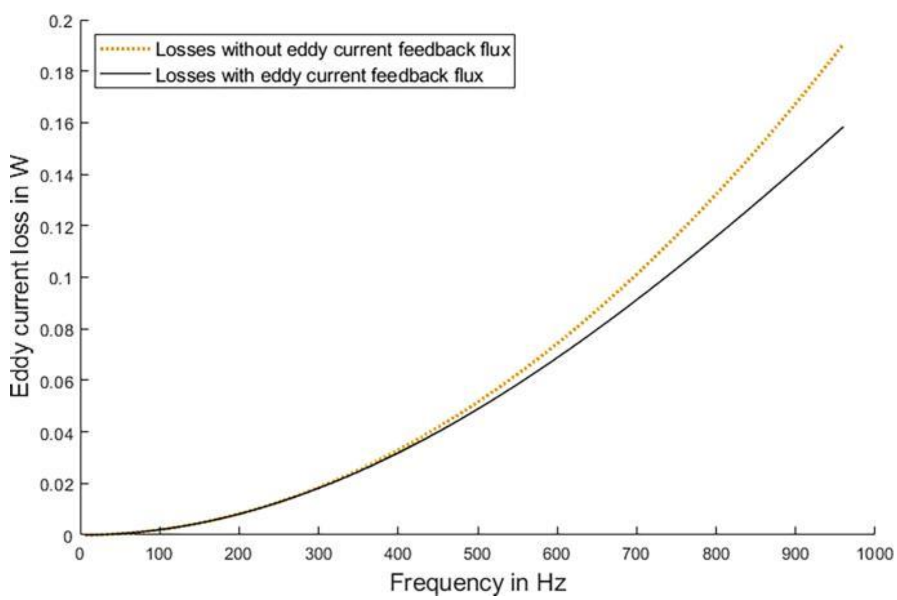

Figure 20: Permanent Magnet (PM) Eddy Current Losses

These induced currents cause additional heating and may lead to partial demagnetization. To reduce these losses, segmented magnets or insulated magnet structures are used.

Mechanical Losses

Mechanical losses are related to the moving parts of the machine and are different from electrical losses.

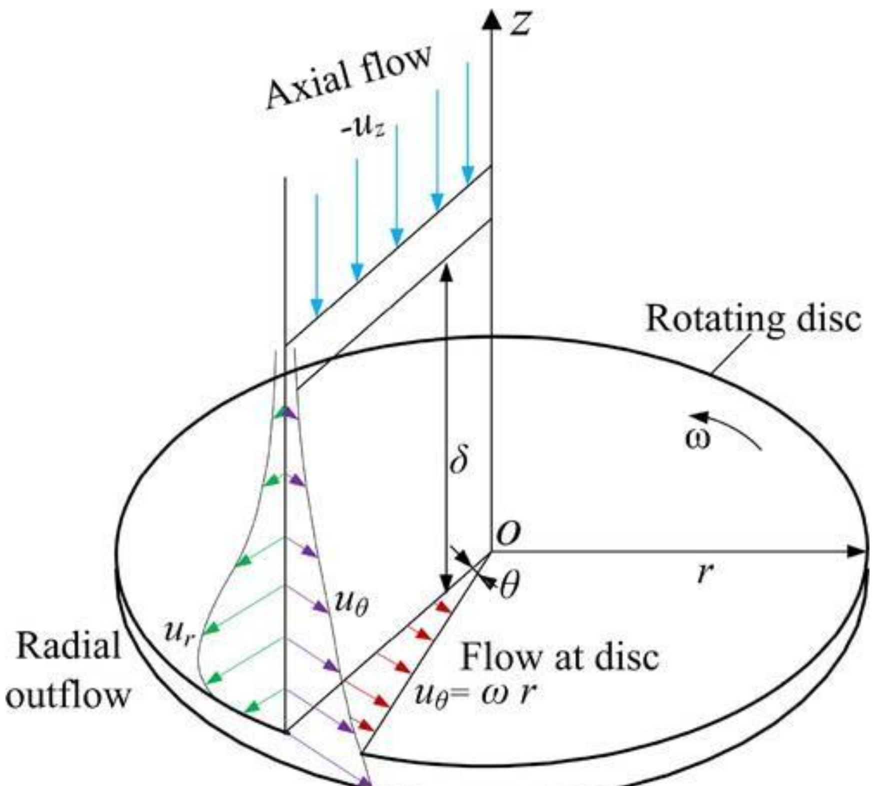

Figure 21: Mechanical Losses

These losses mainly include:

- Bearing friction
- Air friction (windage losses)
- Rotor imbalance

Mechanical losses can be minimized by using high-quality bearings, proper rotor balancing, and optimized aerodynamic design.

Overall Efficiency

The efficiency of the machine represents how effectively electrical power is converted into mechanical power.

The efficiency is defined as: $\eta = P\_out / P\_in$
And the input power can be written as:
$P\_in = P\_out + P\_cu + P\_core + P\_PM + P\_mech$

Where:
- P_cu = copper losses
- P_core = core losses
- P_PM = permanent magnet losses
- P_mech = mechanical losses

This shows that reducing all types of losses improves the overall efficiency of the machine.

Comparison of Loss Mechanisms

Before analyzing performance, it is important to compare the different loss types.

Table 3: Comparison of Loss Mechanisms

Loss Type	Cause	Dependency	Impact on Machine	Reduction Method
Core Loss	Magnetic field variation	Frequency, flux density	Heating in core	Better materials, lower flux variation
Copper Loss	Winding resistance	Current (I^2)	Thermal stress in windings	Thick wires, cooling, optimized winding
PM Loss	Eddy currents in magnets	Magnetic variation	Magnet heating	Segmentation, insulation
Mechanical Loss	Friction & air resistance	Speed	Energy dissipation	Bearings, balancing, aerodynamics

This table summarizes how each loss mechanism affects the performance of the AFM machine and how it can be reduced.

The efficiency of axial flux machines depends on how well different types of losses are minimized. Although AFMs provide high torque density and shorter magnetic paths, several loss mechanisms still affect their performance.

Core losses occur due to alternating magnetic fields in the stator and rotor, and they increase with frequency and flux density. Copper losses are caused by the resistance of stator windings and are proportional to the square of the current, making them a major source of heat.

Permanent magnet losses result from eddy currents induced inside the magnets due to changes in the magnetic field, which can lead to heating and possible demagnetization. Mechanical losses are related to moving parts such as bearings and air friction, and they increase with speed.

Overall efficiency is determined by the ratio of output power to input power, where all these losses reduce the useful output. Therefore, improving efficiency requires careful design of materials, winding configuration, cooling methods, and mechanical components to minimize total losses.

2.5: Methods for Performance Evaluation

Evaluating the performance of axial flux permanent magnet (AFPM) machines requires a combination of simulation and experimental methods. These approaches help in analyzing electromagnetic behavior, efficiency, losses, and dynamic response under different operating conditions. The evaluation methods are generally divided into steady-state, transient, loss separation, and experimental test-bench approaches.

Steady-state evaluation focuses on analyzing the machine under constant speed and torque conditions. It is mainly used to study back-EMF waveforms, torque-speed characteristics, and efficiency mapping. Measurements such as voltage, current, torque, and temperature are taken using instruments like dynamometers, torque sensors, and power analyzers to validate the machine design.

Transient evaluation deals with dynamic conditions such as startup, acceleration, and load changes. This method is important for analyzing current and torque overshoot, commutation behavior, and thermal effects during operation. Simulation tools like MATLAB/Simulink and transient finite element analysis (FEA) are commonly used, in addition to real experimental testing for accurate validation.

Loss separation methods are used to identify and quantify different types of losses inside the machine. Copper losses are calculated using current and resistance, while core losses are estimated using no-load tests or FEA. Eddy current losses in magnets are analyzed using transient simulations or temperature measurements, and mechanical losses are obtained from no-load torque measurements. Additional losses such as stray load losses are determined by subtracting known losses from total measured losses.

R&D test benches represent the most advanced evaluation method, where a complete experimental setup is used to measure electrical, mechanical, and thermal parameters simultaneously. These systems include torque transducers, encoders, power analyzers, and cooling systems, allowing detailed analysis of efficiency, torque ripple, thermal behavior, and long-term performance.

Before selecting the appropriate evaluation method, it is useful to compare the main characteristics of each approach:

Table 4: Methods for Performance Evaluation

Method Type	Purpose	Tools Used	Advantages	Limitations
Steady-State	Constant speed/torque analysis	Dynamometer, power analyzer	reliable, efficiency mapping	Doesn't capture dynamic behavior
Transient	Dynamic performance analysis	MATLAB, Simulink, transient FEA	Captures real-time response	Complex and time-consuming

Method Type	Purpose	Tools Used	Advantages	Limitations
Loss Separation	Identify individual losses	Tests + FEA	Accurate loss breakdown	Requires multiple measurements
R&D Test Bench	Full system validation	Sensors + data acquisition systems	High accuracy, complete analysis	Expensive and complex setup

This table summarizes the main performance evaluation methods and highlights their differences in terms of purpose, tools, advantages, and limitations.

In this chapter, the main concepts related to BLDC machines and axial flux permanent magnet (AFPM) systems were discussed from both control and performance perspectives.

First, BLDC control methods were introduced, including both sensorless and sensorized approaches. Sensorless methods rely on estimating rotor position using electrical signals such as back-EMF, while sensorized methods use physical sensors like Hall sensors to achieve more accurate and stable control, especially at low speeds.

Then, torque estimation and embedded torque sensing technologies were presented. Several sensing techniques were discussed, including strain gauges, fiber Bragg grating (FBG) sensors, magnetic (Hall-based) methods, piezoelectric sensors, and MEMS-based sensors. Each method has its own advantages and limitations in terms of accuracy, cost, robustness, and suitability for different environments.

After that, the efficiency and loss mechanisms in AFPM machines were analyzed. The main losses include core losses, copper losses, permanent magnet losses, and mechanical losses. These losses directly affect the overall efficiency of the machine, and minimizing them requires proper design of materials, geometry, and cooling systems.

Finally, different performance evaluation methods were explained. These include steady-state analysis, transient analysis, loss separation techniques, and advanced R&D test benches. Each method provides important insights into machine behavior under different operating conditions and helps in validating both simulation and experimental results.

In the next chapter, the focus will shift from theoretical analysis to practical implementation. The design and development of the proposed system will be presented, including the selection of the BLDC motor, control strategy, and hardware components.

This chapter will also describe the system architecture, including the power electronics (inverter), control unit, sensors, and measurement systems used in the project. In addition, the integration of torque sensing and control algorithms will be discussed in detail.

Finally, simulation results and/or experimental setup details will be introduced to demonstrate how the designed system operates under real conditions, preparing for performance validation and result analysis in the following chapters.

Chapter Three

Chapter Three

Electromagnetic Modeling and Analytical Foundations

Chapter 3: Electromagnetic Modeling & Analytical Foundations of Axial Flux BLDC Machines

Following the review of machine topologies, control strategies, torque sensing technologies, and performance evaluation methods presented in Chapter Two, this chapter shifts the focus toward the analytical and electromagnetic foundations that govern the operation of axial flux BLDC machines. The purpose of this chapter is to establish a solid theoretical framework that links electromagnetic principles with machine design parameters, enabling accurate prediction of performance characteristics prior to numerical simulation and experimental validation.

In axial flux machines, electromagnetic behavior differs significantly from conventional radial flux machines due to the axial direction of magnetic field distribution and the disc-type geometry. These differences directly affect air-gap flux density, torque production, harmonic content, and overall efficiency. Therefore, understanding the fundamental electromagnetic relationships is essential for proper machine sizing, control, and optimization.

This chapter begins by introducing the key electromagnetic concepts relevant to axial flux machines, including air-gap magnetic field distribution, magnetomotive force (MMF), and harmonic effects. These fundamentals provide insight into how magnetic fields are generated, distributed, and interact within the machine structure. Special attention is given to the influence of geometry, magnet arrangement, and winding configuration on the resulting electromagnetic performance.

Building on these fundamentals, the chapter then derives the governing equations for back electromotive force (Back-EMF) and electromagnetic torque in axial flux BLDC topologies. These derivations form the mathematical basis for understanding how electrical input is converted into mechanical output, and how machine constants such as torque constant and back-EMF constant are determined.

Furthermore, the chapter presents analytical sizing equations used to estimate torque density and power density. These equations are essential for comparing axial flux and radial flux machines and for guiding the initial design process. Additional sections address lumped parameter modeling and circuit representation of the machine, enabling simplified analysis of electrical behavior, as well as winding design considerations and slot/pole combinations that directly influence torque ripple, efficiency, and harmonic content.

By integrating electromagnetic theory with practical design considerations, this chapter serves as a critical bridge between the conceptual understanding introduced earlier and the detailed electromagnetic design and simulation presented in the following chapters.

Subsections:

3.1 Electromagnetic Fundamentals Relevant to Axial Flux Machines
3.2 Back-EMF and Torque Equation Derivations for Axial Flux Machines
3.3 Sizing Equations and Performance Metrics
3.4 Lumped Parameter Modeling and Equivalent Circuits
3.5 Winding Design and Slot/Pole Configuration Considerations

3.1 Electromagnetic Fundamentals Relevant to Axial Flux Machines

The performance of axial flux brushless DC (BLDC) machines is fundamentally governed by electromagnetic principles that describe how magnetic fields are generated, distributed, and interact with current-carrying conductors. Unlike radial flux machines, where the magnetic field flows radially, axial flux machines exhibit a magnetic field that travels parallel to the axis of rotation. This unique configuration leads to distinct electromagnetic characteristics that must be carefully analyzed.

One of the most important aspects in axial flux machines is the air-gap magnetic field distribution. The air-gap represents the region between the stator and rotor where the magnetic field is established. In an ideal case, the magnetic flux density in the air-gap follows a quasi-sinusoidal or trapezoidal distribution, depending on the magnet shape and winding configuration. This distribution directly affects the induced back electromotive force (Back-EMF) and the torque production of the machine.

The magnetic flux density in the air-gap can be approximated as:

$$B_g = \frac{\mu_0 \, H_c \, l_m}{g + \frac{l_m}{\mu_r}}$$

B_g: is the air-gap flux density,
mu_0: is the permeability of free space,
mu_r: is the relative permeability of the magnet material,
H_m: is the magnetizing field strength,
l_m: is the magnet thickness,
g: is the air-gap length.

This equation shows that the air-gap flux density is strongly influenced by both the physical dimensions of the magnet and the air-gap. A smaller air-gap generally results in higher flux density, which improves torque capability but increases manufacturing complexity.

Another key concept is the magnetomotive force (MMF), which represents the driving force that establishes magnetic flux in the machine. MMF is generated by both permanent magnets and stator windings. In axial flux BLDC machines, the combination of rotor permanent magnets and stator currents produces a rotating magnetic field that interacts to generate torque.

In practical machines, the MMF distribution is not perfectly sinusoidal due to slotting effects, magnet shape, and winding layout. This leads to the presence of harmonics in the magnetic field.

Harmonics play a significant role in determining machine performance. While the fundamental component contributes to useful torque, higher-order harmonics can lead to undesirable effects such as torque ripple, acoustic noise, and additional losses. In axial flux machines, harmonic content is influenced by factors such as pole number, slot configuration, and magnet geometry.

Understanding and minimizing harmonic effects is essential for improving torque smoothness and overall efficiency.

In summary, the electromagnetic behavior of axial flux BLDC machines is primarily determined by air-gap flux distribution, magnetomotive force, and harmonic content. These elements directly influence torque production, efficiency, and dynamic performance. A clear understanding of these fundamentals is essential before proceeding to the derivation of back-EMF and torque equations in the following section.

3.2 Back-EMF and Torque Equation Derivations for Axial BLDC

The back electromotive force (Back-EMF) and electromagnetic torque are two of the most critical quantities in the analysis and design of axial flux BLDC machines. These parameters directly describe the energy conversion process between the electrical and mechanical domains. Therefore, deriving accurate expressions for both is essential for predicting machine performance.

Back-EMF Derivation

Back-EMF is the voltage induced in the stator windings due to the relative motion between the magnetic field produced by the rotor magnets and the stator conductors. According to Faraday's law of electromagnetic induction, the induced voltage is proportional to the rate of change of magnetic flux linkage.

In axial flux BLDC machines, the waveform of Back-EMF is typically trapezoidal due to the shape of the magnets and winding distribution, which makes it suitable for six-step (trapezoidal) control.

Electromagnetic Torque Derivation

The electromagnetic torque is produced due to the interaction between the stator current and the magnetic field generated by the rotor. The torque can be derived from the principle of energy conversion, where electrical power is converted into mechanical power.

In axial flux BLDC machines, the derivation of back electromotive force (Back-EMF) and electromagnetic torque is based on fundamental electromagnetic laws, particularly Faraday's law of induction and the principle of energy conversion. Unlike simplified models, a more accurate analytical formulation considers the spatial distribution of the air-gap flux density, which is generally expressed using a Fourier series to account for both fundamental and harmonic components.

The magnetic flux linking the stator windings is obtained by integrating the air-gap flux density over the effective pole area. This flux linkage varies with rotor position, and its time derivative produces the induced Back-EMF. By relating the electrical angular speed to the mechanical speed through the number of pole pairs, a complete expression for the phase Back-EMF can be derived.

Similarly, the electromagnetic torque is obtained from the instantaneous power balance between electrical input and mechanical output. By substituting the Back-EMF expression into the power equation, the torque can be expressed in terms of current, speed, and machine constants. These derivations provide a rigorous foundation for understanding torque production and are essential for accurate modeling and control of axial flux BLDC machines.

Key Equations for Back-EMF and Torque in Axial-Flux BLDC Machines

Back-EMF Derivation

1) Air-gap flux density (assumed approximation):

$$B(\theta) = \sum_{n=1,3,5,\ldots}^{\infty} B_n \cos(np\theta) \quad (1)$$

2) Flux per pole:

$$\Phi(\theta) = \int_{ri}^{r_o} \int_{0}^{\frac{2\pi}{2p}} B(\theta) r \, d\theta \, dr \quad (2)$$

3) Flux linkage of one phase:

$$\lambda(\theta) = N \, \Phi(\theta) \quad (3)$$

4) Back-EMF of one phase (Faraday's law):

$$e(\theta) = -\frac{d\lambda(\theta)}{dt} \quad (4)$$

5) Using chain rule:

$$e(\theta) = -N \frac{d\Phi(\theta)}{d\theta} \frac{d\theta}{dt} \quad (5)$$

6) Electrical angular speed:

$$\omega_e = \frac{d\theta}{dt} = p \, \omega_m \quad (6)$$

7) Phase back-EMF expression:

$$e(\theta) = -N \, \omega_e \frac{d\Phi(\theta)}{d\theta} = E_{max} \, f(\theta) = K_e \, \omega_e \, f(\theta) \quad (7)$$

Torque Derivation

1) Instantaneous electromagnetic power:

$$P_{em}(t) = e(t) \, i(t) \quad (8)$$

2) Mechanical power:

$$P_m(t) = T_e(t) \, \omega_m \quad (9)$$

3) Power balance (neglecting losses):

$$e(t) \, i(t) = T_e(t) \, \omega_m \quad (10)$$

4) Electromagnetic torque:

$$T_e(t) = \frac{e(t) \, i(t)}{\omega_m} = \frac{K_e \, \omega_e \, f(\theta) \, i(t)}{\omega_m} = p \, K_e \, f(\theta) \, i(t) \quad (11)$$

5) Phase torque (for each phase):

$$T_{phase} = K_t \, f(\theta) \, i(t) \quad (12)$$

6) Total electromagnetic torque (three-phase machine):

$$T_e = \sum_{k=a,b,c} T_{phase,k} = K_t \, I_{eq} \quad (13)$$

Where:

B_n : amplitude of the n^{th} harmonic of air-gap flux density (T)
p : number of pole pairs
θ : electrical angle (rad)
r_i, r_o : inner and outer radius (m)
N : number of series turns per phase
ω_m : mechanical angular speed (rad/s)
ω_e : electrical angular speed (rad/s)
$f(\theta)$: back-EMF / flux waveform function
K_e : back-EMF constant (V·s/rad)
K_t : torque constant (N·m/A)
$i()$: phase current (A)
I_{eq} : equivalent current term depending on waveform and conduction mode

Relationship between constants:
$K_t = p \, K_e$
(SI units)

Figure 22: Complete Set of Back-EMF and Torque Equations

The set of equations presented in the figure provides a comprehensive analytical framework for describing the electromagnetic behavior of axial flux BLDC machines. Equation (1) models the air-gap flux density as a sum of harmonic components, which reflects the non-ideal magnetic field distribution caused by practical design factors such as magnet shape and slotting.

Equations (2) and (3) define the magnetic flux per pole and the corresponding flux linkage in the stator windings. These are essential intermediate steps that connect the physical magnetic field to the electrical quantities. Using Faraday's law, equations (4) through (7) derive the Back-EMF as a function of rotor position and electrical angular speed, showing that the induced voltage depends on both machine geometry and rotational speed.

On the torque side, equations (8) to (13) are derived from the instantaneous power balance principle. These equations demonstrate that the electromagnetic torque is directly related to the interaction between the stator current and the magnetic field. The final expressions show that torque is proportional to current, with the proportionality constant defined as the torque constant.

Additionally, the relationship between the Back-EMF constant and torque constant highlights an important property of electric machines in SI units, where both constants are numerically equal when properly defined. Overall, these equations form the theoretical basis for performance prediction, control design, and optimization of axial flux BLDC machines.

The Back-EMF and torque equations establish a direct relationship between electrical inputs and mechanical outputs. Back-EMF is proportional to speed, while torque is proportional to current. These relationships form the basis for control strategies and performance prediction. Understanding these equations is essential before proceeding to machine sizing and performance evaluation, which are discussed in the next section.

3.3 Sizing Equations and Performance Metrics

Sizing equations play a fundamental role in the preliminary design of axial flux BLDC machines, as they establish analytical relationships between machine geometry, magnetic loading, and electric loading. These equations provide an initial estimation of the torque and power capabilities before conducting detailed electromagnetic simulations.

In axial flux topologies, torque is generated over a disc-shaped air-gap area, making the machine dimensions—particularly the inner and outer radii—critical factors in determining performance. Unlike radial flux machines, the torque production in axial flux machines is strongly influenced by the effective radius, leading to higher torque potential for compact designs.

To evaluate and compare machine performance, two key indicators are commonly used: torque density and power density. These metrics normalize the output with respect to machine volume, allowing for a fair comparison between different machine topologies and design configurations. The following equations summarize the main analytical relationships used for sizing and performance evaluation.

The sizing of axial flux BLDC machines is a critical step in the design process, as it determines the machine's ability to deliver the required torque and power within given dimensional and thermal constraints. Unlike detailed electromagnetic models, sizing equations provide analytical approximations that allow designers to estimate machine performance at an early stage.

In axial flux machines, the geometry plays a dominant role, particularly the outer and inner radii of the rotor, since torque is produced over a disc-shaped area rather than a cylindrical surface. Therefore, torque and power capabilities are strongly linked to the effective radius, magnetic loading, and electric loading of the machine.

Two key performance indicators are commonly used:

1. Torque density: torque per unit volume
2. Power density: power per unit volume

These metrics are essential for comparing axial flux machines with radial flux machines and for evaluating the efficiency of the design.

Key Sizing Equations and Performance Metrics for Axial-Flux BLDC Machines

1) Average air-gap flux density (fundamental component)

$$B_{avg} = \frac{4}{\pi} B_{g,pk} k_B \quad (3.1)$$

where $B_{g,pk}$ is the peak air-gap flux density, and k_B is the flux waveform factor.

2) Electric loading (linear current density)

$$A_e = \frac{N_c I}{2\pi r_{avg}} \quad (3.2)$$

where N_c is the total number of active conductors, I is the phase current, and $r_{avg} = \frac{r_o + r_i}{2}$ is the average radius.

3) Electromagnetic torque

$$T = \frac{2}{3} \pi \, B_{avg} \, A_e \left(r_o^3 - r_i^3\right) \quad (3.3)$$

4) Mechanical output power

$$P = T \, \omega_m \quad (3.4)$$

5) Active volume of the machine

$$V = \pi \left(r_o^2 - r_i^2\right) l \quad (3.5)$$

where l is the axial length (stack length) of the machine.

6) Torque density

$$T_d = \frac{T}{V} = \frac{2}{3} \frac{B_{avg} \, A_e}{l} \frac{\left(r_o^3 - r_i^3\right)}{\left(r_o^2 - r_i^2\right)} \quad (3.6)$$

7) Power density

$$P_d = \frac{P}{V} = \frac{T \, \omega_m}{V} = T_d \, \omega_m \quad (3.7)$$

8) Peripheral (linear) speed at average radius

$$v = \omega_m \, r_{avg} \quad (3.8)$$

9) Specific magnetic loading

$$B_{spec} = B_{avg} \quad (3.9)$$

10) Specific electric loading

$$A_{spec} = A_e \quad (3.10)$$

Where:

B_{avg} : average air-gap flux density (T)
$B_{g,pk}$: peak air-gap flux density (T)
k_B : flux waveform factor (–)
A_e : electric loading (A/m)
N_c : total number of active conductors
I : phase current (A)
r_o : outer radius (m)
r_i : inner radius (m)
r_{avg} : average radius $= \frac{r_o + r_i}{2}$ (m)
T : electromagnetic torque (N·m)
P : output power (W)
ω_m : mechanical angular speed (rad/s)
l : axial length (m)
V : active volume (m^3)
T_d : torque density (N·m/m^3)
P_d : power density (W/m^3)
v : peripheral speed (m/s)
B_{spec} : specific magnetic loading (T)
A_{spec} : specific electric loading (A/m)

Note: The above equations are based on ideal assumptions, including uniform air-gap flux density, sinusoidal current distribution, and neglecting losses, leakage, and saturation effects.

Figure 23: Core Sizing Equations and Performance Metrics

The presented equations highlight the strong dependence of torque production on the machine geometry, particularly the radii. The term $(r_o^3 - r_i^3)$ shows that torque increases significantly with the outer radius, which explains why axial flux machines are well known for their high torque capability.

Additionally, both magnetic loading Bavg and electric loading Ae directly influence the torque. Increasing these parameters improves performance but is limited by material saturation, thermal constraints, and insulation limits.

The torque and power density expressions provide a normalized way to evaluate machine performance independent of size. Axial flux machines typically achieve higher torque density compared to radial flux machines due to their larger effective radius and compact axial structure.

However, practical limitations such as cooling, mechanical strength, and manufacturing complexity must be considered when optimizing these parameters.
The presented sizing equations provide a clear analytical framework for estimating the performance of axial flux BLDC machines at the early design stage. They demonstrate that torque production is primarily influenced by the average air-gap flux density, electric loading, and the geometric dimensions of the machine, particularly the radii.

Furthermore, torque density and power density serve as essential performance metrics for evaluating the effectiveness of a given design. Axial flux machines inherently offer high torque density due to their larger effective radius and compact axial structure. However, practical limitations such as thermal constraints, material saturation, and mechanical considerations must be taken into account when optimizing these parameters.

Overall, these equations form a critical foundation for machine design and provide valuable insight before moving to detailed modeling and simulation in the subsequent sections.

3.4 Lumped Parameter Modeling and Equivalent Circuits

The equivalent circuit modeling of axial flux BLDC machines is a fundamental approach used to represent the electrical behavior of the motor in a simplified and analyzable form. This model converts the electromagnetic interactions within the machine into electrical components such as resistances, inductances, and controlled voltage sources.

Such modeling is essential for predicting machine performance under different operating conditions, including steady-state and dynamic regimes. It also serves as a foundation for control strategies, particularly in current control and speed regulation applications.

In a BLDC motor, each phase can be modeled using a voltage balance equation that accounts for three main components: the resistive voltage drops, the inductive voltage due to current variation, and the back electromotive force (Back-EMF). The Back-EMF is generated because of the rotor's rotation within the magnetic field; it depends directly on the angular velocity.

Additionally, the electromagnetic torque is directly related to the phase current, which makes current control a key aspect in regulating motor performance. These relationships form the basis of the equivalent circuit representation.

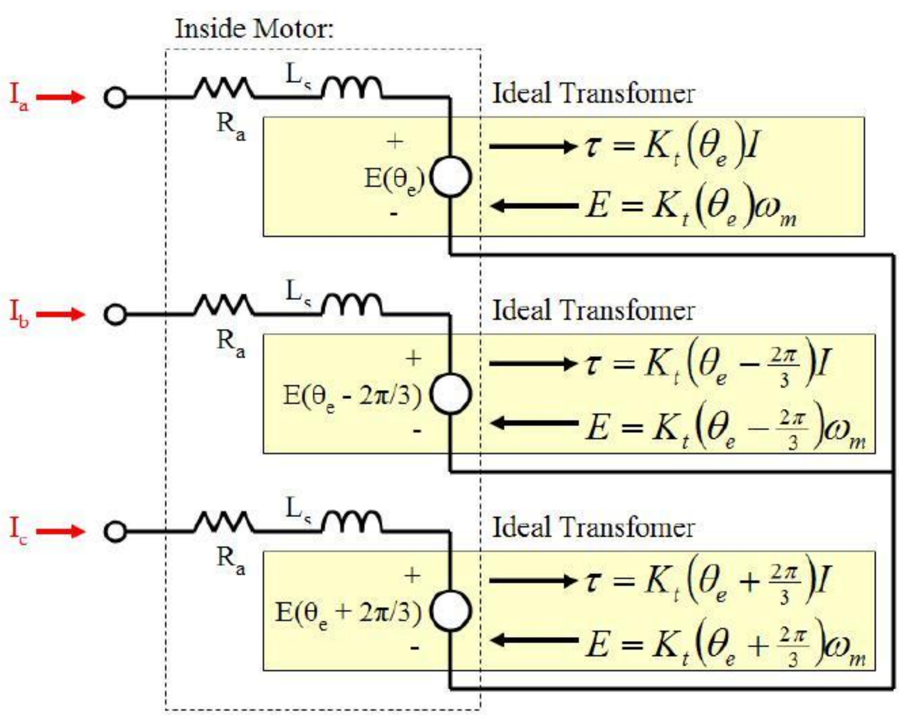

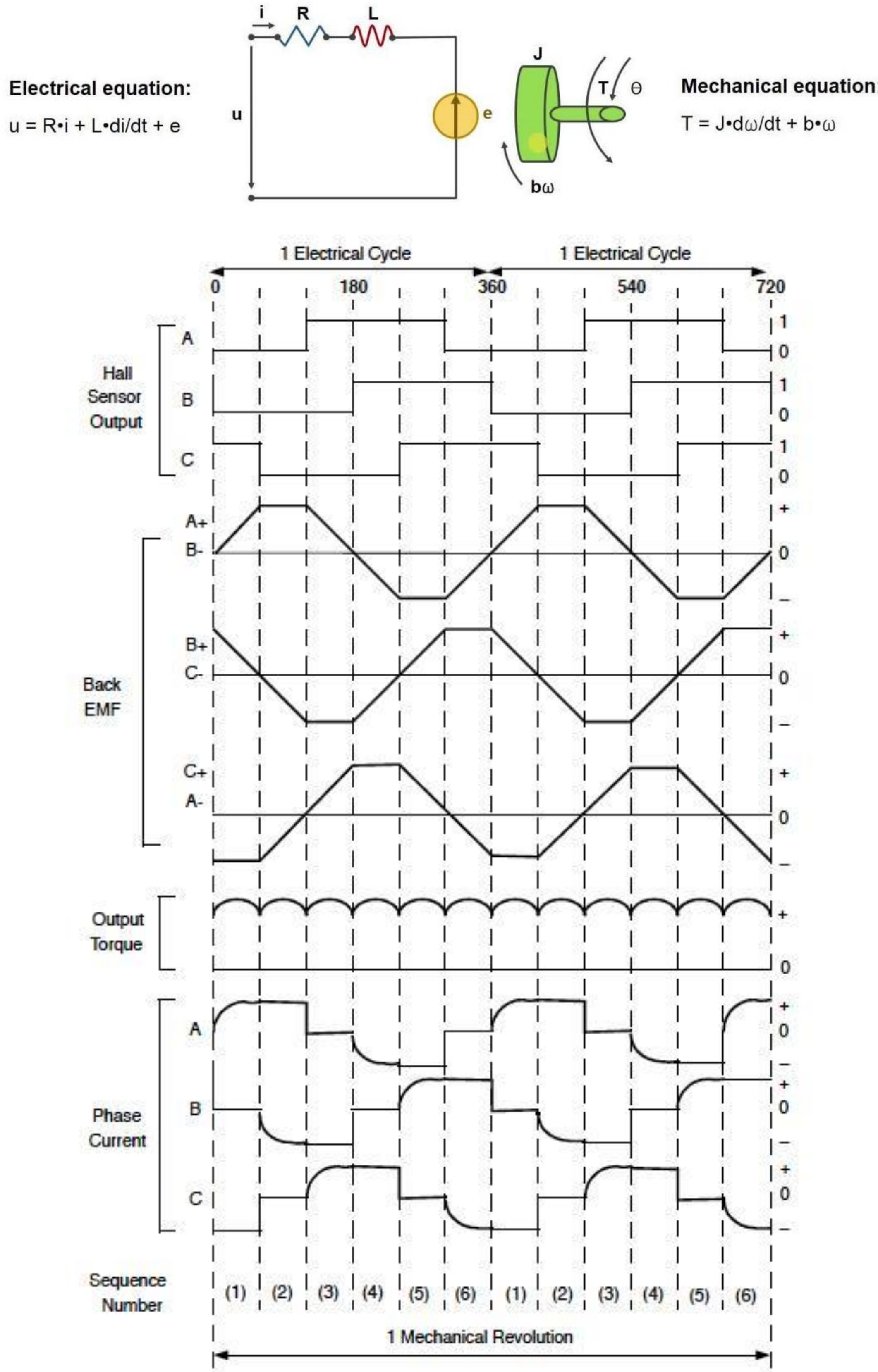

Figure 24: Lumped Parameter Modeling and Equivalent Circuits

The voltage equation shows that the applied voltage is distributed across three elements: the stator resistance, the stator inductance, and the back-EMF. The resistive term represents copper losses, while the inductive term reflects the dynamic behavior of the current.

The Back-EMF term plays a critical role in limiting the current as speed increases, making it a natural feedback mechanism in the motor. The proportionality between Back-EMF and angular speed highlights how electrical and mechanical domains are coupled.

Similarly, the torque equation demonstrates that electromagnetic torque is directly proportional to the current, which simplifies control design. In many practical systems, the torque constant and Back-EMF constant are numerically equal (in SI units), reinforcing the relationship between electrical and mechanical energy.

The equivalent circuit model provides a powerful yet simple representation of axial flux BLDC machine behavior. It captures the essential العلاقة between voltage, current, speed, and torque, making it highly useful for both analysis and control design.

Despite its simplicity, the model offers sufficient accuracy for many engineering applications. However, for more precise analysis, additional factors such as magnetic saturation, temperature effects, and non-ideal waveforms may need to be incorporated.

Overall, this model serves as a critical bridge between theoretical machine design and practical implementation, enabling efficient development of high-performance BLDC drive systems.

3.5 Winding Design and Slot/Pole Configuration Considerations

The winding design and slot/pole configuration are critical aspects in the performance optimization of axial flux BLDC machines. These elements directly influence key characteristics such as torque production, back-EMF waveform, efficiency, and cogging torque.

In axial flux machines, the compact geometry and disc-type structure impose unique constraints on winding layout and slot distribution. Therefore, careful selection of the number of slots and poles, as well as the winding type, is essential to achieve optimal electromagnetic performance and smooth operation.

The winding design determines how conductors are arranged within the stator slots and how they interact with the magnetic field produced by the rotor magnets. The induced EMF in each phase depends on the number of turns, flux linkage, and electrical frequency.

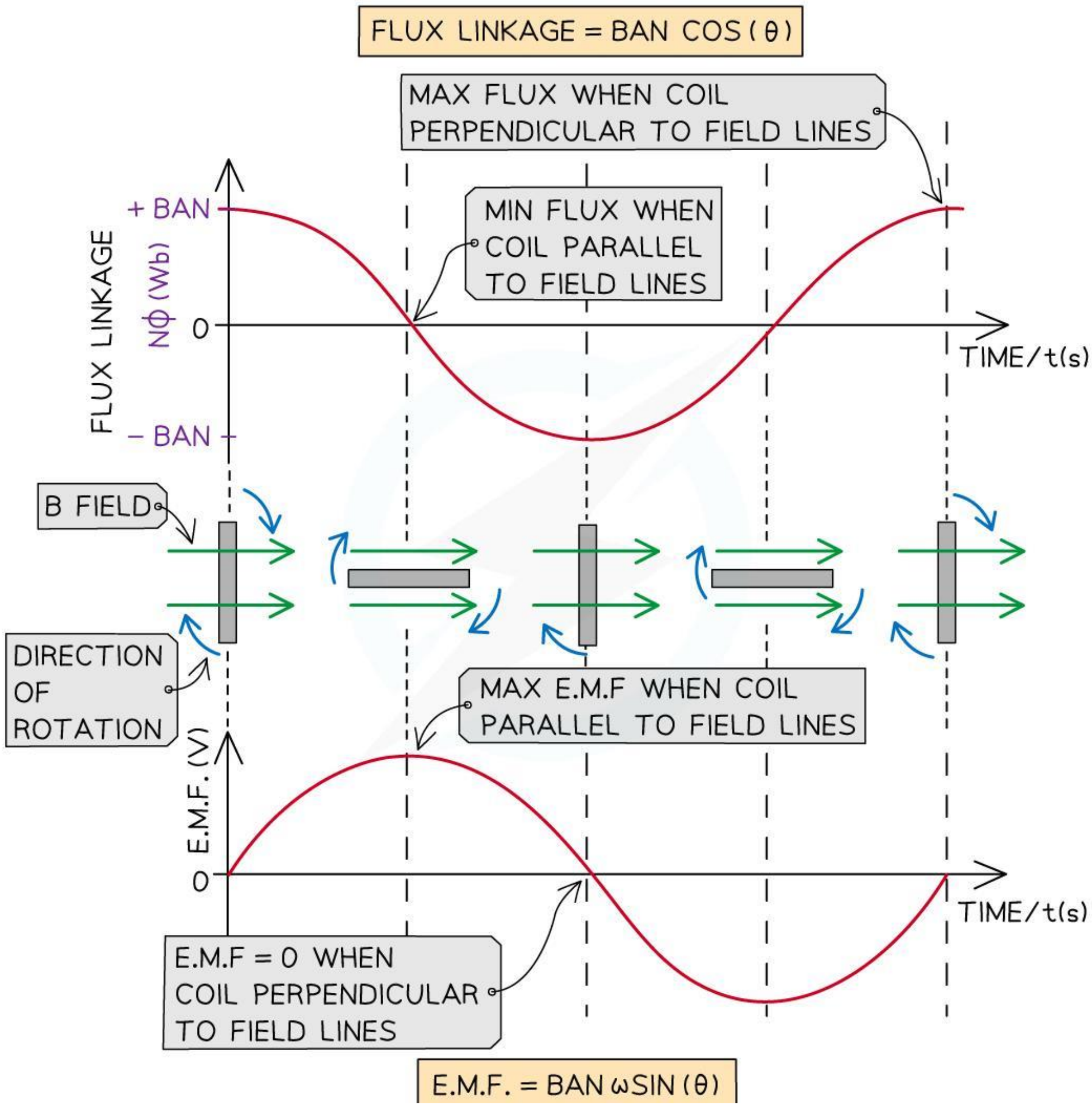

Figure 25: Winding Design and Slot/Pole Configuration Considerations

Slot/pole combinations define the spatial distribution of magnetic fields and directly affect harmonic content, torque ripple, and efficiency. Fractional-slot windings are often used in axial flux machines to reduce cogging torque and improve performance.

The electrical frequency is related to the mechanical speed and number of poles, forming a key relationship in machine operation. These equations summarize the fundamental relationships governing winding behavior.

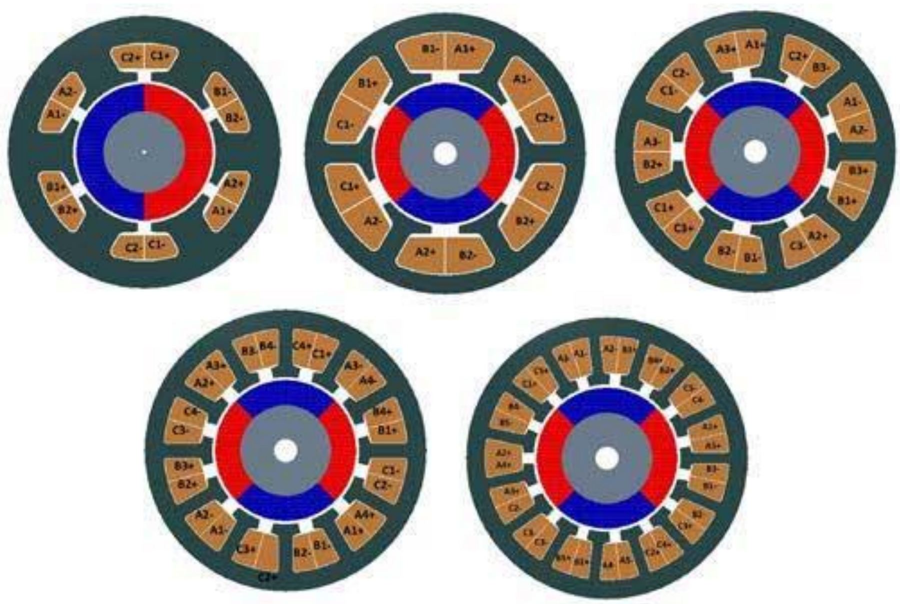

Figure 26: Winding Design and Slot/Pole Configuration Considerations

The induced EMF equation highlights the dependence of generated voltage on the number of turns, magnetic flux, and electrical frequency. Increasing the number of turns enhances voltage but may increase resistance and losses.

The relationship between electrical frequency and mechanical speed shows that higher pole numbers result in higher electrical frequency for the same speed. This affects switching requirements and core losses.

Slot/pole combinations significantly influence machine behavior. Proper selection can reduce torque ripple and improve efficiency. Fractional-slot configurations, in particular, help distribute the magnetic forces more evenly, resulting in smoother torque production.

Additionally, winding factor plays a crucial role in determining how effectively the winding utilizes the magnetic field. A higher winding factor leads to better performance and improved energy conversion.

Table 5: Slot/Pole Configuration Comparison

Configuration Type	Characteristics	Advantages	Disadvantages
Integer Slot Winding	Slots per pole per phase is an integer	Simple design, easy manufacturing	Higher cogging torque
Fractional Slot Winding	Non-integer slots per pole per phase	Reduced cogging torque, smoother output	More complex design
Concentrated Winding	Coils wound around single teeth	Compact, high torque density	Higher harmonic content
Distributed Winding	Coils spread over slots	Lower harmonics, smoother EMF	Larger size, more copper usage

The design of stator windings and the selection of slot/pole configurations are fundamental to achieving high-performance axial flux BLDC machines. These parameters directly affect electromagnetic characteristics, efficiency, and torque quality.

By carefully selecting appropriate configurations, designers can minimize undesirable effects such as torque ripple and cogging torque while maximizing efficiency and power density. Although more advanced configurations may introduce design complexity, they often result in significantly improved performance.

Ultimately, winding design represents a critical trade-off between manufacturability, performance, and cost, making it a key focus area in modern machine design.

This chapter established the analytical and theoretical foundation required for the design of axial flux BLDC machines. The electromagnetic principles, governing equations, and performance metrics presented here provide a coherent framework for understanding how machine geometry, magnetic fields, and electrical variables interact to produce torque and power.

Through the development of back-EMF and torque equations, along with sizing relations and equivalent circuit models, the chapter translated physical machine behavior into quantifiable design parameters. In addition, the discussion on winding design and slot/pole configurations highlighted the practical impact of design choices on efficiency, torque quality, and overall machine performance.

While this chapter focused on analytical modeling and theoretical formulation, the next step in the design process requires transitioning toward practical implementation. Therefore, Chapter 4 builds upon these results by addressing topology selection and defining the mechanical and electrical specifications of the proposed machine. This includes selecting the most suitable axial flux configuration, as well as considering real-world constraints such as packaging, cooling, structural integrity, and operational requirements, ensuring that the theoretical design can be effectively realized in practice.

Chapter Four

Chapter Four

Topology Selection and Specifications

Chapter 4: Topology Selection and Mechanical/Electrical Specifications

This chapter focuses on the practical implementation aspects of the proposed axial flux BLDC machine. Building upon the analytical foundations established in the previous chapter, it addresses the selection of an appropriate machine topology and defines the key mechanical and electrical specifications required for the design.

The chapter begins with a review of candidate axial flux machine configurations and justifies the selected topology based on performance and structural considerations. It then outlines the main mechanical constraints, including packaging limitations, thermal management, and rotor-shaft mechanics. Finally, the electrical requirements of the system are defined in terms of power, torque, speed range, and operating conditions, providing a complete specification framework for the machine design.

Subsections:

4.1 Review of Candidate AF BLDC Topologies and Selection Rationale
4.2 Mechanical Constraints
4.3 Electrical Requirements

4.1 Review of Candidate AF BLDC Topologies

The selection of an appropriate topology is a critical step in the design of axial flux BLDC machines, as it directly affects electromagnetic performance, mechanical complexity, thermal behavior, and overall efficiency. Several axial flux configurations have been developed, each with distinct structural characteristics and performance advantages.

Based on the discussion presented in Chapter 2, axial flux machines offer superior torque density and better efficiency at low speeds compared to radial flux machines. Furthermore, different axial flux topologies vary in terms of rotor–stator arrangement, magnetic flux paths, and mechanical construction, making the selection process an essential design decision.

Overview of Candidate Topologies

Axial flux BLDC machines can be broadly classified based on the number and arrangement of stators and rotors. The most common configurations include:

1. Single Stator – Single Rotor (SSSR)
2. Double Stator – Single Rotor (DSSR)
3. Single Stator – Double Rotor (SSDR)
4. Yokeless and Segmented Armature (YASA) topology
5. Axial Flux Internal Rotor (AFIR) configuration

Each topology presents trade-offs between torque capability, manufacturing complexity, cooling efficiency, and structural robustness.

The YASA topology is known for its high torque density and elimination of stator yoke, which reduces iron losses and weight. However, it introduces higher manufacturing complexity and requires precise assembly.

The double stator–single rotor configuration improves torque production by utilizing both sides of the rotor, resulting in better magnetic flux utilization. Nevertheless, it increases structural complexity and may introduce challenges in cooling and alignment.

The single stator–single rotor topology is the simplest configuration, offering ease of manufacturing, lower cost, and straightforward mechanical integration. Although it may produce lower torque compared to multi-stator configurations, it is highly suitable for experimental setups and compact designs.

The AFIR configuration provides good mechanical support and protection for internal components but may suffer from reduced cooling effectiveness compared to open-structure designs.

Table 6: Comparative Analysis of Topologies

Topology	Torque Density	Mechanical Complexity	Cooling Capability	Cost	Suitability
SSSR	Moderate	Low	Good	Low	Prototyping, simple designs
DSSR	High	Medium–High	Moderate	Medium	High torque applications
SSDR	High	Medium	Good	Medium	Balanced performance
YASA	Very High	High	Good	High	Advanced, high-performance
AFIR	Moderate	Medium	Limited	Medium	Enclosed/protected designs

Based on the design objectives of this project, the single stator–single rotor (SSSR) configuration was selected. This decision is justified by the following considerations:

- Simplicity in mechanical construction and assembly
- Lower manufacturing cost and ease of prototyping
- Sufficient performance for the targeted power and torque levels
- Better suitability for experimental validation and testing

Additionally, the selected topology allows straightforward integration with measurement systems, such as sensors and controllers, which are required for evaluating torque and efficiency.

The topology selection process represents a balance between performance and practicality. While advanced configurations such as YASA and multi-stator designs offer higher torque density, the single stator–single rotor topology provides an optimal compromise for this project in terms of simplicity, cost, and implementation feasibility.

This selected configuration forms the basis for the subsequent mechanical and electrical design considerations presented in the following sections.

4.2 Mechanical Constraints

The mechanical design of axial flux machines plays a crucial role in ensuring structural integrity, thermal stability, and reliable operation. Due to their disc-shaped geometry and compact axial length, axial flux machines impose unique mechanical constraints that must be carefully considered during the design process.

This section outlines the main mechanical challenges associated with the proposed machine, including packaging limitations, thermal management, and rotor–shaft mechanical structure. Practical design considerations and constraints are highlighted to ensure a feasible and efficient implementation.

Packaging Constraints

Axial flux machines are characterized by a compact disc geometry, where the rotor and stator are arranged in parallel planes with a small axial separation. This configuration results in limited space for winding placement, structural supports, cooling mechanisms, and electrical connections.

In this project, the machine is designed with a disc diameter of approximately 30 cm, with a base thickness of 2 mm. Neodymium permanent magnets with a thickness of 2 mm are mounted on the rotor disc, while the stator disc accommodates the winding coils.

The air gap between the rotor and stator is a critical parameter that significantly affects machine performance. A small air gap improves magnetic coupling and torque production but increases sensitivity to mechanical misalignment. In this design, the air gap is selected within the range of 0.5 mm to 1.0 mm, providing a balance between performance and mechanical feasibility.

Cooling and Thermal Considerations

Thermal management is essential in axial flux machines due to concentrated losses within a compact structure. The primary sources of heat include copper losses, core losses, and eddy current losses in permanent magnets.

In this project, a forced-air cooling method is adopted, where airflow is directed across the exposed stator surfaces to enhance heat dissipation. The copper losses in the winding are expressed as: $\mathbf{P_{copper} = 3\, I^2_{rms}\, R}$

Additionally, core losses consist of hysteresis and eddy current losses, while eddy currents within permanent magnets contribute to localized heating. Proper thermal design is necessary to prevent overheating and ensure reliable operation.

Shaft and Rotor Mechanics

The mechanical structure of the system consists of two main parts: an axial flux motor and an axial flux generator. These components are mechanically coupled using a stainless-steel shaft and a jaw shaft coupler.

The shaft connects the rotor of the motor to the rotor of the generator, allowing torque transmission between the two systems. This configuration enables experimental evaluation of machine performance, including torque and efficiency measurements. Mechanical alignment, rigidity, and vibration control are important considerations to ensure stable operation and minimize mechanical losses.

Bearings and Structural Considerations

Bearings play a vital role in supporting the rotating components and maintaining precise alignment between the rotor and stator. Due to the small air gap in axial flux machines, even minor misalignments can significantly degrade performance.

Proper bearing selection is essential to handle axial and radial loads while minimizing friction and wear. Additionally, the overall structural design must ensure sufficient stiffness to prevent deformation under operating conditions.

Mechanical constraints in axial flux machine design require careful consideration of packaging limitations, thermal management, and structural integrity. The compact geometry introduces challenges in space utilization, cooling, and alignment, which must be addressed through appropriate design choices.

By integrating suitable cooling methods, maintaining precise air gap control, and ensuring robust mechanical coupling, the proposed design achieves a balance between performance and practical feasibility. These mechanical considerations form a foundation for the electrical specifications discussed in the next section.

4.3 Electrical Requirements

Defining the electrical requirements of the axial flux BLDC machine is essential to establish the operational framework and performance targets of the system. These requirements determine the constraints for electromagnetic design, winding configuration, power electronics, and control strategy.

This section outlines the key electrical specifications of the proposed machine, including power rating, torque capability, speed range, and voltage/current limits, ensuring that the design meets the intended application and operational conditions.

Power Rating

The machine is designed to operate at a rated power of 500 W, which defines the continuous power level that the motor can deliver under normal operating conditions. This rating is selected based on the intended application and serves as a primary constraint for sizing and thermal design.

Torque Requirements

Torque is a fundamental performance parameter, particularly for axial flux machines known for their high torque density. The required torque is derived from the power and speed relationship, ensuring that the machine can deliver sufficient mechanical output across its operating range.

The system is designed to provide stable torque output suitable for experimental evaluation and performance testing.

Speed Range

The operating speed range is selected to align with the advantages of axial flux machines, particularly their efficiency at relatively low to moderate speeds. The chosen speed range ensures compatibility with the mechanical setup and allows accurate measurement of torque and efficiency.

The relationship between speed and torque is considered during design to maintain consistent performance across operating conditions.

Voltage and Current Specifications

The machine is powered باستخدام a three-phase PWM-driven BLDC driver, providing flexible control over speed and torque.

The electrical specifications are defined as follows:

- Voltage range: 6 V to 60 V
- Rated current: 20 A

These values are selected to ensure safe operation, compatibility with available power electronics, and sufficient current capacity to meet torque demands.

Control Strategy Considerations

A three-phase PWM control scheme is employed to drive the motor, enabling efficient regulation of speed and torque. This approach allows precise control of the machine under varying load conditions and supports experimental analysis using microcontrollers and sensors.

The defined electrical requirements provide a clear operational framework for the axial flux BLDC machine. By specifying power, torque, speed, and electrical limits, this section ensures that the machine design aligns with both performance objectives and practical implementation constraints.

These specifications, combined with the mechanical considerations discussed earlier, establish a complete design foundation for the development and testing of the proposed system.

This chapter addressed the practical aspects of axial flux BLDC machine design by selecting an appropriate topology and defining the key mechanical and electrical specifications. The single stator–single rotor configuration was chosen based on its simplicity, cost-effectiveness, and suitability for experimental validation. In addition, the main mechanical constraints, including packaging, cooling, and structural considerations, were identified, along with the electrical requirements necessary to achieve the desired performance. These elements collectively establish a realistic and implementable design framework.

Building on this foundation, Chapter 5 transitions from system-level specifications to detailed design and implementation. It focuses on applying analytical equations and design parameters to determine the physical dimensions, winding configuration, and electromagnetic characteristics of the machine. This includes detailed calculations and design procedures that translate the theoretical and specification-based framework into a fully defined and realizable axial flux BLDC machine.

Chapter Five

Chapter Five

Detailed Electromagnetic Design and Optimization

After selecting the axial flux BLDC topology and defining the mechanical and electrical specifications in the previous chapters, this chapter focuses on the detailed electromagnetic design and optimization of the proposed machine. The objective of this chapter is to translate high-level design targets, such as torque density, efficiency, and compactness into quantitative electromagnetic dimensions and parameters that can be later validated using finite element analysis.

The electromagnetic design stage plays a critical role in axial flux machines due to the strong coupling between magnetic loading, electric loading, air-gap geometry, and thermal limitations.

Unlike radial flux machines, axial flux BLDC motors exhibit non-uniform air-gap flux distribution and higher sensitivity to magnet geometry and segmentation, which necessitates a careful and iterative design approach.

Subsections:

5.1: Design Variables and Optimization Objectives
5.2: Electromagnetic Design Equations and Iterative Sizing Procedure
5.3: Winding Choices: Concentrated vs Distributed Windings
5.4: Magnet Design and Permanent Magnet Segmentation Strategies
5.5: Loss Estimation Methods Used in Preliminary Design

Chapter 5: Detailed Electromagnetic Design and Optimization

The detailed electromagnetic design of axial flux BLDC machines requires a systematic approach that balances performance, efficiency, and physical constraints. At this stage of the design process, the interaction between electromagnetic parameters and machine geometry becomes increasingly significant, as small variations in dimensions or material selection can lead to noticeable changes in overall performance. In axial flux machines, electromagnetic behavior is strongly influenced by the distribution of magnetic flux across the air-gap and the effective utilization of the active machine area. As a result, design decisions related to winding configuration, pole–slot combination, and magnet geometry must be carefully evaluated to achieve the desired torque production while minimizing losses and unwanted torque pulsations.

This chapter adopts an iterative design methodology in which key electromagnetic parameters are progressively refined based on analytical relations and engineering constraints. The purpose of this approach is not only to satisfy the design specifications but also to ensure that the resulting machine configuration is practical, manufacturable, and suitable for subsequent numerical validation. By establishing a well-defined electromagnetic design framework, this chapter forms a critical link between the conceptual design stage and the numerical simulation phase, providing a solid foundation for accurate finite element modelling and performance evaluation in the following chapter.

Furthermore, the electromagnetic design process must consider practical implementation constraints such as material availability, manufacturing tolerances, and thermal limits. These factors directly influence the reliability and repeatability of the designed machine and play a significant role in determining whether the theoretical design can be successfully translated into a functional prototype. Addressing these considerations at an early stage reduces the need for extensive design modifications in later phases and contributes to a more efficient overall development process.

5.1: Design variables and optimization objectives

The electromagnetic performance of an axial flux BLDC motor is highly dependent on a set of interrelated design variables that govern magnetic loading, electric loading, and geometric constraints. Unlike conventional radial flux machines, axial flux topologies exhibit stronger coupling between design parameters, which requires a structured identification of variables before proceeding with analytical sizing and numerical validation.

In this section, the primary electromagnetic design variables are identified and categorized according to their functional role in torque production, loss behavior, and manufacturability. In parallel, the optimization objectives of the proposed machine are defined to guide the iterative design process adopted in this chapter.

5.1.1: Identification of Key Electromagnetic Design Variables

The electromagnetic design variables of the axial flux BLDC motor can be broadly classified into geometric, magnetic, and electrical parameters. Each category influences the machine performance in a different manner, while collectively determining the feasibility and effectiveness of the final design.

Before analyzing these variables individually, it is important to summarize them in a structured form to clarify their role within the design and optimization process.

Table 7: Identification of Key Electromagnetic Design Variables

Category	Design Variable	Symbol	Description
Geometric	Outer rotor radius	R_o	Determines active area and torque capability
Geometric	Inner rotor radius	R_i	Affects material utilization and flux path length
Geometric	Air-gap length	g	Influences magnetic coupling and flux density

Category	Design Variable	Symbol	Description
Magnetic	Number of poles	2_P	Determines electrical frequency and torque density
Magnetic	Magnet thickness	t_m	Controls air-gap flux magnitude
Magnetic	Magnet arc ratio	α_m	Affects flux waveform and harmonic content
Electrical	Number of turns per phase	N	Determines back-EMF and torque constant
Electrical	Phase current	I	Directly related to torque production
Electrical	Current density	J	Influences copper losses and thermal behavior

Table 5.1: Key Electromagnetic Design Variables of the Axial Flux BLDC Motor provides a comprehensive overview of the main electromagnetic design variables considered in this project. Geometric parameters primarily affect the effective active area and flux paths, while magnetic variables govern flux distribution and torque generation. Electrical variables directly influence torque magnitude, losses, and thermal performance. Identifying these parameters at an early stage enables a systematic and traceable optimization process in subsequent sections.

5.1.2: Influence of Design Variables on Machine Performance

Each design variable listed in Table 5.1 contributes to machine performance in a nonlinear and interdependent manner. For instance, increasing the outer rotor radius enhances torque capability by enlarging the effective torque arm, but simultaneously increases material usage and mechanical stress. Similarly, reducing the air-gap length improves magnetic coupling but introduces tighter manufacturing tolerances and potential mechanical reliability issues.

To illustrate these interdependencies conceptually, a high-level design interaction diagram is introduced. A conceptual diagram below showing how geometric, magnetic, and electrical variables influence torque density, efficiency, losses, and manufacturability.

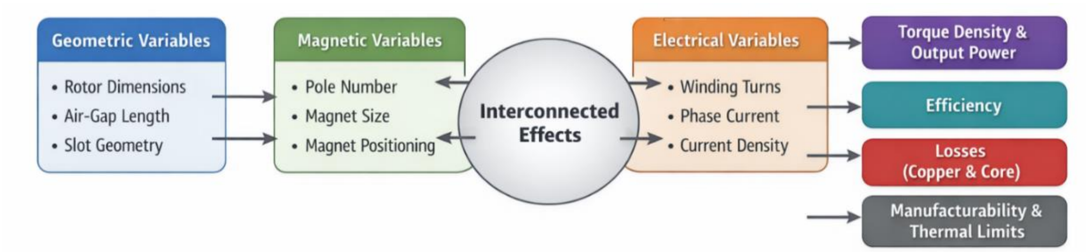

Figure 27: Relationship Between Electromagnetic Design Variables and Performance Metrics

Figure 5.1: Relationship Between Electromagnetic Design Variables and Performance Metrics, highlights the interconnected nature of electromagnetic design variables and performance metrics. Changes in a single parameter often propagate through multiple performance aspects, reinforcing the need for an optimization-oriented design approach rather than isolated parameter tuning.

5.1.3: Optimization Objectives

Based on the identified design variables, the optimization objectives of the proposed axial flux BLDC motor are defined to guide the iterative design and evaluation process. These objectives reflect both performance targets and practical constraints relevant to real-world implementation. The optimization goals are summarized in the following table 5.2: Electromagnetic Optimization Objectives.

Table 8: Electromagnetic Optimization Objectives.

Category	Optimization Goal	Rationale
Performance	Maximize average electromagnetic torque	Improve power density and load capability
Performance	Minimize torque ripple	Ensure smooth operation and reduced vibration
Efficiency	Minimize copper and core losses	Improve overall system efficiency
Thermal	Limit current density	Maintain acceptable temperature rise

Category	Optimization Goal	Rationale
Practical	Ensure manufacturable dimensions	Enable reliable prototype fabrication

Table 5.2 defines the criteria used to evaluate and refine the electromagnetic design. Rather than optimizing a single parameter, the design process seeks a balanced solution that satisfies multiple, sometimes conflicting, objectives. This multi-objective perspective is essential for achieving a practical and high-performance axial flux BLDC motor.

5.1.4: Role of Design Variables in the Iterative Optimization Process

The identified design variables and optimization objectives form the foundation of the iterative sizing and refinement procedure employed throughout this chapter. Initial parameter values are selected based on analytical relations and engineering judgment, after which their impact on performance is evaluated and adjusted accordingly.

This iterative approach ensures that design decisions are informed by both theoretical considerations and practical constraints, ultimately leading to a machine configuration that is suitable for detailed finite element validation in Chapter 6.

In summary, the identification of key electromagnetic design variables and the definition of optimization objectives provide a structured foundation for the detailed design of the proposed axial flux BLDC motor. By clearly linking geometric, magnetic, and electrical parameters to performance metrics such as torque, efficiency, and losses, this section establishes a coherent framework for informed design decision-making.

The defined variables and objectives guide the iterative refinement process and ensure that performance targets are addressed alongside practical implementation constraints. Based on this foundation, the following section develops the analytical design equations and iterative sizing procedure used to quantify these relationships and progress toward a feasible and optimized machine design.

5.2: Design equations and iterative sizing procedure

Following the identification of key design variables and optimization objectives in Section 5.1, this section presents the analytical electromagnetic design equations and the iterative sizing procedure adopted for the proposed axial flux BLDC motor. The purpose of this section is to establish quantitative relationships between the selected design variables and the resulting electromagnetic performance, forming the analytical basis for preliminary machine sizing.

Analytical modelling at this stage enables rapid evaluation of design trends and provides physical insight into the influence of key parameters on torque production, flux distribution, and electrical characteristics. Although these models involve simplifying assumptions, they play a crucial role in narrowing the design space before detailed finite element analysis is performed.

5.2.1: Fundamental Electromagnetic Torque Equation

The electromagnetic torque of an axial flux BLDC motor can be expressed in terms of air-gap flux and stator current. For a surface-mounted permanent magnet axial flux machine, the average electromagnetic torque can be approximated as:

$$ {}_{t}k \cdot {}_{ph}I \cdot {}_{g}\Phi \cdot \frac{p}{2} = {}_{avg}T $$

Where:

- ✓ *P*: is the number of pole pairs
- ✓ *Qg*: is the average air-gap flux per pole
- ✓ *Iph*: is the phase current
- ✓ *Kt*: is the torque constant determined by winding configuration and machine geometry.

This expression highlights the direct dependence of torque on both magnetic loading and electric loading, reinforcing the need for coordinated optimization of magnet dimensions, winding turns, and current density.

5.2.2: Air-Gap Flux and Magnetic Loading Estimation

Accurate estimation of air-gap flux is essential for reliable torque prediction. The average air-gap flux density can be approximated using magnet properties and effective air-gap length, accounting for leakage and fringing effects.

Before proceeding with numerical validation, the key magnetic quantities used in the analytical model are summarized in the following table; 5.3: Magnetic Quantities Used in Analytical Electromagnetic Design.

Table 9: magnetic parameters used to estimate air-gap flux and magnetic loading

Parameter	Symbol	Description
Residual flux density	*Br*	Magnet material property
Effective air-gap flux density	*Bg*	Average flux density in the air-gap
Air-gap area	*Ag*	Effective magnetic area
Air-gap flux	*Qg*	Flux linking stator windings

Table 5.3 summarizes the magnetic parameters used to estimate air-gap flux and magnetic loading. These quantities form the basis for calculating electromagnetic torque and induced voltage. By defining them explicitly, the analytical design remains transparent and traceable throughout the sizing process.

5.2.3: Back-EMF and Electrical Sizing Relations

The back-electromotive force (back-EMF) is a key electrical characteristic that determines voltage requirements and compatibility with the selected inverter. The phase back-EMF can be approximated as:

$$\omega \cdot {}_{e}k = {}_{ph}E$$

Where:
Ke: is the back-EMF constant
W: is the mechanical angular speed

The back-EMF constant is directly related to the number of windings turns and air-gap flux, establishing a direct link between electromagnetic design and electrical constraints such as supply voltage and speed range.

5.2.4: Iterative Sizing Procedure

Due to the strong coupling between electromagnetic variables, a single-pass analytical calculation is generally insufficient to satisfy all design objectives simultaneously. Instead, an iterative sizing procedure is adopted, in which key parameters are progressively adjusted until convergence is achieved.

Before detailing the procedure, a high-level representation of the iterative design flow is introduced in figure 5.2: Iterative Electromagnetic Sizing Procedure for the Axial Flux BLDC Motor which illustrates the closed-loop nature of the electromagnetic sizing process.

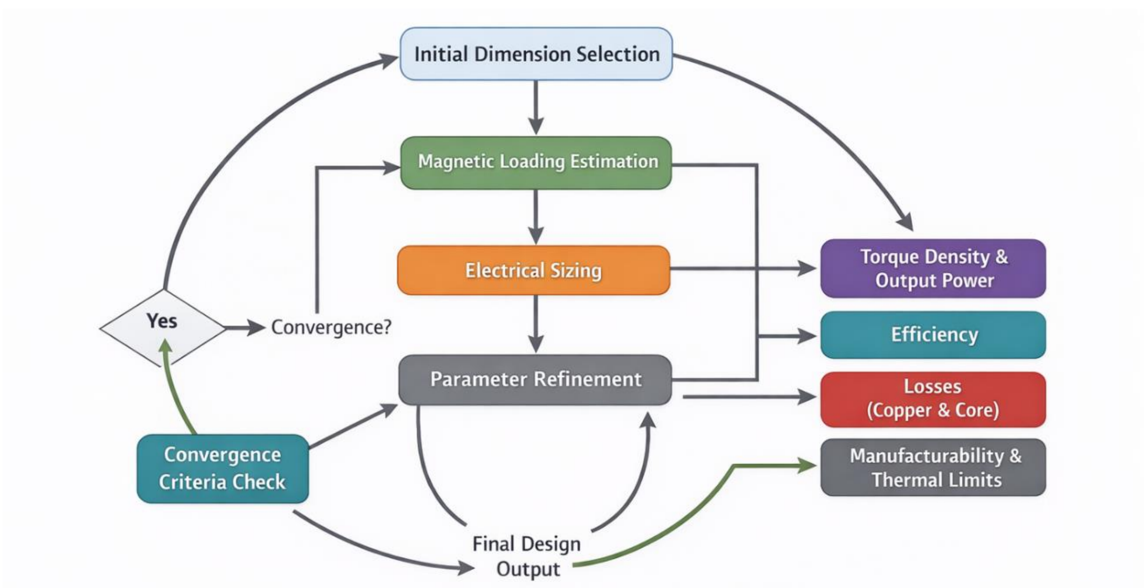

Figure 28: Iterative Electromagnetic Sizing Procedure for the Axial Flux BLDC Motor

A flowchart illustrating the iterative process starting from initial dimension selection, followed by magnetic loading estimation, electrical sizing, loss evaluation, and parameter refinement. Each iteration refines geometric, magnetic, and electrical parameters based on performance evaluation and constraint checks, ensuring convergence toward an optimized and feasible design solution.

To demonstrate the outcome of the iterative sizing approach, Table 5.5 compares the initial parameter estimates with the refined values adopted for the final analytical design. The refined set represents a balanced solution that supports torque capability, efficiency, and manufacturability, and it is used consistently as the baseline for subsequent modelling and validation.

Table 5.5: Comparison Between Initial and Refined Electromagnetic Design Parameters, demonstrates how the electromagnetic design evolved through an iterative process, showing the transition from preliminary analytical estimates to refined values suitable for numerical simulation and experimental validation.

Table 10: Initial and Refined Electromagnetic Design Parameters

Parameter	**Symbol**	**Initial Value**	**Refined Value**	**Design Impact**
Outer rotor radius	*Ro*	75 mm	80 mm	Torque capability and active area
Inner rotor radius	*Ri*	30 mm	35 mm	Material utilization
Air-gap length	*g*	1.2 mm	1.0 mm	Magnetic coupling
Number of poles	*2p*	14 poles	16 poles	Torque density and frequency
Magnet thickness	t_m	3.0 mm	4.0 mm	Air-gap flux level
Magnet arc ratio	α_m	0.65	0.70	Improves flux waveform
Turns per phase	*N*	16 turns	18 turns	Back-EMF and torque constant
Phase current	*Iph*	14 A	12 A	Torque and losses
Current density	*J*	6.0 A/mm²	5.0 A/mm²	Thermal feasibility

Table 5.5 shows that the refinement process does not rely on increasing current to achieve performance; instead, improvements are obtained through coordinated adjustments in geometry and magnetic loading. Increasing the effective radius and magnet thickness, reducing the air-gap, and slightly increasing the number of turns collectively enhance air-gap flux linkage and torque constant. At the same time, the refined design reduces current density and rated phase current to improve thermal behavior and limit copper losses, resulting in a more feasible and reproducible design suitable for finite element validation and later experimental testing.

5.2.5: Design Iteration Criteria and Convergence

To ensure systematic convergence, the iterative sizing process is guided by predefined criteria, including torque target satisfaction, voltage compatibility, current density limits, and preliminary loss constraints. Parameter adjustments are performed incrementally to avoid excessive deviation from feasible design regions.

This structured approach allows efficient exploration of the design space while maintaining consistency with the optimization objectives defined in Section 5.1.

In this section, analytical electromagnetic design equations have been introduced to establish quantitative relationships between design variables and machine performance. The iterative sizing procedure provides a practical framework for refining geometric, magnetic, and electrical parameters while accounting for performance objectives and implementation constraints.

The resulting analytically sized design serves as a validated starting point for detailed finite element modelling and simulation, which are presented in the following chapter.

5.3: Winding choices

The selection of an appropriate winding configuration is a critical aspect of the electromagnetic design of axial flux BLDC machines. Winding topology directly affects torque production, back-electromotive force waveform, loss distribution, thermal behavior, and manufacturability. Unlike radial flux machines, axial flux topologies offer greater flexibility in winding arrangement, which necessitates careful evaluation of available options.

This section discusses the winding choices adopted for the proposed axial flux BLDC motor, focusing on the comparison between concentrated and distributed windings, as well as the selection of coil pitch and phase connection. The objective is to justify the chosen winding configuration in relation to the performance and optimization objectives defined earlier in this chapter.

5.3.1: Concentrated and Distributed Windings in Axial Flux Machines

In axial flux BLDC motors, windings can be implemented in either concentrated or distributed forms. Concentrated windings are typically wound around individual stator teeth, whereas distributed windings are spread over multiple slots per pole per phase. Each configuration exhibits distinct electromagnetic and practical characteristics. Before discussing the implications of each winding type, a comparative overview is presented.

Table 11: Concentrated and Distributed Windings

Aspect	Concentrated Windings	Distributed Windings
End-winding length	Short	Long
Copper losses	Lower	Higher
Torque ripple	Higher	Lower
Harmonic content	Higher	Lower
Manufacturing complexity	Low	High
Suitability for axial flux	High	Moderate

Table 5.4: Comparison Between Concentrated and Distributed Windings highlights the fundamental trade-offs between concentrated and distributed windings. Concentrated windings offer reduced end-winding length and lower copper losses, which are particularly advantageous for compact axial flux machines. However, they tend to introduce higher space harmonics and torque ripple. Distributed

windings provide smoother electromagnetic behavior but at the expense of increased copper losses and manufacturing complexity. Considering the compactness and manufacturability requirements of the proposed design, a concentrated winding configuration is selected.

5.3.2: Electromagnetic Implications of Winding Selection

The choice of winding configuration has a direct impact on the shape of the air-gap flux linkage and the resulting back-EMF waveform. Concentrated windings generally produce more trapezoidal back-EMF waveforms, which are well suited for BLDC operation with classical commutation strategies. In contrast, distributed windings tend to produce more sinusoidal waveforms, making them preferable for field-oriented control.

To illustrate the difference in flux linkage and back-EMF characteristics, a schematic representation is introduced in figure 5.3: Conceptual Comparison of Flux Linkage and Back-EMF for Concentrated and Distributed Windings.

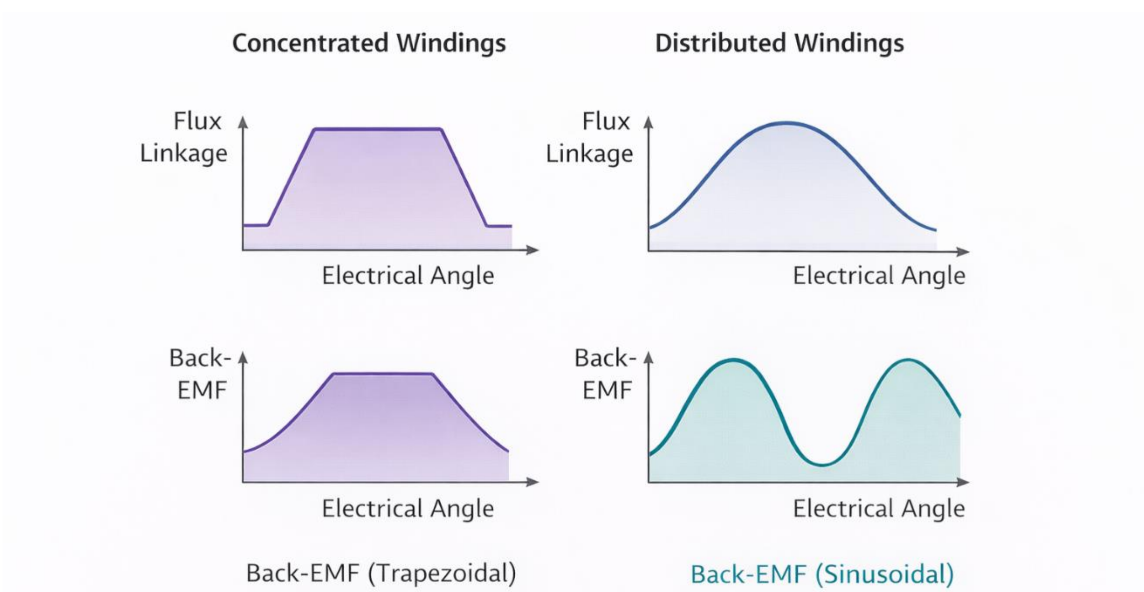

Figure 29: Conceptual Comparison of Flux Linkage and Back-EMF

A comparative diagram showing trapezoidal back-EMF for concentrated windings and sinusoidal back-EMF for distributed windings. The following figure 5.3 illustrates how winding configuration influences electromagnetic waveforms and control compatibility. The trapezoidal nature of the back-EMF generated by concentrated windings aligns with the selected BLDC control strategy discussed in Chapter 8, reinforcing the coherence between electromagnetic design and control implementation.

5.3.3: Coil Pitch Selection

Coil pitch, defined as the angular span of a coil relative to the pole pitch, plays an important role in determining harmonic content and torque ripple. Full-pitch coils maximize fundamental EMF but may increase harmonic components, whereas short-pitch coils can reduce specific harmonics at the expense of reduced EMF magnitude.

In the proposed design, coil pitch is selected to balance fundamental torque production and harmonic suppression. The selection is guided by analytical evaluation and compatibility with the chosen pole–slot combination.

5.3.4: Phase Connection and Winding Configuration

The phase connection of the stator windings, typically configured in either star (Y) or delta (Δ) connection, affects voltage levels, current ratings, and inverter requirements. A star connection offers higher phase voltage and lower current for a given power level, making it suitable for applications with voltage-limited inverters.

Based on the electrical constraints and desired operating range of the proposed axial flux BLDC motor, a star-connected winding configuration is adopted. This choice ensures compatibility with the inverter voltage rating while maintaining acceptable current density and thermal performance.

5.4: Magnet design and PM segmentation strategies

The last section has examined the winding choices available for axial flux BLDC machines, focusing on the comparison between concentrated and distributed windings, coil pitch selection, and phase connection. The analysis demonstrates that concentrated windings, combined with an appropriate coil pitch and star phase connection, provide a practical balance between electromagnetic performance, and control compatibility. These winding decisions directly influence magnet utilization and flux distribution, forming a natural transition to the magnet design and permanent magnet segmentation strategies discussed in this section.

Permanent magnets represent one of the most influential elements in the electromagnetic design of axial flux BLDC machines. Magnet material properties, geometry, and placement directly determine the air-gap flux distribution, torque capability, back-EMF characteristics, and loss behavior. In axial flux topologies, magnet design becomes even more critical due to the planar flux paths and the large effective air-gap area.

This section addresses the design of permanent magnets used in the proposed machine, with particular emphasis on magnet geometry, material selection, and segmentation strategies. The objective is to achieve sufficient magnetic loading for torque production while minimizing losses and ensuring thermal and mechanical feasibility.

5.4.1: Permanent Magnet Material Selection

The selection of permanent magnet material has a significant impact on electromagnetic performance and thermal stability. High-energy-density rare-earth magnets, such as Neodymium-Iron-Boron (NdFeB), are commonly employed in axial flux machines due to their high residual flux density and coercivity.

In this project, NdFeB magnets are selected to provide adequate air-gap flux density while maintaining compact machine dimensions. The choice is guided by the need to balance magnetic performance with cost, and availability.

5.4.2: Magnet Geometry and Placement

Magnet geometry, including thickness, arc length, and radial span, strongly influences the resulting air-gap flux waveform. Increasing magnet thickness enhances magnetic flux but may lead to diminishing returns due to saturation and increased cost. Similarly, magnet arc ratio affects harmonic content and torque ripple. Before analyzing the effects of segmentation, the main magnet geometric parameters adopted in the design are summarized in the following table.

Table 12: Permanent Magnet Geometric Parameters

Parameter	Adopted Value	Design Impact
Magnet material	NdFeB	High magnetic energy density
Magnet thickness	4.0 mm	Controls air-gap flux magnitude
Magnet arc ratio	0.70	Influences flux waveform
Magnet radial span	Ri to Ro	Defines active magnetic area
Magnetization direction	Axial	Suitable for axial flux topology

Table 5.6: Permanent Magnet Geometric Parameters summarizes the permanent magnet parameters used in the analytical design. These values are selected to provide sufficient air-gap flux while avoiding excessive magnet volume and unnecessary material cost. The chosen arc ratio and thickness also support compatibility with the concentrated winding configuration.

5.4.3: Permanent Magnet Segmentation Strategy

At higher operating speeds and under time-varying magnetic fields, permanent magnets are subject to eddy current losses, which can lead to localized heating and reduced efficiency. In axial flux machines, these losses can be significant due to the large magnet surface area exposed to harmonic fields.

To mitigate eddy current losses, magnet segmentation is employed. By dividing each magnet pole into multiple electrically isolated segments, circulating current paths within the magnet material are interrupted, significantly reducing eddy current magnitude.

Before discussing the loss reduction mechanism, a conceptual illustration of magnet segmentation is introduced in the figure 5.4: Conceptual Illustration of Permanent Magnet Segmentation in an Axial Flux Rotor. A rotor disk showing surface-mounted permanent magnets, comparing a single-piece magnet with a segmented magnet configuration.

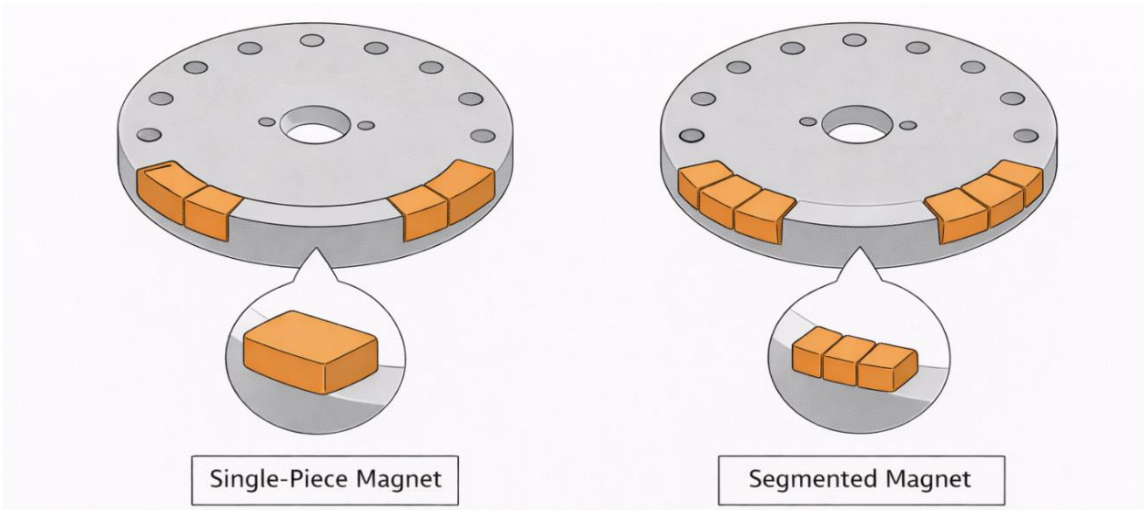

Figure 30: Conceptual Illustration of Permanent Magnet Segmentation in an Axial Flux Rotor

Figure 5.4 conceptually demonstrates how magnet segmentation reduces the effective loop area available for eddy current circulation. This strategy enhances thermal performance and supports stable operation at higher speeds without significantly compromising torque production.

5.4.4: Electromagnetic and Thermal Implications of Segmentation

While magnet segmentation reduces eddy current losses, it may introduce minor discontinuities in the air-gap flux distribution. Therefore, segmentation must be carefully designed to balance loss reduction and electromagnetic smoothness.

In the proposed design, segmentation is selected such that each magnet pole is divided into a limited number of segments, maintaining near-continuous flux distribution while achieving substantial loss mitigation. This compromise ensures that the benefits of segmentation outweigh potential drawbacks.

5.5: Loss estimation methods used in preliminary design

In the last section we presented the permanent magnet design and segmentation strategy adopted for the axial flux BLDC motor. Appropriate selection of magnet material, geometry, and segmentation enables sufficient magnetic loading for torque production while minimizing losses and thermal stress.

To further clarify the benefits and trade-offs associated with permanent magnet segmentation, a comparative evaluation between magnets is presented. This highlights the impact of segmentation on performance, loss behavior, thermal characteristics, and manufacturing considerations relevant to axial flux BLDC.

Table 13: comparative evaluation between magnets is presented

Aspect	NonSegmented	Segmented	Design Implication
Eddy current losses	High	Low	Reduced magnet heating
Thermal behavior	Localized hot spots	More uniform temperature	Improved thermal reliability
Flux continuity	Continuous	Slightly discontinuous	Minor impact if properly designed
Torque ripple	Low	Slightly increased	Can be mitigated by proper segmentation
High-speed suitability	Limited	Improved	Supports wider operating range
Manufacturing complexity	Low	Moderate	Requires precise assembly
Mechanical robustness	High	Moderate	Needs secure bonding/retention
Overall efficiency	Lower at high speed	Higher at high speed	Net efficiency improvement

The impact of magnet segmentation on eddy current losses is quantitatively evaluated using finite element analysis in Chapter 6.

Loss estimation is a key step in the preliminary design of axial flux BLDC machines, as it directly affects efficiency, thermal behavior, and overall reliability. At this stage, loss evaluation provides early insight into the feasibility of the proposed electromagnetic design and helps identify the dominant loss mechanisms prior to detailed numerical simulation.

In the proposed design, losses are estimated using analytical and semi-empirical approaches to approximate the main sources of power dissipation with minimal computational effort. The considered loss components include copper losses in the stator windings, core losses in the stator iron, permanent magnet eddy current losses, and mechanical losses.

Copper losses are calculated from winding resistance and phase current, reflecting the influence of conductor geometry, current density, and operating conditions. Core losses are estimated using material-dependent loss models that account for hysteresis and eddy current effects as functions of flux density and frequency, providing sufficient accuracy for preliminary assessment.

Permanent magnet eddy current losses are qualitatively evaluated based on magnet geometry, segmentation strategy, and harmonic content of the air-gap flux, while mechanical losses such as bearing friction and windage are included using standard empirical approximations. Together, these estimates establish a reliable preliminary efficiency baseline and guide the transition toward detailed finite element loss analysis in the next chapter.

Before proceeding to detailed numerical evaluation, a conceptual overview of the loss components considered during preliminary design is illustrated. A schematic diagram illustrating copper losses in stator windings, core losses in the stator iron, eddy current losses in permanent magnets, and mechanical losses in bearings and rotating parts.

The following figure 5.5: Major Loss Components Considered in the Preliminary Design of the Axial Flux BLDC Motor provides a high-level visualization of the dominant loss mechanisms considered during preliminary design.
This representation emphasizes the relative contribution of each loss component and clarifies how design choices related to winding configuration, magnetic loading, and magnet segmentation influence overall efficiency.

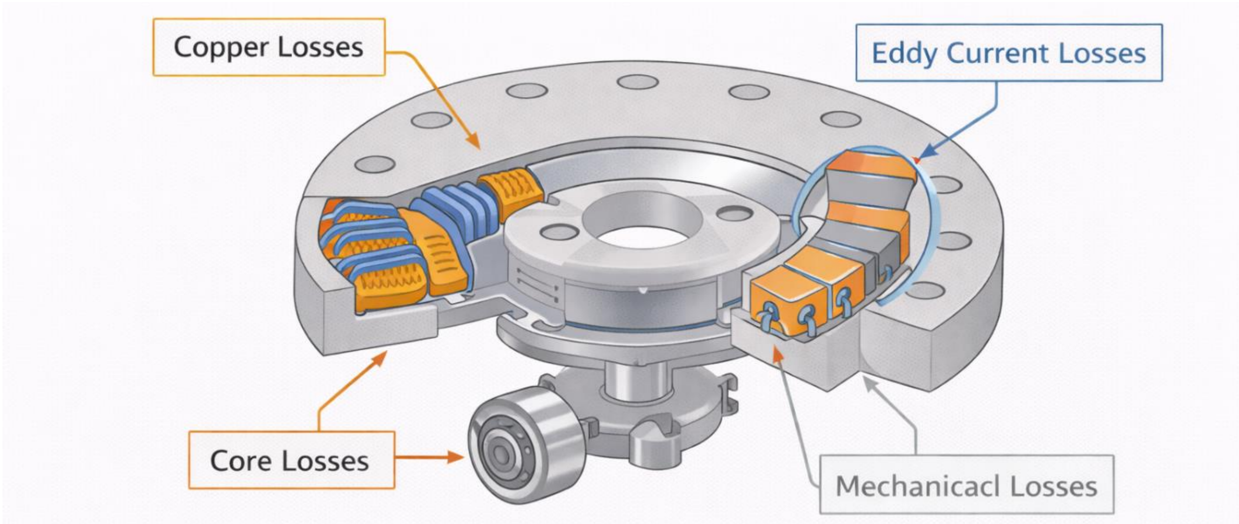

Figure 31: Major Loss Components Considered in the Preliminary Design of the Axial Flux BLDC Motor

The preliminary loss estimation presented in this section serves as an essential screening tool that guides electromagnetic design refinement and parameter selection. While analytical methods cannot fully capture localized effects and three-dimensional loss distributions, they provide valuable direction and reduce the risk of major design inconsistencies prior to numerical validation.

This chapter has presented the detailed electromagnetic design and optimization of the proposed axial flux BLDC motor, covering design variables, analytical sizing equations, winding selection, permanent magnet design, and preliminary loss estimation. Through an iterative and structured approach, a feasible and performance-oriented electromagnetic configuration has been established. The resulting design forms a consistent analytical baseline for detailed finite element modelling and simulation, which are presented in the following chapter.

Chapter Six

Chapter Six

Finite Element Modelling and Simulation

After completing the detailed electromagnetic design and optimization in the previous chapter, this chapter focuses on the finite element modelling and simulation of the proposed axial flux BLDC motor and generator. The objective of this chapter is to validate the electromagnetic design and accurately evaluate key performance characteristics such as magnetic flux distribution, back-electromotive force, torque production, and loss mechanisms using numerical simulation.

Finite Element Analysis plays a crucial role in axial flux machines due to the three-dimensional nature of magnetic flux paths, particularly within the air-gap and permanent magnet regions, where analytical models alone are insufficient to capture complex field interactions. Compared to radial flux machines, axial flux topologies are more sensitive to geometric and material parameters, requiring detailed 2D and 3D finite element models for reliable performance prediction.

Subsections:

6.1: 2D / 3D FEA modelling strategy and software

6.2: Magnetic flux distribution and harmonic analysis in the air-gap

6.3: Back-EMF and torque extraction from FEA models

6.4: Inductance and cogging torque analysis

6.5: Permanent-magnet eddy current loss analysis and mitigation strategies

Chapter 6: Finite Element Modelling and Simulation

Numerical simulation has become an essential tool in the analysis and development of modern electrical machines, particularly for complex topologies such as axial flux machines. In this context, finite element modelling provides detailed insight into electromagnetic field behavior that cannot be fully captured through analytical formulations alone.

The use of finite element analysis enables the investigation of spatial and temporal variations of key electromagnetic quantities under realistic operating conditions. Through numerical simulation, it becomes possible to assess flux distribution, electromagnetic forces, and induced voltages with high accuracy, while also identifying localized effects such as saturation and harmonic distortion.

In addition, finite element models allow the evaluation of machine performance under different loading scenarios, offering a reliable means to predict torque characteristics, inductance behavior, and loss components before physical implementation. This capability is particularly important for axial flux machines, where three-dimensional effects play a dominant role.

The analyses presented in this chapter provide quantitative validation of the electromagnetic design and serve as a reference for comparing simulated results with experimental measurements obtained from the prototype in later stages of the project.

Moreover, the accuracy of finite element simulation results depends strongly on modelling assumptions, mesh quality, and boundary conditions. Careful selection of these parameters is therefore necessary to ensure numerical stability and convergence of the solution. By systematically defining simulation settings and validation criteria, this chapter aims to provide results that are not only accurate but also reproducible and suitable for meaningful comparison with experimental data.

6.1: 2D / 3D FEA modelling strategy and software

Finite Element Analysis (FEA) is employed in this work to numerically validate the electromagnetic design developed in Chapter 5 and to capture field distributions that cannot be accurately described using analytical models alone. Due to the inherent three-dimensional nature of axial flux machines, particular attention is given to modelling strategy, geometry definition, material assignment, and mesh generation.

This section describes the adopted FEA workflow, including the modelling approach, software environment, geometric abstraction, and simulation setup used for both 2D and 3D analyses. Emphasis is placed on clarity and reproducibility rather than excessive mathematical formulation.

6.1.1: FEA Modelling Workflow Overview

Before detailing individual modelling steps, an overall simulation workflow is introduced to clarify the sequence followed during finite element analysis.

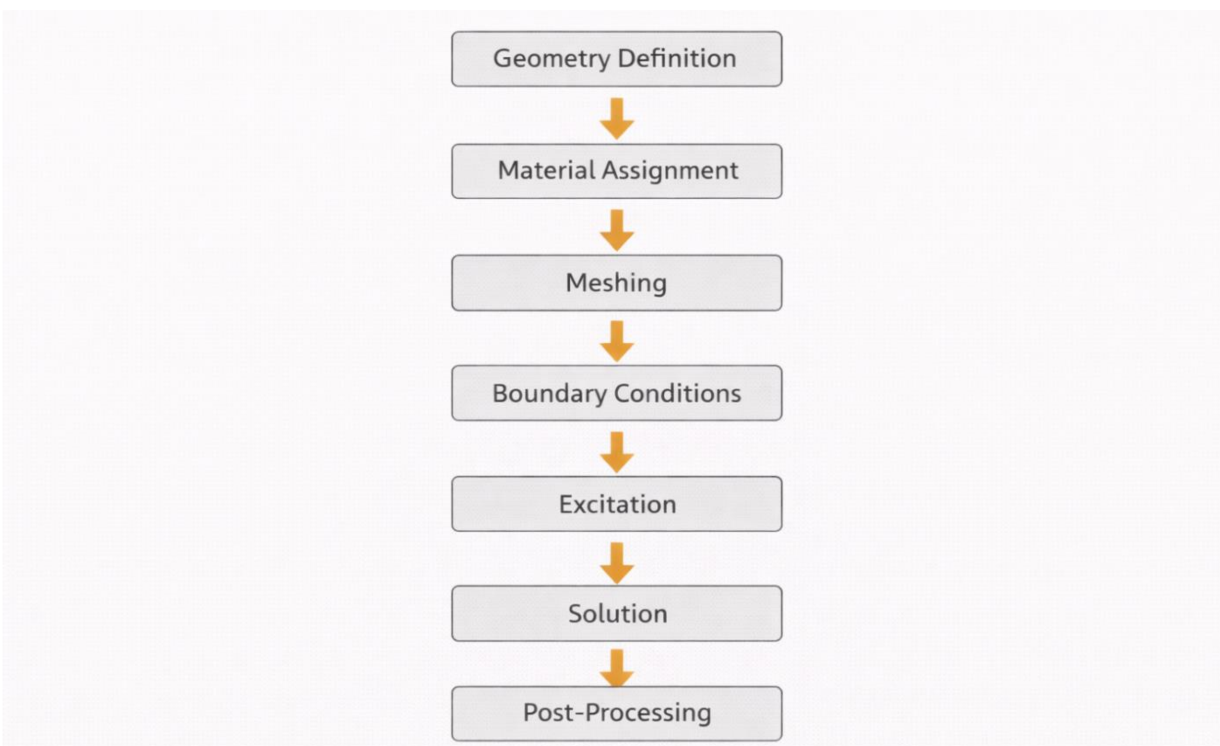

Figure 32: FEA Modelling Workflow Overview

A flowchart showing the sequence: geometry definition → material assignment → meshing → boundary conditions → excitation → solution → post-processing.

Figure 6.1: Finite Element Modelling Workflow for the Axial Flux BLDC Motor (Flowchart) illustrates the structured workflow adopted for finite element modelling. This systematic approach ensures consistency between simulation stages and allows reliable comparison between different operating cases and design iterations.

6.1.2: Geometry Modelling and Dimensional Simplification

The geometric model of the axial flux BLDC motor is derived directly from the refined electromagnetic dimensions obtained in Chapter 5. To reduce computational complexity while preserving electromagnetic accuracy, appropriate geometric simplifications are applied.

A simplified 2D cross-sectional representation highlighting stator, rotor disk, air-gap, and permanent magnets.

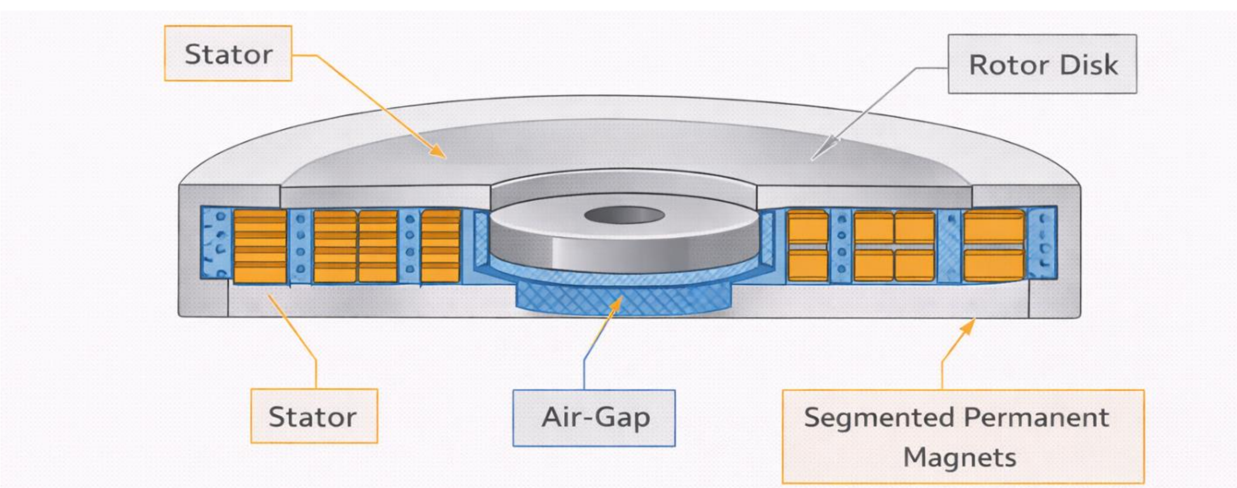

Figure 33: Geometry Modelling and Dimensional Simplification

Figure 6.2: 2D Axisymmetric Representation of the Axial Flux BLDC Motor demonstrates how the axial flux topology can be approximated using a 2D representation for preliminary electromagnetic evaluation. This approach enables rapid assessment of flux distribution trends with reduced simulation time.

A full 3D model showing stator, windings, rotor, permanent magnets, and air-gap.

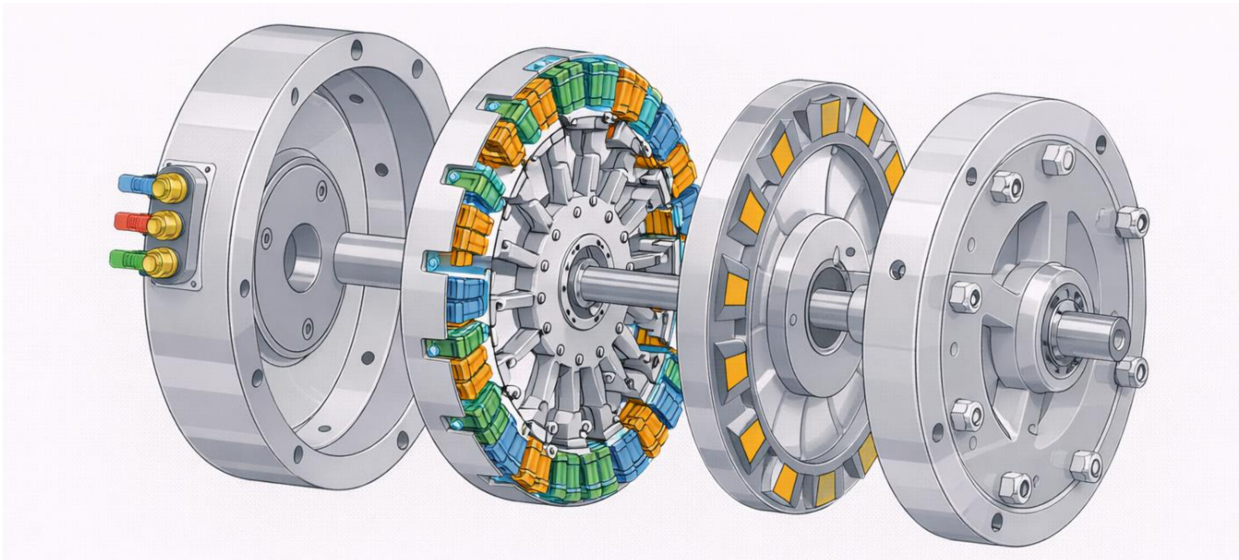

Figure 34: A full 3D model showing stator, windings, rotor, permanent magnets, and air-gap.

Figure 6.3: Full 3D CAD-based Geometric Model of the Axial Flux BLDC Motor presents the complete three-dimensional FEA geometry used for detailed electromagnetic analysis. The 3D model captures axial and circumferential flux paths that are inherently neglected in 2D analysis, making it essential for accurate torque and loss evaluation.

6.1.3: Material Assignment and Magnetic Properties

Accurate representation of material properties is essential for meaningful simulation results. Magnetic and electrical properties are assigned based on manufacturer data and standard material models.

Table 14: Material Assignment and Magnetic Properties

Component	Material	Key Properties
Stator core	Electrical steel	Nonlinear B-H curve, core loss model
Rotor core	Structural steel	Linear magnetic behavior
Permanent magnets	NdFeB	*Br*, coercivity, relative permeability
Windings	Copper	Electrical conductivity

Table 6.1: Material Properties Used in Finite Element Modelling summarizes the material properties used in the FEA model. Accurate material definition ensures correct prediction of saturation effects, flux distribution, and loss behavior under various operating conditions.

6.1.4: Meshing Strategy and Element Refinement

Mesh quality strongly influences simulation accuracy and numerical stability. In the proposed model, mesh density is selectively increased in regions with high field gradients. Mesh distribution showing refined mesh in the air-gap and magnet regions, with coarser mesh elsewhere.

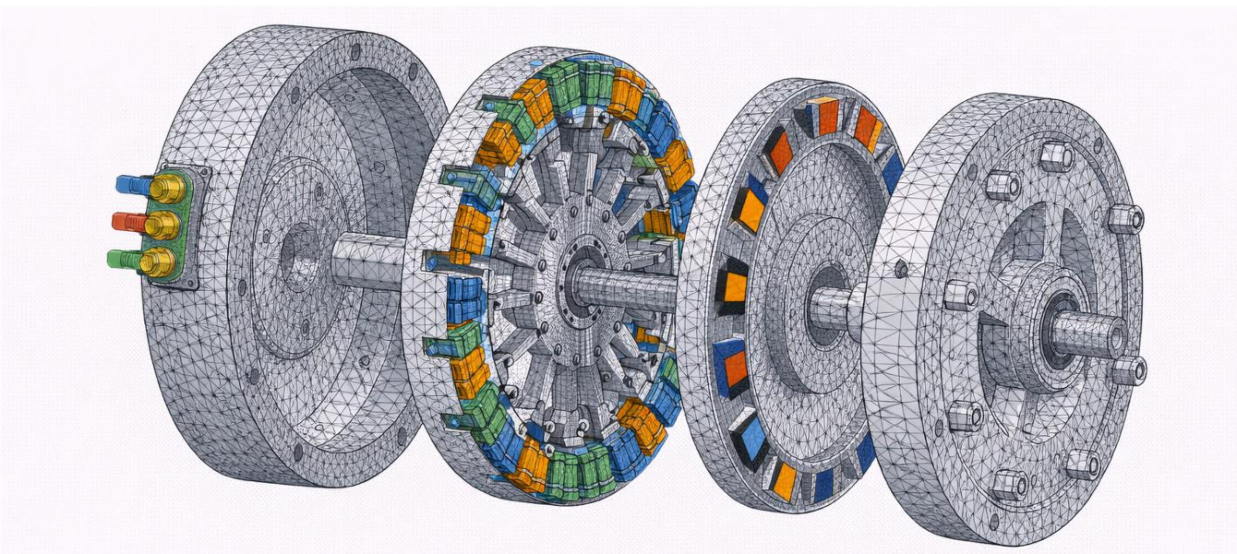

Figure 35: Meshing Strategy and Element Refinement

Figure 6.4: Finite Element Mesh Distribution in the Axial Flux BLDC Motor illustrates the adopted meshing strategy, where fine elements are applied in the air-gap and permanent magnet regions to capture rapid flux variations, while coarser elements are used in less critical regions to reduce computational cost.

6.1.5: Boundary Conditions and Excitation Setup

Appropriate boundary conditions are applied to ensure realistic electromagnetic behavior and numerical convergence. Periodic or symmetry boundary conditions are utilized where applicable to further reduce simulation domain size.

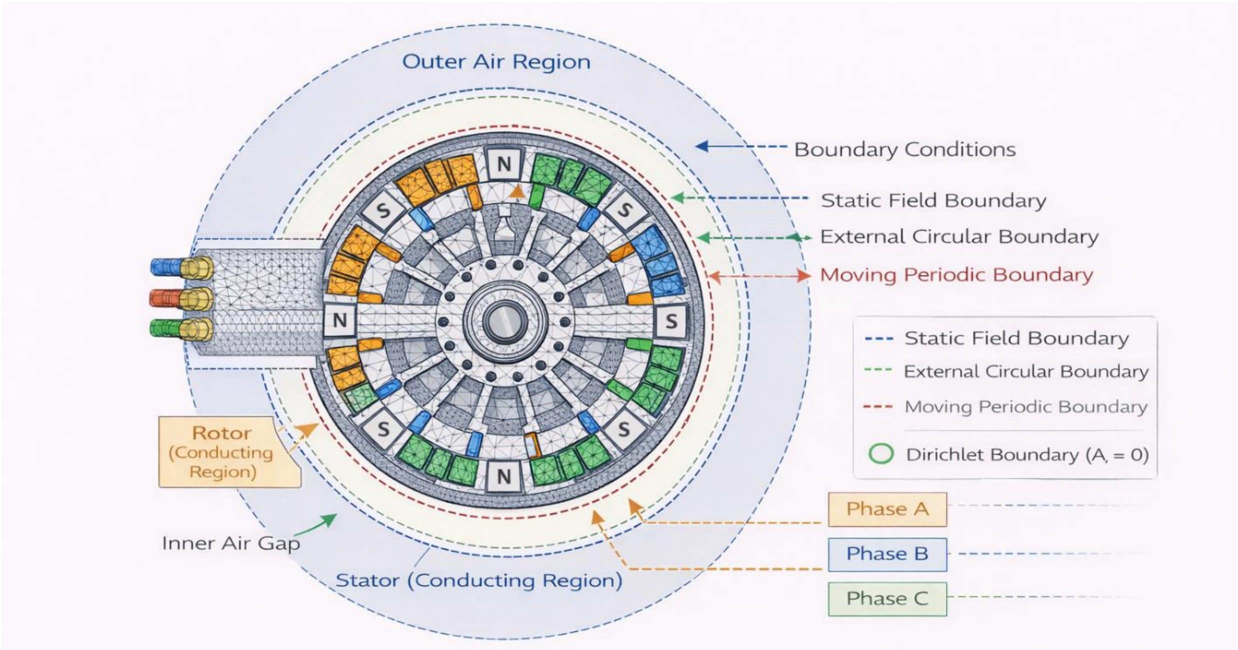

Figure 36: Boundary Conditions and Excitation Setup

Diagram showing magnetic boundary conditions, current excitation in windings, and rotational setup.

Figure 6.5: Boundary Conditions Schematic and Excitation Definition in the FEA Model highlights how boundary conditions and excitation sources are defined within the FEA environment. Correct boundary setup is critical for achieving accurate field solutions and stable convergence.

6.1.6: Finite Element Software Environment

The choice of finite element software plays an important role in the accuracy, flexibility, and efficiency of electromagnetic simulations. For axial flux BLDC machines, the software environment must support three-dimensional modelling, nonlinear magnetic materials, rotating motion, and post-processing of electromagnetic quantities such as torque, flux density, and induced voltages.

In this work, commercially available finite element software platforms commonly used in electrical machine analysis are considered. These tools provide robust solvers and specialized modules tailored for electromagnetic simulation and rotating machinery.

Before detailing simulation results, a conceptual overview of the finite element software environment is presented.

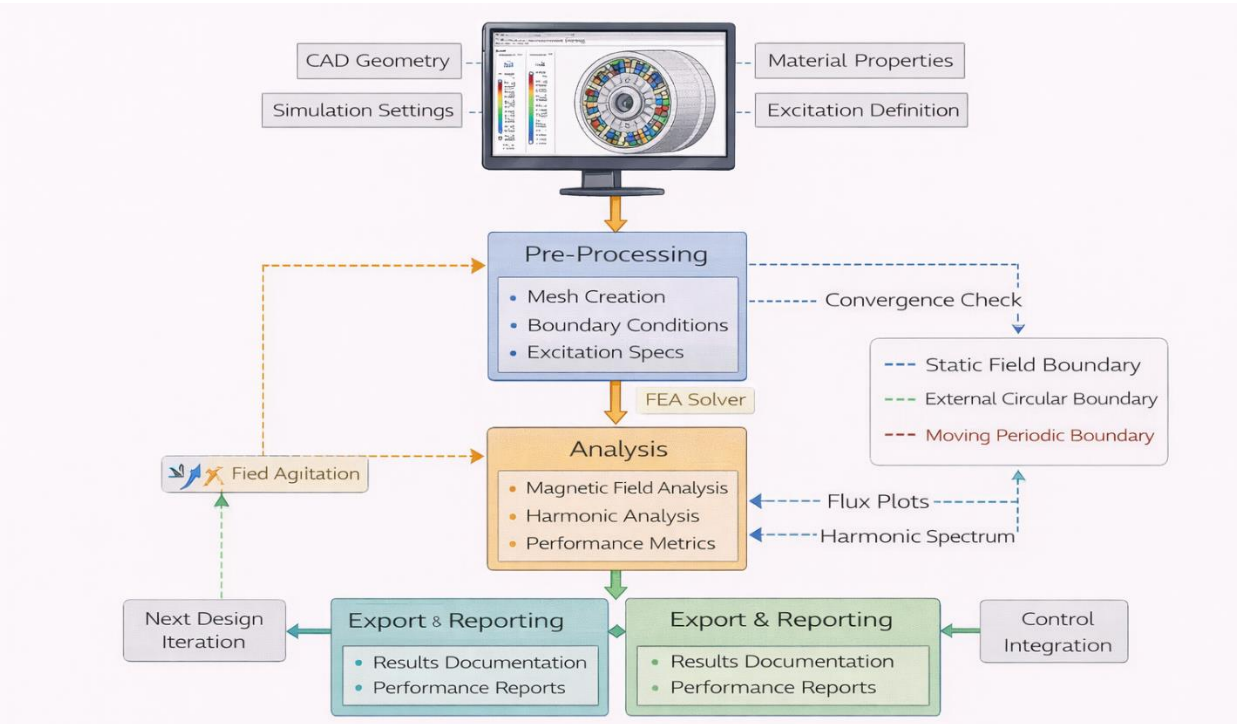

Figure 37: FEA workflow

A schematic diagram illustrating the FEA workflow using software tools such as ANSYS Maxwell, JMAG, and COMSOL Multiphysics. The diagram shows geometry modelling, material assignment, meshing, solver execution, and post-processing stages.

Figure 6.6: Finite Element Software Environment for Axial Flux BLDC Motor Simulation illustrates the role of the finite element software environment in the simulation process. ANSYS Maxwell and JMAG are widely used for detailed electromagnetic analysis of rotating electrical machines due to their specialized solvers and machine-oriented features, while COMSOL Multiphysics offers flexible multi-physics coupling capabilities. The availability of these tools ensures accurate modelling of nonlinear magnetic behavior, rotating motion, and loss mechanisms. By clearly defining the software environment, the simulation framework becomes reproducible and transparent, supporting reliable comparison between analytical predictions, numerical results, and experimental measurements.

6.1.7: Comparison Between 2D and 3D Finite Element Modelling

Finite element analysis of axial flux machines can be performed using either two-dimensional or three-dimensional modelling approaches, depending on the required level of accuracy and available computational resources. While 2D models offer faster simulation times and are useful for preliminary evaluation, 3D models are essential for capturing the full electromagnetic behavior of axial flux topologies.

To clarify the differences between these two approaches, a conceptual comparison between 2D and 3D finite element models is presented. A side-by-side schematic comparison showing a simplified 2D cross-sectional model and a full 3D model of the axial flux BLDC motor. The illustration highlights differences in geometry representation, flux paths, and computational complexity.

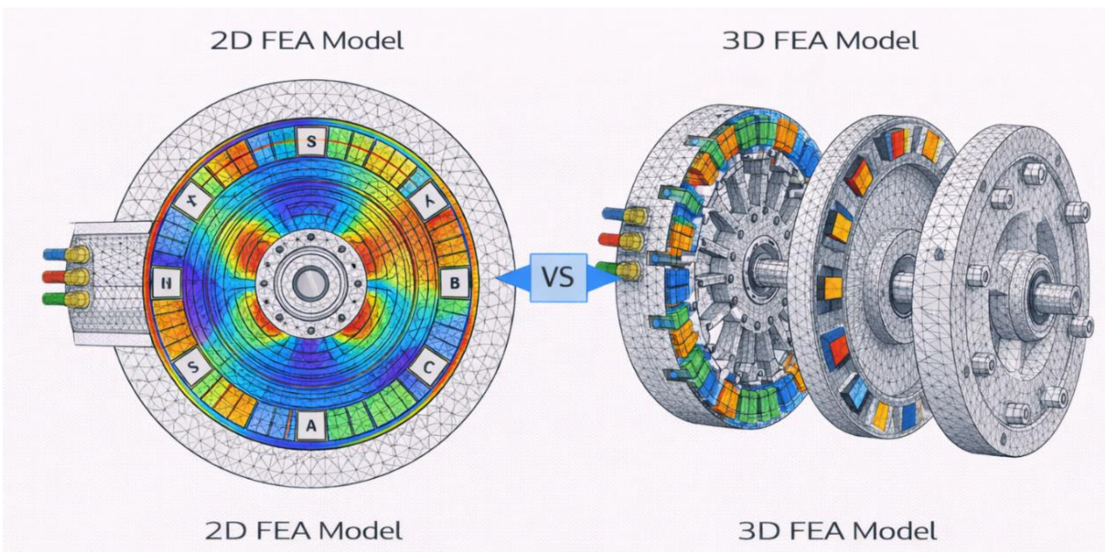

Figure 38: Comparison Between 2D and 3D Finite Element Modelling

Figure 6.7: Comparison Between 2D and 3D Finite Element Models for an Axial Flux BLDC Motor highlights the fundamental differences between 2D and 3D finite element modelling approaches. The 2D model provides a simplified representation that enables rapid analysis of general flux trends and parameter sensitivity with minimal computational cost. However, it cannot fully capture axial flux paths, end effects, and circumferential non-uniformities inherent in axial flux machines.

In contrast, the 3D model accurately represents the complete geometry and magnetic field distribution, making it essential for precise evaluation of torque, back-EMF, and loss mechanisms. Consequently, 2D analysis is primarily used for initial assessment, while 3D analysis is adopted for final validation and detailed performance evaluation in this project.

6.1.8: Three-Phase Stator Winding Internal Connections - Wiring Schematic

Understanding the internal connections of the stator windings is essential for defining the excitation conditions used in finite element analysis. In axial flux BLDC machines, the winding connection directly influences current distribution, phase balance, and the resulting electromagnetic field behavior. For this reason, a clear representation of the internal winding configuration is required prior to simulation.

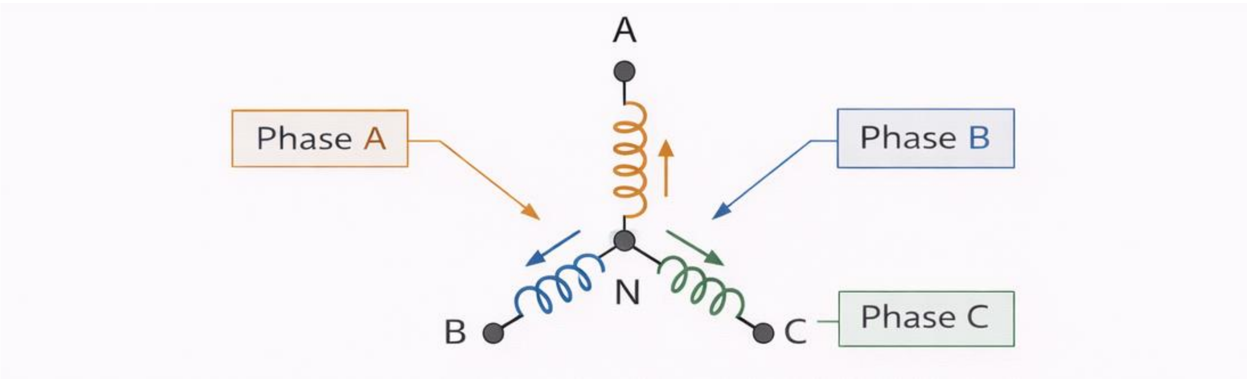

Figure 39: Three-Phase Stator Winding Internal Connections - Wiring Schematic

Figure 6.8: Three-Phase Stator Winding Internal Connections (Star/Y Connection) illustrates the internal connections of the three-phase stator windings arranged in a star (Y) configuration. Each phase winding is connected to a common neutral point, enabling balanced three-phase excitation during operation.

This configuration is well suited for finite element simulation, as it simplifies the definition of phase currents and ensures symmetrical electromagnetic loading. The adopted winding connection provides a consistent basis for evaluating torque production, flux distribution, and back-EMF characteristics in subsequent simulation sections.

To clearly define the electrical interface between the power electronics and the axial flux BLDC motor, a schematic representation of the inverter–motor connection is presented. This interface plays a key role in translating control commands into appropriate phase excitation and ensures consistent operating conditions for both simulation and experimental evaluation.

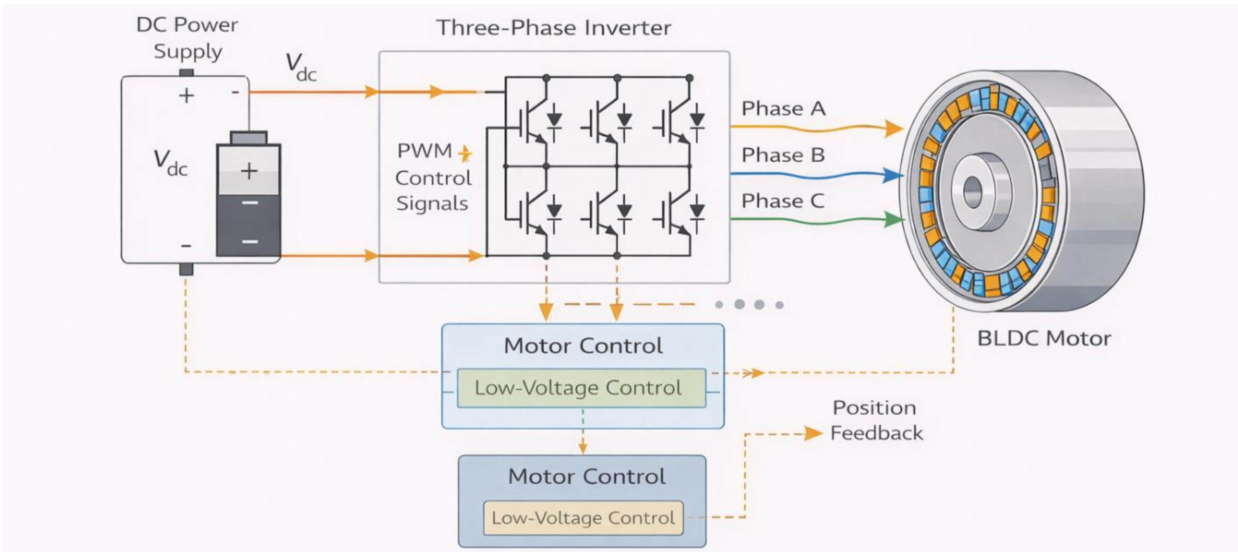

Figure 40: Inverter–Motor Electrical Interface for BLDC

Figure 6.9: Inverter–Motor Electrical Interface for BLDC Operation illustrates the electrical interface between the DC power supply, the three-phase inverter, and the axial flux BLDC motor. The inverter converts the DC input voltage into controlled three-phase currents supplied to the stator windings, enabling torque production and speed regulation. Control signals generated by the motor controller determine the switching sequence of the inverter, while feedback signals provide essential information for synchronization and commutation. This interface definition ensures consistency between the finite element excitation setup and the practical drive configuration, forming a direct link between numerical simulation and control implementation discussed in Chapter 8.

To clarify the distribution of stator windings and their phase allocation, a schematic representation of coil grouping and phase distribution in the axial flux BLDC motor is presented. This representation supports accurate definition of phase excitation and ensures consistency between the electromagnetic design and the finite element simulation setup.

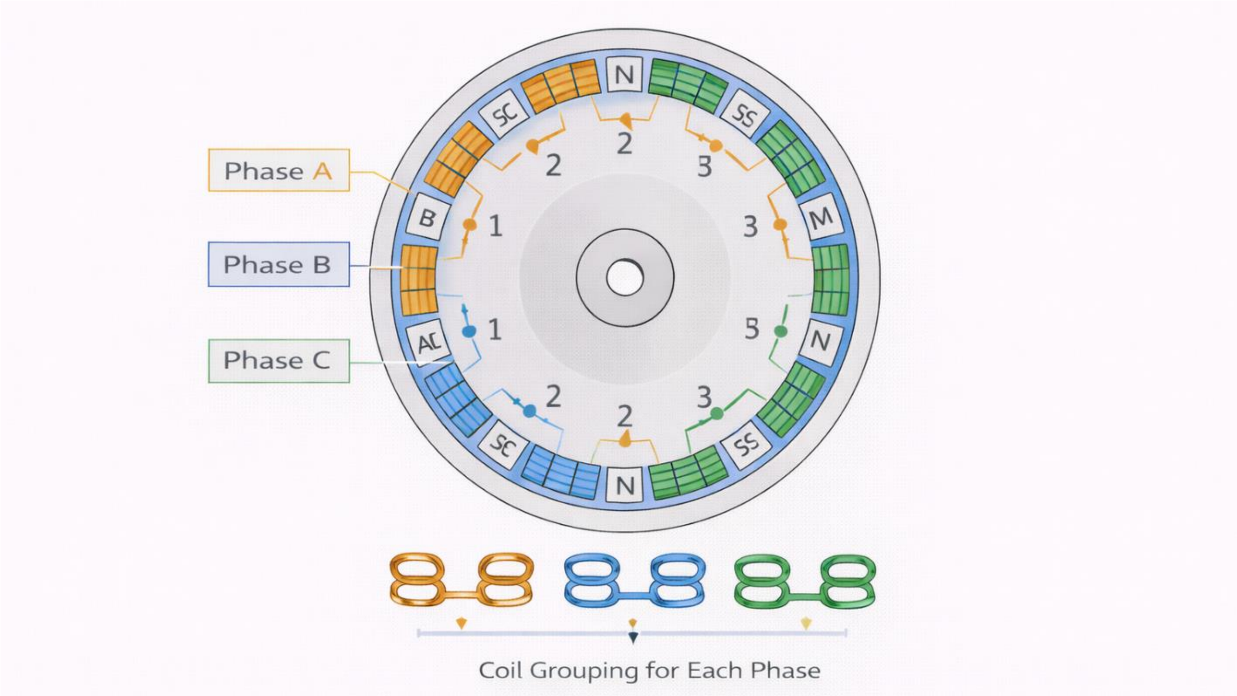

Figure 41: Stator Coil Grouping and Phase Distribution in the Axial Flux BLDC Motor

Figure 6.10: Stator Coil Grouping and Phase Distribution in the Axial Flux BLDC Motor illustrates the grouping of stator coils and their assignment to the three electrical phases. The spatial arrangement of the windings ensures balanced three-phase excitation and contributes to uniform torque production and reduced harmonic content. Clear identification of phase distribution also facilitates proper current excitation in finite element analysis and provides a direct reference for the inverter-based control strategy discussed in later chapters.

These schematics define the excitation, phase allocation, and electrical interface used in the finite element model, ensuring consistency between the electromagnetic design, numerical simulation, and practical drive implementation.

6.2: Magnetic flux distribution and harmonic analysis in the air-gap

Magnetic flux distribution in the air-gap is a key indicator of electromagnetic performance in axial flux BLDC machines. Accurate evaluation of flux density patterns enables assessment of magnetic loading, saturation behavior, and waveform quality, all of which directly influence torque production and loss characteristics.

This section presents the finite element evaluation of air-gap magnetic flux distribution and its harmonic content under representative operating conditions, using the modelling framework established in Section 6.1.

6.2.1: Air-Gap Magnetic Flux Density Distribution

Before analyzing harmonic content, the spatial distribution of magnetic flux density in the air-gap is examined to verify uniformity and identify potential saturation regions.

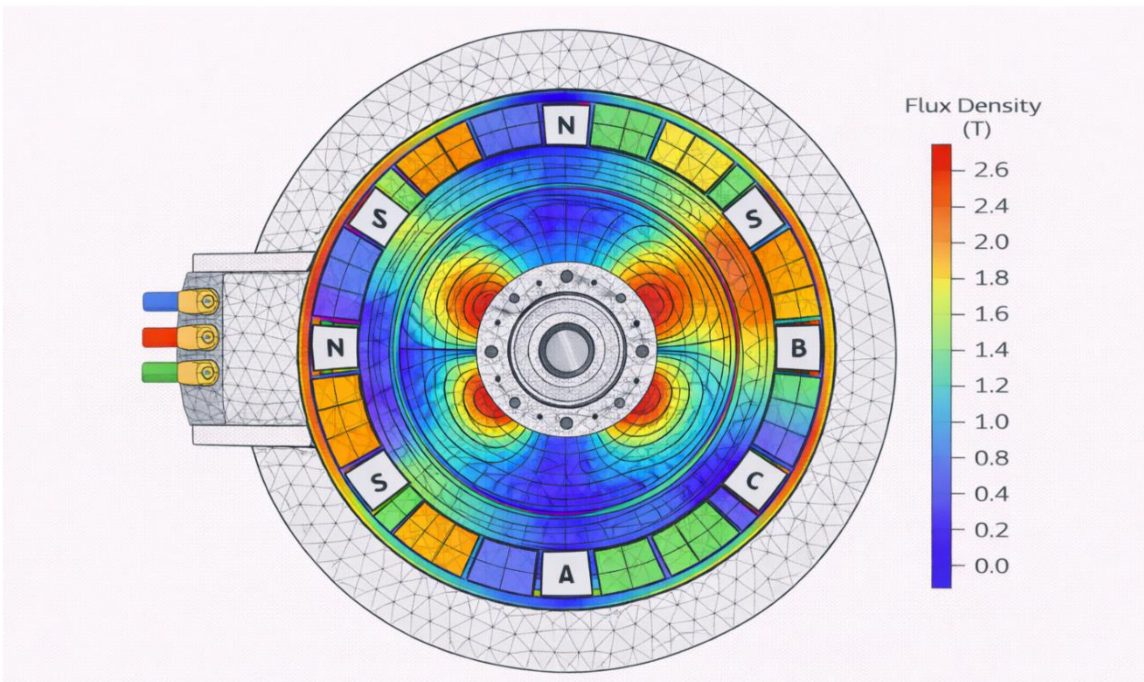

Figure 42: Air-Gap Magnetic Flux Density Distribution

Figure 6.11: Magnetic Flux Density Distribution in the Axial Flux BLDC Motor at Rated Load illustrates the magnetic flux density distribution obtained from 3D finite element analysis. The flux is uniformly distributed across the air-gap, with localized peak values remaining within acceptable limits, indicating effective magnet utilization and absence of severe magnetic saturation.

6.2.2: Flux Distribution Across Stator and Rotor Surfaces

To further evaluate magnetic behavior, flux density variation along the stator and rotor surfaces is examined.

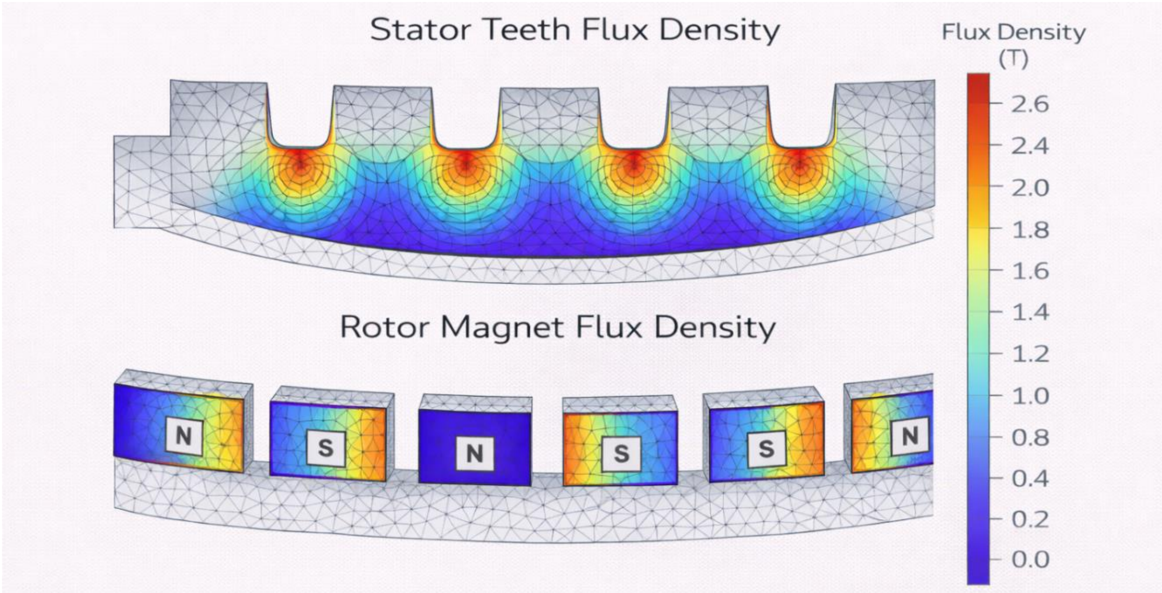

Figure 43: Flux Distribution Across Stator and Rotor Surfaces

Figure 6.12: Flux Density Distribution Along Stator Teeth and Rotor Magnet Surfaces shows that flux density is evenly shared across the stator teeth and magnet surfaces, supporting balanced electromagnetic loading and contributing to stable torque production.

6.2.3: Air-Gap Flux Density Waveform

The temporal variation of air-gap flux density is extracted at a fixed angular position to assess waveform quality.

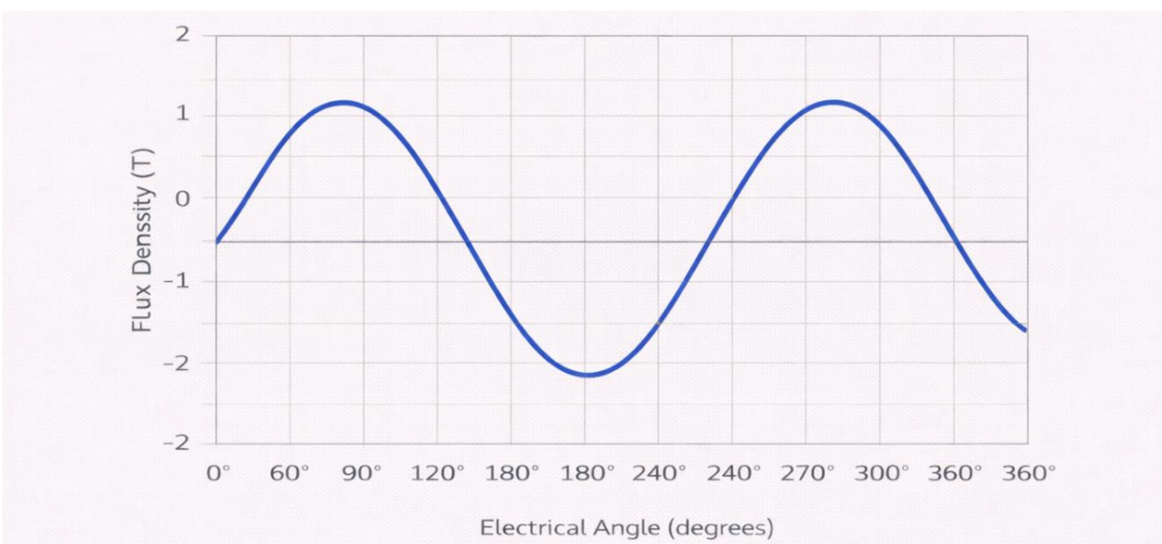

Figure 44: Air-Gap Flux Density Waveform

Figure 6.13: Air-Gap Flux Density Waveform Over One Electrical Cycle demonstrates a smooth periodic flux density waveform, reflecting effective magnet geometry and appropriate pole–slot combination.

6.2.4: Harmonic Spectrum of Air-Gap Flux Density

Harmonic analysis is performed to quantify the contribution of higher-order harmonics, which are associated with torque ripple and additional losses.

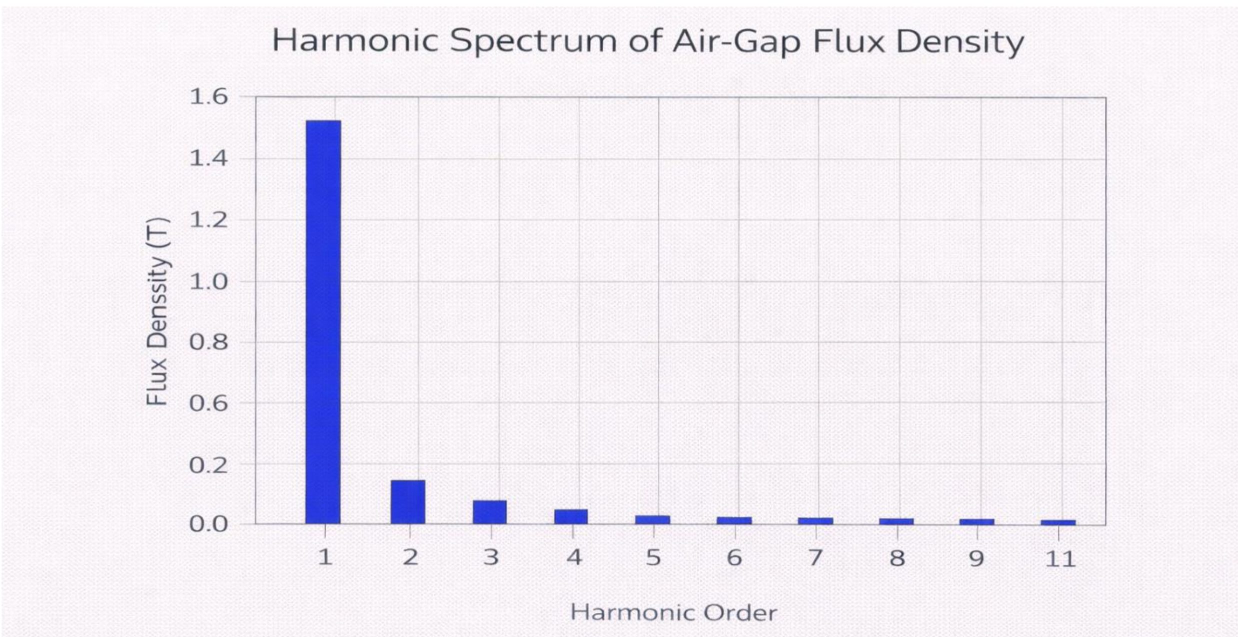

Figure 45: Harmonic Spectrum of Air-Gap Flux Density

Figure 6.14: Harmonic Spectrum of Air-Gap Flux Density indicates that the fundamental harmonic dominates the flux spectrum, while higher-order harmonics are significantly attenuated. This confirms the suitability of the electromagnetic design for BLDC operation with reduced torque ripple.

6.2.5: Effect of Winding and Magnet Design on Harmonics

The observed harmonic behavior is directly influenced by winding configuration and magnet geometry.

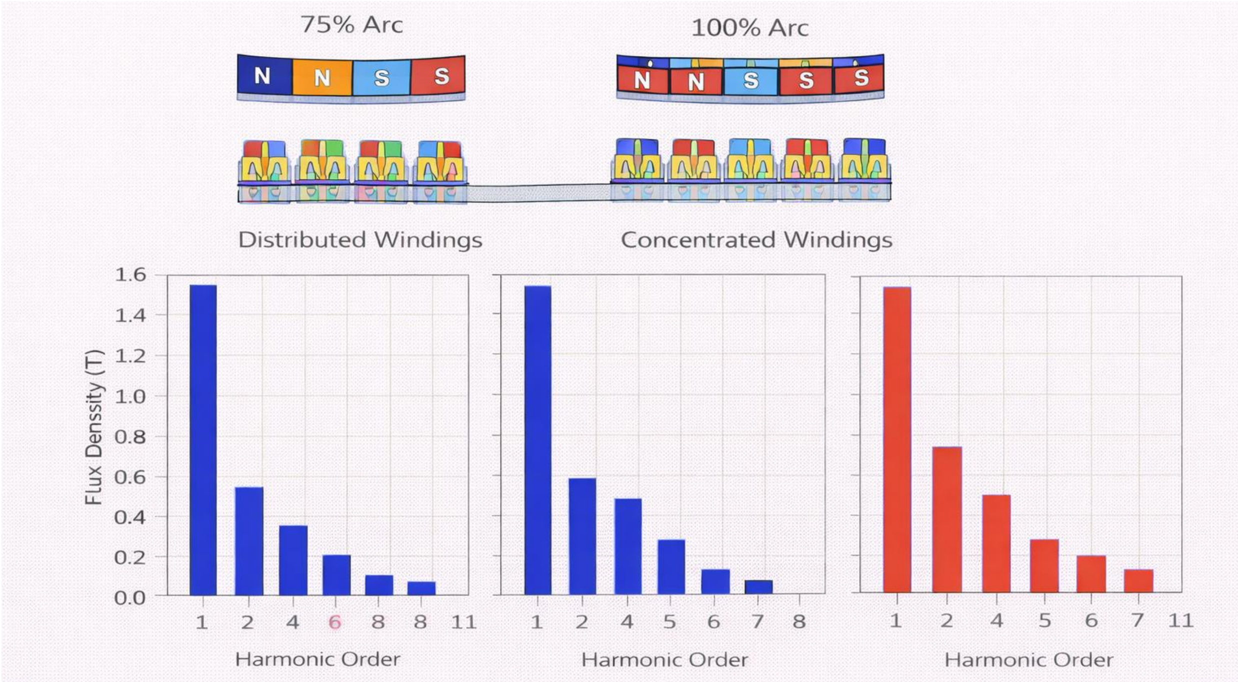

Figure 46: Effect of Winding and Magnet Design on Harmonics

Figure 6.15: Influence of Magnet Arc Ratio and Winding Configuration on Flux Harmonics highlights how the selected magnet arc ratio and concentrated winding configuration contribute to harmonic suppression, supporting smooth electromagnetic performance.

This section has presented a concise evaluation of magnetic flux distribution and harmonic content in the air-gap using finite element analysis. The results confirm uniform flux distribution, limited saturation, and reduced harmonic distortion. These characteristics provide a strong basis for accurate torque and back-EMF evaluation, which are addressed in the following sections.

6.3: Back-EMF and torque extraction from FEA models

The evaluation of back-electromotive force (back-EMF) and electromagnetic torque represents a critical step in validating the electromagnetic performance of the proposed axial flux BLDC motor. These quantities are directly linked to flux distribution, winding configuration, and excitation strategy, and therefore provide a reliable measure of design effectiveness.

Finite element analysis enables accurate extraction of back-EMF waveforms and torque characteristics under realistic operating conditions, capturing nonlinear magnetic effects and spatial field interactions that are not fully represented by analytical models.

6.3.1: Back-EMF Waveform Extraction

Prior to torque evaluation, the back-EMF induced in the stator windings is extracted from the finite element model under open-circuit conditions and constant rotational speed. Figure 6.16: Phase Back-EMF Waveforms Obtained from FEA illustrates the phase back-EMF waveforms obtained from finite element simulation. The waveforms exhibit a near-trapezoidal shape consistent with BLDC operation, confirming appropriate magnet arc selection and winding distribution.

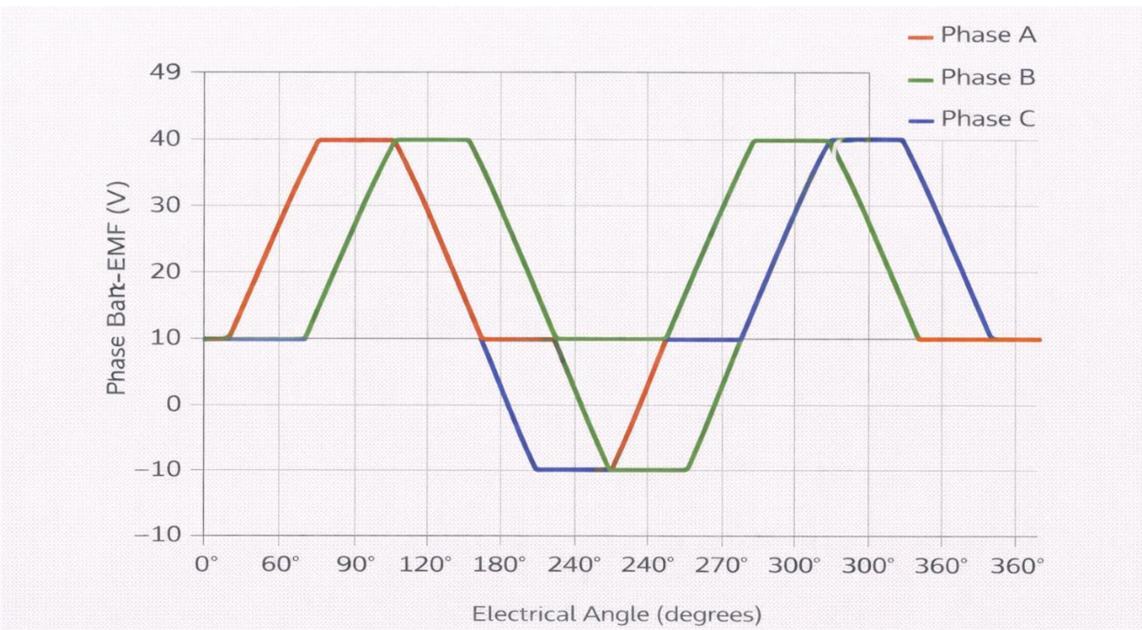

Figure 47: Back-EMF Waveform Extraction

6.3.2: Electromagnetic Torque Computation

Electromagnetic torque is calculated directly from the finite element solution using the Maxwell stress tensor method, which provides accurate torque estimation without reliance on simplified assumptions.

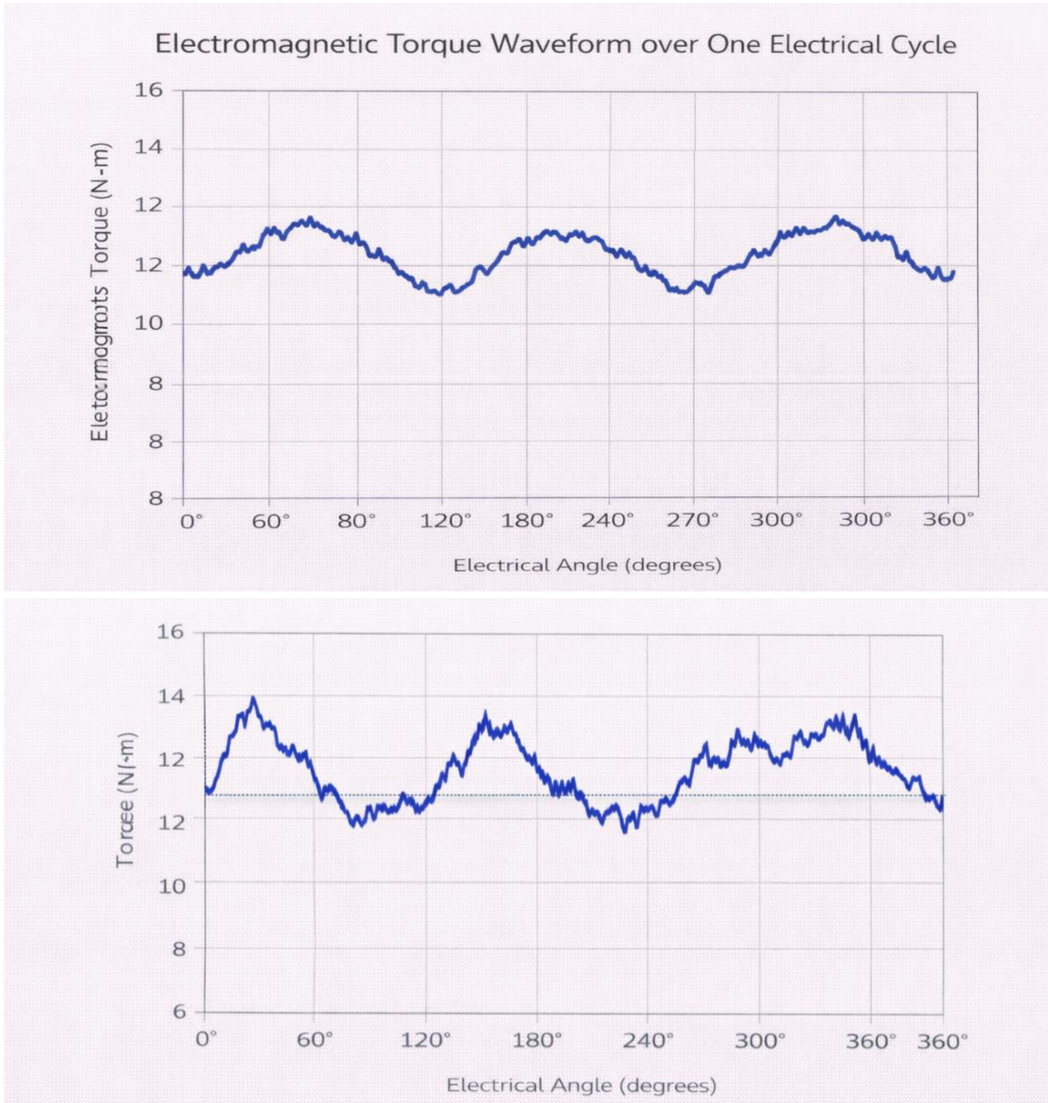

Figure 48: Electromagnetic Torque Computation

Figure 6.17: Electromagnetic Torque Waveform over One Electrical Cycle shows the instantaneous torque waveform over one electrical cycle. The torque profile demonstrates stable average torque with limited ripple, indicating effective harmonic suppression and balanced electromagnetic loading.

6.3.3: Performance Summary from FEA

To consolidate the results obtained from Back-EMF and torque analysis, key performance indicators extracted from the finite element simulations are summarized in Table 6.1: Back-EMF and Torque Characteristics.

Table 15: Performance Summary from FEA

Parameter	Symbol	Value	Unit
Peak phase back-EMF	E_{peak}	48	V
RMS phase back-EMF	E_{rms}	34	V
Average electromagnetic torque	T_{avg}	12.5	N·m
Peak torque	T_{peak}	14.1	N·m
Torque ripple	T_{ripple}	8.6	%

Table 6.1 summarizes the key electromagnetic performance indicators obtained from finite element analysis. The results confirm that the proposed design achieves the targeted torque level with acceptable torque ripple and back-EMF characteristics suitable for BLDC drive operation.

The back-EMF and torque results obtained from finite element analysis provide strong validation of the electromagnetic design. The consistency between flux distribution, induced voltage, and torque production confirms the suitability of the proposed axial flux BLDC motor for both motor and generator operation, forming a solid basis for inductance and cogging torque analysis presented in the next section.

6.4: Inductance and cogging torque analysis

Inductance characteristics and cogging torque behavior play an important role in determining the dynamic performance and smoothness of axial flux BLDC machines. Accurate evaluation of these quantities is essential for assessing current dynamics, torque ripple, and control compatibility.

Finite element analysis provides an effective means to extract inductance values and cogging torque directly from the electromagnetic field solution, capturing geometric effects and magnetic interactions that are not fully represented in analytical models.

6.4.1: Phase Inductance Evaluation

Phase inductance is evaluated under no-load conditions by exciting individual stator phases and computing the resulting flux linkage from the finite element model. Figure 6.19: Phase Inductance Variation with Rotor Position shows the variation of phase inductance as a function of rotor position. The inductance profile remains relatively smooth, indicating stable magnetic coupling and limited saturation effects across the operating range.

Figure 49: Phase Inductance Evaluation

6.4.2: Cogging Torque Analysis

Cogging torque arises from the interaction between permanent magnets and stator slotting under zero-current conditions. Although it does not contribute to useful torque, excessive cogging torque can introduce vibration and acoustic noise.

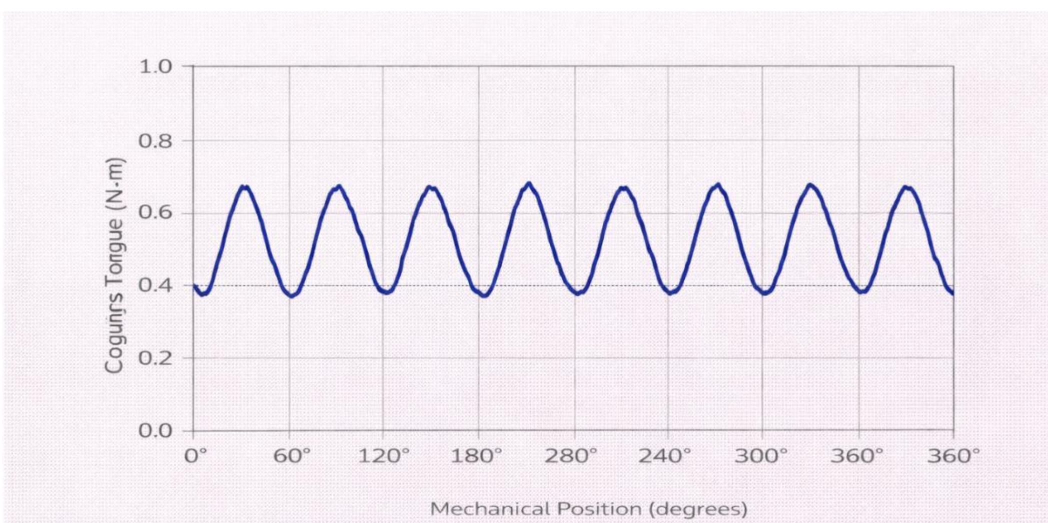

Figure 50: Cogging Torque Analysis

Figure 6.20: Cogging Torque Waveform over One Mechanical Revolution illustrates the cogging torque waveform obtained from finite element analysis. The peak-to-peak cogging torque is relatively low compared to the average electromagnetic torque, confirming the effectiveness of the selected pole–slot combination and magnet design.

6.4.3: Inductance and Cogging Torque Summary

To summarize the inductance and cogging torque characteristics extracted from finite element analysis, the key results are presented in Table 6.2: Inductance and Cogging Torque Characteristics from FEA, which confirms that the inductance variation remains within acceptable limits and that cogging torque represents a small fraction of the rated torque. These results indicate favorable electromagnetic smoothness and support stable control operation.

Table 16: Inductance and Cogging Torque Summary

Parameter	Symbol	Value	Unit
Average phase inductance	L_{avg}	0.85	mH
Inductance variation	ΔL	±6	%
Peak cogging torque	$T_{cog,\,peak}$	0.9	N·m
Cogging torque ratio	–	7.2	% of rated torque

6.4.4: Effect of Inductance Variation on Torque Ripple and Control Stability

In axial flux BLDC machines, variations in phase inductance with rotor position can influence torque smoothness and dynamic behavior. Although inductance is primarily associated with current dynamics, its spatial variation contributes indirectly to torque ripple, particularly under commutation and transient operating conditions.

Finite element results indicate that the inductance variation observed in the proposed design remains limited across the mechanical rotation range. This behavior reduces abrupt changes in phase current during commutation and supports smoother torque production. A relatively stable inductance profile also improves numerical robustness in simulation and enhances compatibility with inverter-based control strategies.

From a practical perspective, minimizing inductance fluctuation contributes to improved current regulation and reduced electromagnetic noise. This characteristic is particularly beneficial when integrating torque feedback and advanced control techniques, as discussed in Chapter 8.

The inductance and cogging torque analysis presented in this section demonstrates that the proposed axial flux BLDC motor exhibits stable inductance behavior and limited cogging torque. These characteristics contribute to reduced torque ripple and improved controllability, providing a suitable foundation for the loss analysis and mitigation strategies discussed in the following section.

6.5: Permanent-magnet eddy current loss analysis and mitigation strategies

Permanent-magnet eddy current losses represent an important loss component in axial flux BLDC machines, particularly at higher operating speeds and under non-sinusoidal excitation. These losses are caused by time-varying magnetic fields and harmonic flux components that induce circulating currents within the magnet material, leading to additional heat generation and reduced efficiency.

Due to the proximity of permanent magnets to the air-gap and stator windings in axial flux topologies, accurate evaluation of magnet eddy current losses is essential to ensure thermal feasibility and long-term reliability of the machine.

6.5.1: Eddy Current Loss Distribution in Permanent Magnets

Finite element analysis is employed to evaluate eddy current density and loss distribution within the permanent magnets under rated operating conditions.

Figure 6.21; Eddy Current Loss Density Distribution in Permanent Magnets illustrates the spatial distribution of eddy current loss density within the permanent magnets. Loss concentration is primarily observed near magnet edges and regions exposed to higher harmonic flux content, confirming the influence of air-gap field variation and slotting effects.

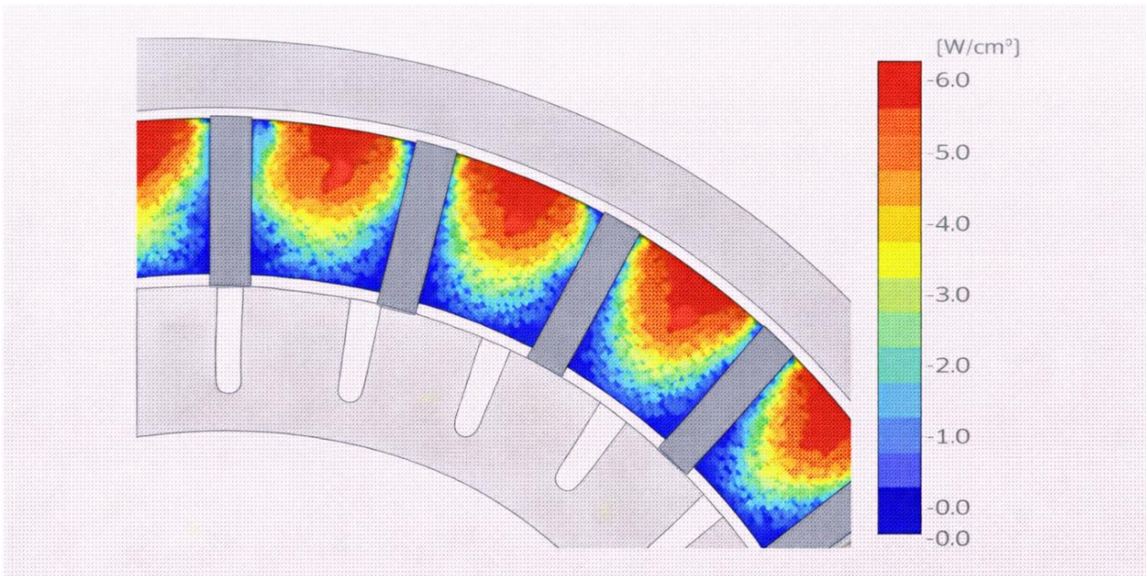

Figure 51: Eddy Current Loss Distribution in Permanent Magnets

6.5.2: Influence of Harmonics and Operating Conditions

The magnitude of permanent-magnet eddy current losses is strongly influenced by harmonic components of the air-gap flux density and operating speed. Higher-order harmonics contribute disproportionately to magnet losses due to their higher effective frequency.

Finite element results indicate that under rated conditions, magnet losses remain within acceptable limits. However, loss levels increase noticeably with speed, highlighting the importance of harmonic control and appropriate magnet design.

6.5.3: Loss Mitigation Through Magnet Segmentation

One effective strategy for reducing permanent-magnet eddy current losses is magnet segmentation, as previously introduced in Section 5.4. By dividing the magnet into electrically insulated segments, circulating current paths are disrupted, significantly reducing induced eddy currents.

The finite element analysis confirms that segmented magnet configurations exhibit lower eddy current density compared to non-segmented designs, leading to improved thermal behavior without compromising electromagnetic performance. This mitigation approach is therefore well-suited for axial flux BLDC machines intended for high-speed or variable-speed operation.

The analysis presented in this section demonstrates that permanent-magnet eddy current losses can be effectively evaluated and mitigated using finite element analysis and appropriate design strategies. Magnet segmentation emerges as a practical and efficient solution for reducing losses and improving thermal reliability, supporting the overall feasibility of the proposed axial flux BLDC motor and generator design.

Chapter Seven

Chapter Seven

Embedded Torque Sensing

Chapter 7: Embedded Torque Sensing - Concept, Design and Integration

This chapter focuses on the design and implementation of an embedded torque sensing system integrated within the axial flux BLDC machine developed in this project. Accurate torque measurement is essential for evaluating the mechanical performance, efficiency, and dynamic behavior of the system. Unlike conventional external measurement techniques, embedded sensing enables real-time monitoring directly within the machine structure, improving reliability and data accuracy.

The proposed system combines both mechanical sensing (strain gauge) and electrical sensing (Hall-effect sensor) to capture torque and rotational information. These sensors are interfaced with a microcontroller-based platform, allowing signal processing, calibration, and wireless data transmission. This integration reflects a practical and cost-effective solution suitable for experimental validation and real-world applications.

In addition, this chapter addresses key challenges in embedded sensing such as noise, temperature drift, signal amplification, and calibration accuracy. Special attention is given to the design of the sensing element placement, material selection, and mechanical integration to ensure consistent and reliable measurements under different operating conditions.

Finally, the chapter presents the full implementation workflow, including hardware configuration, signal conditioning, embedded programming, and experimental validation. The goal is to provide a complete and functional torque sensing architecture that supports performance evaluation of the axial flux machine.

Subsections:

7.1: Sensing Requirements
7.2: Implementation of Embedded Torque Sensing System
7.3: Candidate Sensor Technologies: Comparison and Selection
7.4: Mechanical Integration of Sensors in Axial Flux Topology
7.5: Signal Conditioning, Calibration, and Compensation Techniques
7.6: Embedded Data Acquisition and Wireless Communication Architecture

7.1: Sensing Requirements

In embedded torque sensing systems, defining accurate sensing requirements is critical to ensure reliable performance evaluation of the axial flux machine. The selection of sensors such as strain gauges and Hall-effect sensors must consider several key parameters, including bandwidth, measurement accuracy, thermal stability, and mechanical integration. These factors directly influence the quality of the acquired data and, consequently, the accuracy of torque, speed, and efficiency calculations.

This section outlines the sensing requirements for both strain gauge and Hall-effect sensors, highlighting their operational limits and design considerations within the system.

Strain Gauge Sensor

The strain gauge is used to measure mechanical deformation caused by torque. Since torque variations can be either steady or dynamic, the sensor must be selected and configured to capture both conditions accurately. Additionally, because strain gauges are highly sensitive to environmental conditions, proper signal conditioning and mounting are essential.

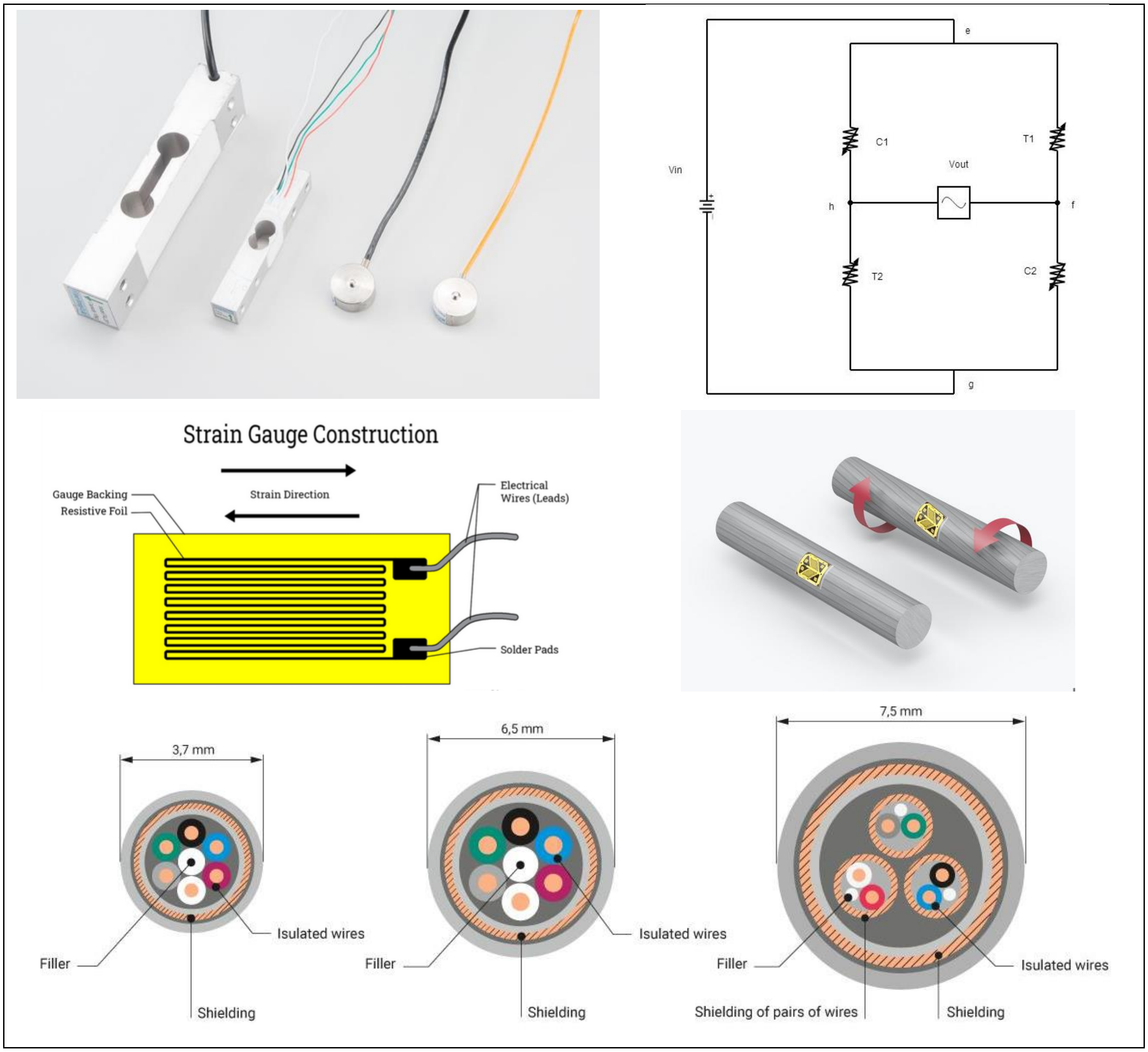

Figure 52: Strain Gauge Sensor

The Strain Guage use Wheatstone bridge pattern which is four element and the output voltage can be determine using the formula; And the output voltage connect to HX711 Interface Module

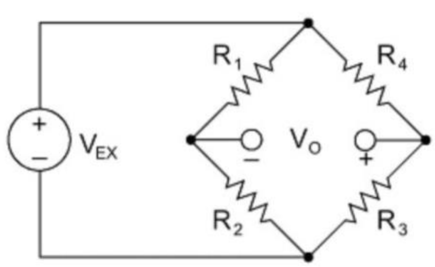

$$V_o = \left(\frac{R_3}{R_3+R_4} - \frac{R_2}{R_1+R_2}\right) * V_{EX}$$

Figure 53: Strain Gauge Sensor Output Voltage

Key Requirements:

1. Bandwidth:
   The required bandwidth depends on the nature of torque variation:
   - Steady-state operation: 10–50 Hz is sufficient.
   - Dynamic torque analysis: 200–500 Hz is required for accurate transient response.

2. Accuracy:
   Torque measurement accuracy directly affects power and efficiency.
   - Target accuracy: ±1% Full Scale (FS)
   - Use of HX711 interface module improves resolution and signal amplification in Wheatstone bridge configurations

3. Temperature Drift:
   Sensitive to temperature changes due to resistance variation.
   - Using a full Wheatstone bridge helps compensate for thermal effects
   - Acceptable drift: ≤ 0.1% FS/°C

4. Mounting Constraints:
   - Must be installed on a clean, flat surface
   - Use appropriate adhesives for strong bonding
   - Shielded wiring is required to minimize electrical noise and measurement errors

Hall-Effect Sensor 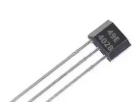

The Hall effect sensor is an electronic device used to detect magnetic fields. It operates based on the Hall effect principle, which was discovered by Edwin Hall in 1879. These sensors are widely used in modern electronic systems due to their reliability, small size, and ability to provide non-contact measurement.

The Hall-effect sensor is used for rotor position and speed measurement. It detects magnetic field changes as the rotor magnets pass by, generating signals used for speed estimation and control. Proper selection and placement are crucial for accurate and stable readings.

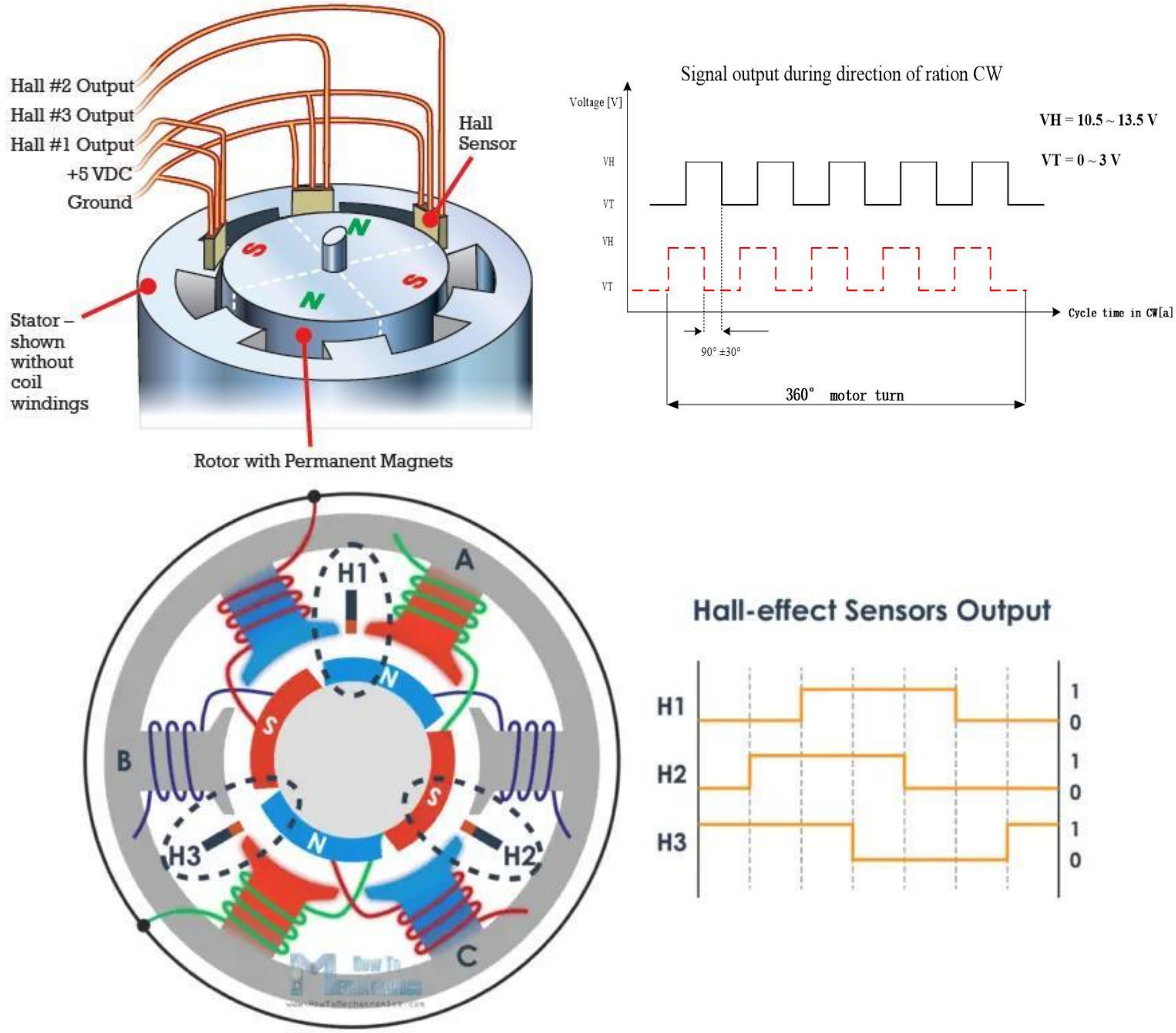

Figure 54: Hall-Effect Sensor

Key Requirements:

1. Bandwidth:
   - Must support detection of maximum rotor speed
   - Sensor frequency response should be at least 10× the maximum electrical frequency
   - Ensures accurate timing and minimizes jitter

2. Accuracy:
    - Speed measurement accuracy requirement: ±0.5% to ±1%
    - This level is sufficient for efficiency and performance evaluation

3. Temperature Drift:
    - Less sensitive compared to strain gauges
    - Typical drift: ≤ 0.05%/°C

4. Mounting Constraints:
    - Precise alignment with rotor magnets is critical
    - Proper air gap distance must be maintained
    - Sensor should be mounted securely to minimize vibration effects and signal noise

Common Applications of Hall Effect Sensor

Hall effect sensors are widely used across multiple fields due to their high accuracy, reliability, and durability. They operate without physical contact, making them ideal for environments where mechanical wear must be minimized. These sensors are commonly found in automotive systems, industrial automation, and modern consumer electronics such as smartphones and portable devices.

General Applications:
1. Automotive systems: Speed detection, crankshaft position sensing
2. Industrial systems: Position and proximity sensing
3. Brushless DC motors: Rotor position detection
4. Current sensing: Measuring electric current without direct contact
5. Security systems: Door position detection

Uses in Smartphones and Portable Devices

Hall effect sensors are widely integrated into smartphones and portable devices to enable a range of smart and energy-efficient functionalities. These sensors allow the device to detect magnetic fields and respond accordingly, which enhances user experience and power management.

For instance, they are used in flip cover detection, where the screen automatically turns on or off when the cover is opened or closed. Additionally, they help in identifying magnetic accessories such as protective cases or attachments. Hall effect sensors also play a key role in compass functionality by detecting the direction of the Earth's magnetic field, which is essential for navigation applications. Furthermore, they contribute to position sensing in certain advanced features, supporting improved interaction and device responsiveness.

In conclusion, the Hall effect sensor is a simple yet powerful device for detecting magnetic fields, offering a reliable and efficient non-contact sensing solution. Its durability, accuracy, and low maintenance requirements make it highly suitable for a wide range of applications, including automotive systems, industrial automation, and consumer electronics such as smartphones.

Moreover, the ability of Hall effect sensors to be integrated into both large-scale systems and compact devices highlights their versatility and importance in modern engineering. As technology continues to advance toward smarter and more automated systems, the role of Hall effect sensors is expected to expand even further, reinforcing their significance in future sensing and control applications.

Table 17: Summary Table of Sensing Requirements

Parameter	Strain Gauge Sensor	Hall-Effect Sensor
Bandwidth	10–50 Hz (steady), 200–500 Hz (dynamic)	≥10× electrical frequency
Accuracy	±1% FS	±0.5% – ±1%
Temperature Drift	≤ 0.1% FS/°C	≤ 0.05%/°C
Mounting Requirements	Flat surface, adhesive, shielding	Precise alignment, air gap, vibration-free

The sensing requirements for both strain gauge and Hall-effect sensors must be carefully defined to ensure accurate torque and speed measurements in the axial flux machine. While strain gauges provide high-resolution torque measurement, they require careful handling of temperature effects and noise. On the other hand, Hall-effect sensors offer robust and stable speed detection with less sensitivity to environmental factors. Together, these sensors form a complementary sensing system that enables reliable performance evaluation and control of the machine.

7.2: Implementation of Embedded Torque Sensing System

In the previous section, we provided a preliminary explanation of the embedded system that will measure the torque values in an axial flux motor. In this section, we will explain the implementation method, the problems we encountered, and how we were able to solve them to achieve the desired results.

First, we will explain about the material we used to make the shaft coupler where we use aluminum because it highly torsional and it useful for the sensor (strain gauge) that we installed on it, and give wide range of reading which increase the Accuracy since accuracy is essential, the variable value obtained from the sensor alone is very small and will also serve as an amplifier.

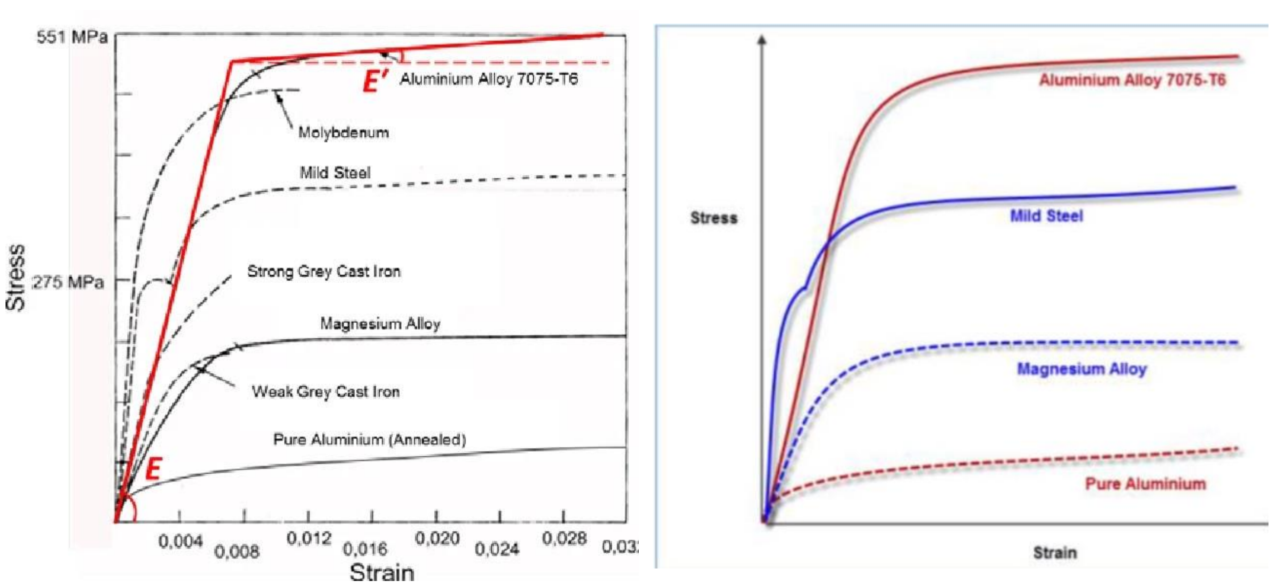

Figure 55: Implementation of Embedded Torque Sensing System

In this graph, the relationship between the applied stress and the resulting strain for different materials is shown. As illustrated in the figure, pure aluminum experiences relatively high strain compared to other materials. Increasing this strain value, in comparison to other materials, provides a positive advantage in determining the torque value, even when the torque is very small at low levels.

Secondly, we use the ESP32 controller due to its high-speed processing capability and its wireless communication feature, which allows data transmission from the controller mounted on the aluminum shaft to another controller that plots the readings.

The Keye studio ESP32 microcontroller acts as the central processing unit of the embedded system, serving as the "brain" that manages inputs, processing, and outputs. It receives input data from sensors, such as strain gauges and Hall effect sensors, which measure parameters like torque and speed. This data is then processed using embedded software to calculate important performance metrics, including torque and efficiency of the machine. The ESP32 is particularly suitable for this application due to its high processing speed and built-in wireless communication capabilities, allowing real-time data transmission and monitoring.

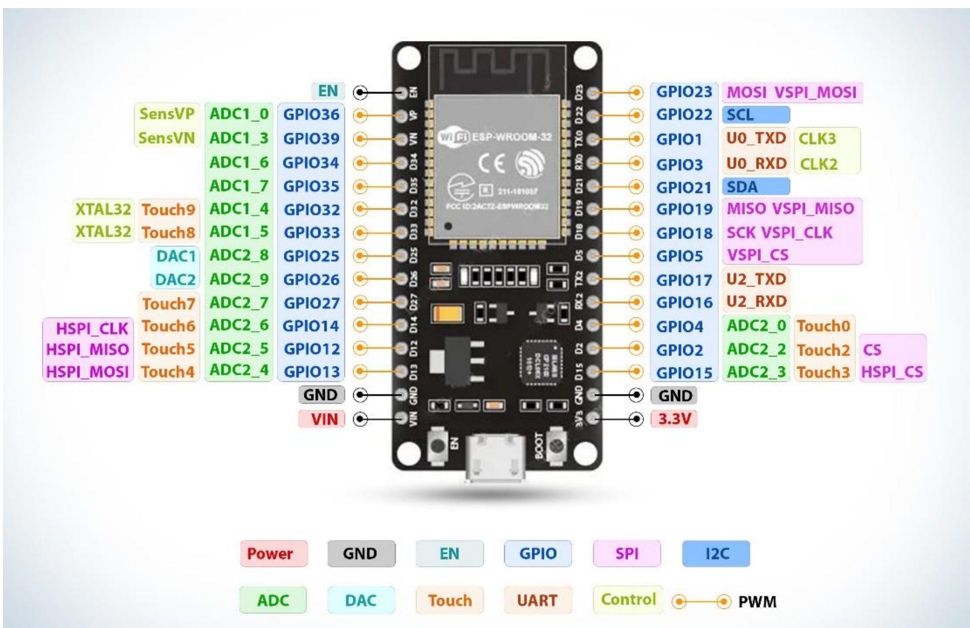

Figure 56: Keye studio ESP32 microcontroller

The sensing system consists of four strain gauges connected in a Wheatstone bridge configuration and mounted at a 45-degree angle. One sensor is positioned at +45°, while the corresponding sensor is placed at −45°. In this configuration, when one sensor contracts, the other expands; the expanding sensor experiences an increase in resistance, while the contracting sensor experiences a decrease in resistance, according to the resistance-strain relationship.

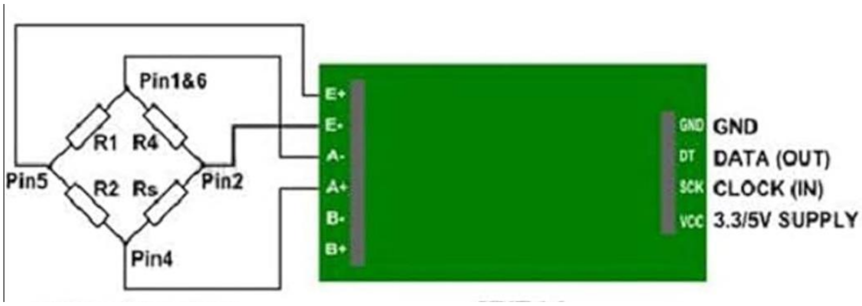

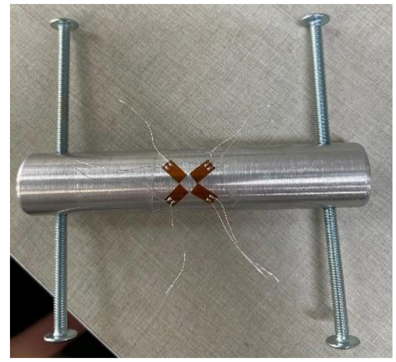

Figure 57: connection of the sensors to the amplifier/analog-to-digital converter

This image illustrates the connection of the sensors to the amplifier/analog-to-digital converter. On the sensor side, we use the terminals E+, E−, A+, and A−. The E+ input represents the positive excitation, while E− represents the negative excitation, which can also be considered as ground. The A+ terminal represents the positive differential input, and A− represents the negative differential input. The A channel is used for high accuracy and high amplification, up to 128 times. The resistors shown represent the strain gauge sensors mounted on the aluminum shaft coupler.

On the controller side, there are four output connections: VCC, which supplies power to the HX711 module, and ground. The DT pin is used to transmit data to the controller for processing and converting it into real values, while the SCK (clock input) receives pulses from the controller to enable data transmission from the DT pin.

In the controller coding, we use the HX711.h library to obtain the raw data. A known torque is applied to the shaft coupler using a torque wrench, and the map () function in the Arduino IDE is used to convert the raw readings into actual torque values from the strain gauge sensor. For wireless communication, we use ESP-NOW to transmit the data between devices.

The HX711 interface module is used to read signals from the strain gauge arranged in a Wheatstone bridge configuration and convert the analog signal into digital data. This digital output is then sent to the microcontroller, enabling accurate processing and measurement of the applied torque.

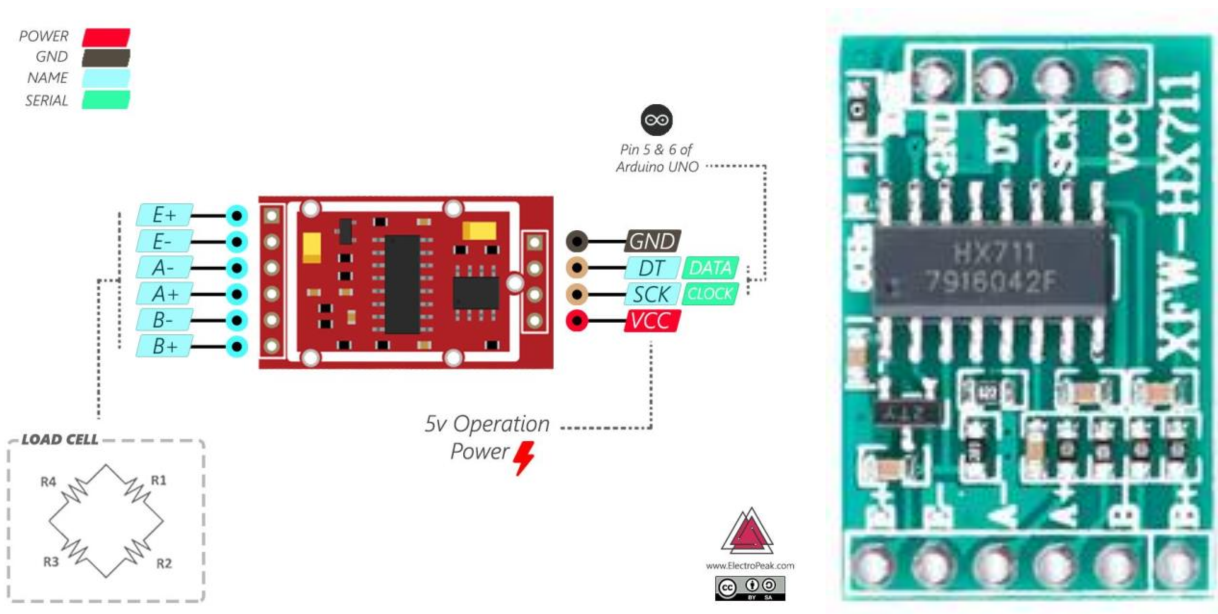

Figure 58: HX711 interface module

The following images illustrate the final assembled Embedded Torque Sensing System after the complete integration of mechanical and electronic components. The system includes the strain gauges mounted on the aluminum shaft coupler, connected to the HX711 amplification module, and interfaced with the ESP32 microcontroller. The setup also shows the proper wiring, sensor placement, and overall structural arrangement used to ensure accurate torque measurement and reliable data transmission. These images represent the practical implementation of the designed sensing system in its operational form.

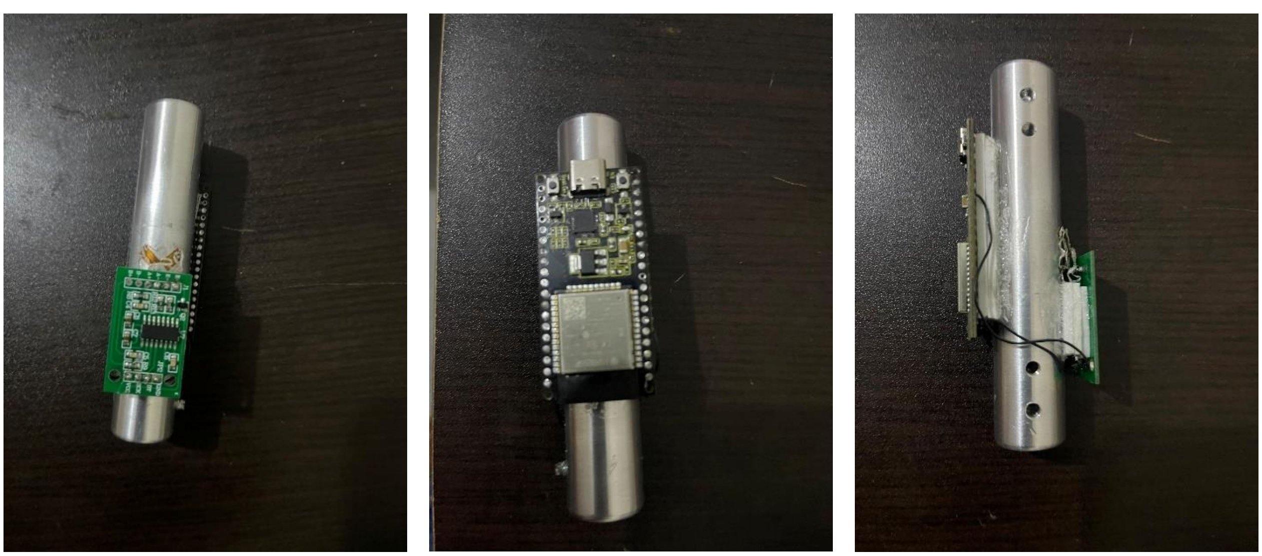

Figure 59: Embedded Torque Sensing System

Raw Data Acquisition and Calibration Process

1. Raw Value Initialization

First, the initial raw data value is recorded, which represents the no-load condition of the shaft (i.e., torque equals zero). The measured raw value at zero torque was 314666, while the recorded value when applying 20 N·m torque was 1880569.

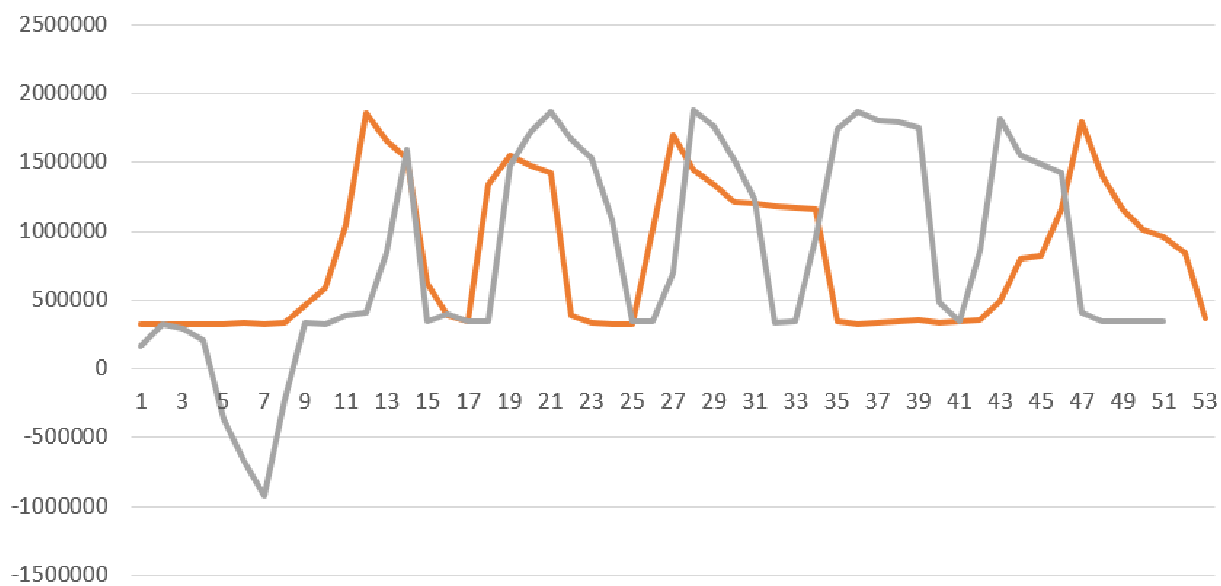

Figure 60: Raw Value Initialization

2. Raw Data Measurement and Scaling

This plot represents the raw data collected when a torque of 20 N·m is applied using a torque wrench. The torque is applied multiple times to ensure that the readings are consistent and close to each other. The maximum recorded value at 20 N·m is selected for accuracy.

```
T =map(R, 314666, 1880569, 0, 20000);
T=T/1000;
```

After that, the map () function in the Arduino IDE is used to scale the raw data into actual torque values. In this mapping process, the value 314666 corresponds to 0 N·m, and the value 1880569 corresponds to 20000 (which is later divided by 1000 to obtain the value in N·m).

3. Code for Raw Data Acquisition

The following code is used to obtain the raw data values from the sensor through the HX711 module, which reads the signal from the strain gauge and sends it to the microcontroller for processing.

```
#include "HX711.h"
#define DT  4
#define SCK 12
float R ;
float T;
HX711 scale;

void setup() {
  Serial.begin(115200);
  scale.begin(DT, SCK);
  delay(1);
  scale.tare();
  Serial.println("Tare done!");
  scale.set_scale(1.0);
}

void loop() {
  R=scale.read_average(10);
  T =map(R, 314666, 1880569, 0, 20000);
  T=T/1000;
  if(T<0)T*-1;
Serial.print(Torque=);
Serial.print(T);
Serial.println("N.m");
  delay(1);
  scale.tare();

}

```

Figure 61: Code for Raw Data Acquisition

The system uses wireless communication between two ESP32 microcontrollers. One ESP32 is mounted on the shaft to read data from the torque sensing system, while the other ESP32 is used as a receiver to monitor the data and plot the readings in real time.

To establish the wireless connection, the first step is to obtain the MAC address of the transmitting controller using a simple code. The MAC address used in this setup is F4:65:0B:C2:58:18.

```
#include "WiFi.h"

void setup() {

  // Setup Serial Monitor
  Serial.begin(115200);

  // Put ESP32 into Station mode
  WiFi.mode(WIFI_MODE_STA);

  // Print MAC Address to Serial monitor
  Serial.print("MAC Address: ");
  Serial.println(WiFi.macAddress());
}

void loop() {
```

The receiver code is then implemented on the second ESP32 to receive the transmitted data from the shaft coupler torque sensing system, enabling real-time monitoring and visualization of the measured values.

```
#include <WiFi.h>
#include <esp_now.h>

typedef struct {
  float torque;
} Message;

Message receivedData;

void OnDataRecv(
  const esp_now_recv_info_t *info,
  const uint8_t *incomingData,
  int len
) {
  memcpy(&receivedData, incomingData, sizeof(receivedData));

  Serial.print("Received Torque = ");
  Serial.print(receivedData.torque);
  Serial.println(" N.m");
}

void setup() {
  Serial.begin(115200);

  WiFi.mode(WIFI_STA);

  Serial.print("Receiver MAC Address: ");
  Serial.println(WiFi.macAddress());

  if (esp_now_init() != ESP_OK) {
    Serial.println("ESP-NOW Init Failed");
    return;
  }

  esp_now_register_recv_cb(OnDataRecv);

  Serial.println("Receiver Ready");
}

void loop() {}
```

The strain gauge sensors, along with the HX711 module and the transmitter code, are used to measure the applied torque and transmit the data wirelessly to the receiving system for further processing and visualization.

```
#include <WiFi.h>
#include <esp_now.h>
#include "HX711.h"
#define DT 4
#define SCK 12
HX711 scale;
float R;
float T;
typedef struct {
  float torque;
} Message;
Message data;
uint8_t receiverAddress[] = {0xF4, 0x65, 0x0B, 0xC2, 0x58, 0x18};
void setup() {
  Serial.begin(115200);
  scale.begin(DT, SCK);
  delay(100);
  scale.tare();
  scale.set_scale(1.0);
  WiFi.mode(WIFI_STA);
  if (esp_now_init() != ESP_OK) {
    Serial.println("ESP-NOW Init Failed");
    return;
  }
  esp_now_peer_info_t peerInfo = {};
  memcpy(peerInfo.peer_addr, receiverAddress, 6);
  peerInfo.channel = 0;
  peerInfo.encrypt = false;
  if (esp_now_add_peer(&peerInfo) != ESP_OK) {
    Serial.println("Failed to add peer");
    return;
  }
  Serial.println("Transmitter Ready");
}
void loop() {
  R = scale.read_average(10);
  T = map((long)R, 314666, 1880569, 0, 20000);
  T = T / 1000.0;
  if (T < 0)
    T = -T;
  data.torque = T;
  esp_err_t result = esp_now_send(
    receiverAddress,
    (uint8_t *)&data,
    sizeof(data)
  );
  if (result == ESP_OK) {
    Serial.print("Sent Torque = ");
    Serial.print(T);
    Serial.println(" N.m");
  } else {
    Serial.println("Send Error");
  }
  delay(100);
}
```

During the implementation of the embedded torque sensing system, several challenges were encountered.

First, the initial readings obtained from the amplifier and analog-to-digital converter showed multiple values even when the torque was zero (at rest), leading to instability in the baseline measurement.

Secondly, even when the system appeared to operate with a fixed initial value, a noticeable drift occurred in the readings, where the values gradually increased without applying any torque to the system.

Thirdly, the raw output values were significantly high, indicating a large deviation from the zero reference before proper calibration. This negatively affected the overall performance and accuracy of the system.

All these issues were resolved by removing and replacing the strain gauge sensors with new ones, as well as changing the amplifier and analog-to-digital converter. Additionally, the amplifier was reconnected to the microcontroller using thin and flexible wires to reduce noise and interference. After these modifications, the system provided stable and accurate readings following proper calibration.

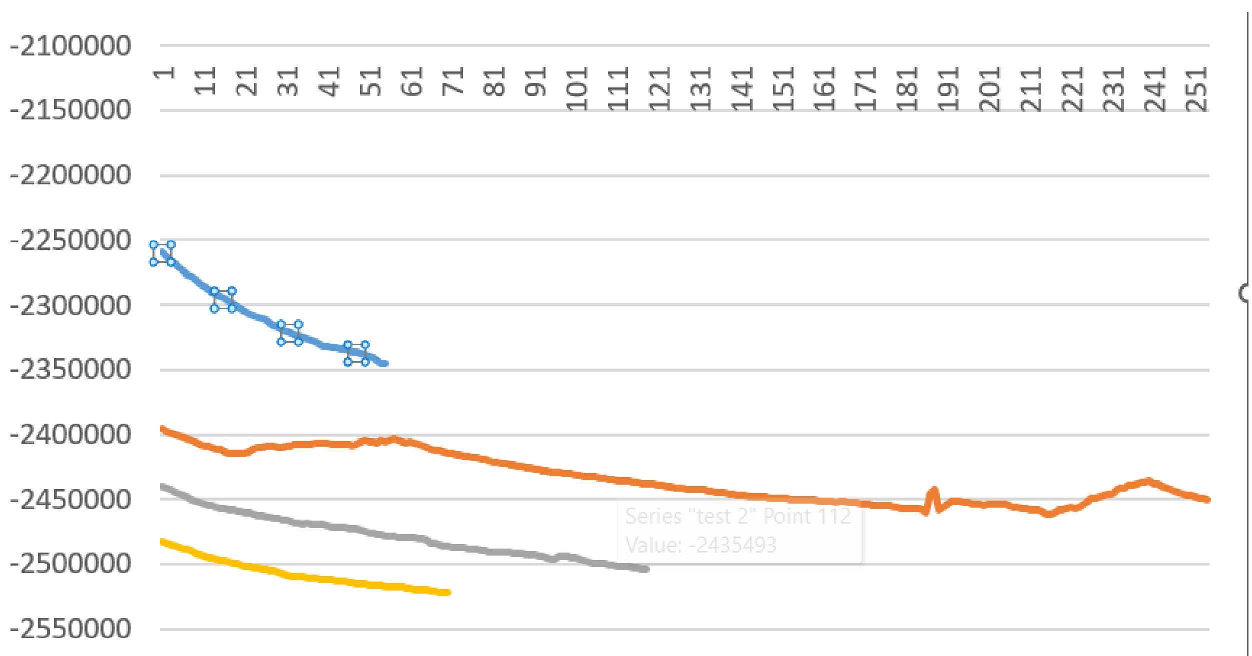

Figure 62: stable and accurate readings following proper calibration

This graph shows that the initial value is not consistent, as the starting point of each curve is different. This variation affects the system calibration because it becomes difficult to determine the exact value corresponding to zero torque. Additionally, it can be observed that some curves, such as the blue one, drift downward even without any applied torque, resulting in a continuous shift in the raw values. This behavior negatively affects the readings when torque is applied and impacts the accuracy of the actual torque measurement.

Furthermore, the initial raw values are extremely high, exceeding two million, which is far from the expected zero reference. Ideally, the initial value should be much closer to zero or at least significantly lower, similar to the value obtained in the first attempt, as shown in the raw readings graph, where the value was approximately three hundred thousand. This is considered a more reasonable baseline. After proper calibration, the system produced highly accurate readings, with no significant effects that would limit the system's performance or measurement accuracy.

In conclusion, the implementation of the embedded torque sensing system demonstrates a practical and effective approach for real-time torque measurement in axial flux machines. By integrating strain gauge sensors in a Wheatstone bridge configuration with the HX711 amplification module and the ESP32 microcontroller, the system achieves accurate signal acquisition and processing.

Despite initial challenges such as signal drift, unstable zero readings, and high raw values, these issues were successfully mitigated through proper sensor replacement, improved wiring techniques, and careful calibration. The use of wireless communication further enhances the system by enabling real-time monitoring and data visualization. Overall, the developed system provides reliable and precise torque measurements, making it suitable for performance evaluation and efficiency analysis of the machine.

Following the successful implementation of the embedded torque sensing system, it is essential to evaluate alternative sensing technologies that can be used for torque measurement in axial flux machines. This section presents a comparative analysis of different sensor technologies, including strain gauges, Hall-effect-based methods, and other advanced sensing approaches.

Each technology is assessed based on key performance factors such as accuracy, sensitivity, response time, cost, and ease of integration. The objective is to justify the selection of the most suitable sensing method for the application while highlighting the advantages and limitations of each approach.

7.3: Candidate Sensor Technologies: Comparison and Selection

The selection of an appropriate sensing technology is a critical step in the design of a reliable torque measurement system for axial flux machines. Several sensing approaches can be considered, each with different operating principles, advantages, and limitations. Among the most commonly used technologies are strain gauge–based sensors, Hall-effect sensors, optical sensing methods, and magnetoelastic sensors. The choice between these technologies depends on factors such as measurement accuracy, sensitivity, environmental robustness, cost, and ease of integration into the mechanical structure.

Strain gauge–based sensing is one of the most widely adopted techniques for torque measurement due to its high accuracy and direct relationship between mechanical deformation and electrical signal output. In this method, strain gauges are mounted on the shaft or coupler, forming a Wheatstone bridge that converts small deformations caused by torque into measurable voltage changes. This approach provides precise and stable measurements when properly calibrated, making it highly suitable for experimental and embedded applications. However, it requires careful installation, temperature compensation, and signal amplification, which may increase system complexity.

Hall-effect sensors offer an alternative non-contact measurement method by detecting changes in magnetic fields generated by rotational elements. These sensors are advantageous in environments where mechanical contact is undesirable, as they reduce wear and maintenance requirements. They are generally easier to install and more robust against mechanical fatigue. Nevertheless, their accuracy is typically lower compared to strain gauge systems, and they may be affected by external magnetic interference, which can introduce measurement errors in sensitive applications.

Optical sensing techniques, including encoders and fiber-optic sensors, provide high-resolution measurements and fast response times. These systems are particularly effective in applications requiring precise angular displacement or speed measurements, which can be indirectly related to torque. Despite their advantages, optical systems tend to be more expensive and sensitive to environmental conditions such as dust, vibration, and misalignment, limiting their practicality in certain industrial or embedded setups.

Magnetoelastic sensors represent another non-contact approach, where torque-induced stress alters the magnetic properties of a material, and this variation is measured to estimate torque. These sensors are durable and suitable for harsh environments, offering good long-term stability. However, they often require specialized materials and calibration procedures, which can increase implementation cost and complexity.

To provide a clearer comparison, the following table summarizes the key characteristics of these sensing technologies:

Table 18: key characteristics of these sensing technologies

Technology	Accuracy	Contact Type	Cost	Complexity	Environmental Sensitivity
Strain Gauge	High	Contact	Low–Medium	Medium	Medium
Hall-Effect	Medium	Non-contact	Low	Low	High (magnetic noise)
Optical Sensors	High	Non-contact	High	High	High (dust, alignment)
Magnetoelastic	Medium–High	Non-contact	Medium–High	High	Low–Medium

Based on this comparative analysis, the strain gauge–based sensing method was selected for the implemented system. This choice is justified by its superior accuracy, direct measurement capability, and suitability for calibration in controlled experimental conditions.

Although it requires additional signal conditioning and careful installation, these challenges can be effectively managed, as demonstrated in the previous section. Consequently, the strain gauge approach provides the most reliable and precise solution for torque measurement in the developed embedded system.

7.4: Mechanical Integration of Sensors in Axial Flux Topology

The mechanical integration of the sensing system within the axial flux machine topology represents a crucial aspect of the overall system design, as it directly affects measurement accuracy, reliability, and system durability. Due to the unique geometry of axial flux machines, where the torque is transmitted along a relatively compact axial structure, careful consideration must be given to the placement and mounting of the sensing elements to ensure accurate strain transfer and minimal disturbance to the mechanical behavior of the system.

In this work, the strain gauges were integrated onto the shaft coupler, which serves as the primary torque transmission element between the driving and driven components. This location was selected because it experiences measurable torsional deformation under load while remaining accessible for sensor installation. The strain gauges were arranged in a Wheatstone bridge configuration to maximize sensitivity and compensate for temperature variations and unwanted mechanical effects. Proper surface preparation of the coupler, including cleaning and polishing, was essential to ensure strong adhesion of the gauges and accurate strain transfer.

The routing of electrical connections from the rotating shaft to the stationary data acquisition system posed an additional design challenge. To address this, thin and flexible wires were used to connect the strain gauges to the signal conditioning circuit, minimizing mechanical resistance and reducing the influence on shaft dynamics. These wires were carefully secured to avoid fatigue or damage during operation. Furthermore, the compact nature of the axial flux topology required that all components, including the HX711 amplifier and the ESP32 microcontroller, be arranged in a manner that maintains system balance and avoids introducing vibrations or misalignment.

Another important consideration was the protection of the sensing elements from environmental and operational factors such as vibration, electromagnetic interference, and mechanical stress concentrations. Protective coatings and proper insulation were applied to the strain gauges and wiring to enhance durability and ensure stable performance over time. Additionally, the integration design ensured that the sensing system did not significantly alter the stiffness or mass distribution of the shaft, preserving the original mechanical characteristics of the machine.

Overall, the successful mechanical integration of the sensing system within the axial flux topology demonstrates that accurate torque measurement can be achieved without compromising the structural integrity or performance of the machine. The chosen integration approach provides a balanced solution between measurement precision, mechanical compatibility, and system robustness, making it suitable for experimental and practical applications.

7.5: Signal Conditioning, Calibration, and Compensation Techniques

Accurate torque measurement in embedded systems relies heavily on proper signal conditioning, calibration, and compensation techniques. Since the output of strain gauges is inherently very small and highly sensitive to external influences, it is necessary to process and refine the signal before it can be reliably interpreted. In this system, the signal obtained from the strain gauge Wheatstone bridge is first amplified and digitized using the HX711 module, which provides high-resolution analog-to-digital conversion suitable for low-level signals.

Signal conditioning plays a fundamental role in improving the quality of the measured data. The raw signal obtained from the sensor is typically affected by noise, environmental disturbances, and minor mechanical vibrations. The HX711 module helps reduce noise through internal filtering and amplification; however, additional stabilization is achieved through software techniques. Repeated measurements are taken and compared to ensure consistency, and unstable readings are discarded. This approach improves the reliability of the acquired data and minimizes the effect of transient fluctuations.

Calibration is a critical step to establish a relationship between the raw sensor output and the actual torque values. In this implementation, calibration was performed by first determining the initial raw value corresponding to zero torque, followed by applying a known torque using a torque wrench. The corresponding raw readings were recorded, and a mapping function was used to convert the raw data into torque values. This linear mapping ensures that the system can accurately translate sensor output into meaningful physical measurements. The calibration process significantly reduces measurement errors and aligns the system output with real-world values.

Compensation techniques are essential to address issues such as drift, offset variation, and environmental effects. During the implementation, it was observed that the system exhibited changes in the initial value and gradual shifts in the readings even without applied torque. These issues were mitigated by improving sensor quality, optimizing wiring connections using thin and flexible conductors, and ensuring stable mechanical mounting. Additionally, recalibration was performed after hardware modifications to ensure consistency.

The combination of proper signal conditioning, accurate calibration, and effective compensation techniques results in a stable and reliable torque sensing system. These processes ensure that the system maintains high accuracy despite inherent sensor limitations and external disturbances, making it suitable for precise performance evaluation in axial flux machine applications.

7.6: Embedded Data Acquisition and Wireless Communication Architecture

The embedded data acquisition and wireless communication architecture form the backbone of the torque sensing system, enabling real-time measurement, processing, and transmission of data. This architecture is designed to ensure reliable acquisition of sensor signals from the rotating shaft while allowing seamless communication with an external monitoring unit. The system is based on two ESP32 microcontrollers, where one is mounted on the rotating shaft to acquire sensor data, and the other is used as a receiver for monitoring and visualization.

The data acquisition process begins with the strain gauge sensors, whose signals are first conditioned and digitized using the HX711 module. The processed digital data is then read by the ESP32 microcontroller located on the shaft. Due to the rotating nature of the system, it is not practical to use wired communication; therefore, a wireless communication protocol is implemented. The ESP32 provides built-in Wi-Fi capabilities, which are utilized to transmit the acquired data to a second ESP32 acting as a receiver.

Establishing wireless communication requires identifying the unique MAC address of the receiver ESP32. This address is used to configure a direct communication link between the two devices, ensuring that the transmitted data reaches the intended destination. Once the connection is established, the transmitter continuously sends torque data packets, which are received, decoded, and processed by the receiver unit. The received data is then displayed and plotted in real time, allowing continuous monitoring of the system performance.

The architecture is designed to ensure low latency and reliable data transfer, which are essential for accurate real-time analysis. Additionally, the use of two dedicated microcontrollers separates the tasks of data acquisition and data visualization, improving system efficiency and stability. This distributed design also minimizes the computational load on each unit and enhances overall system responsiveness.

Overall, the implemented embedded architecture provides a robust and efficient solution for real-time torque measurement in a rotating system. By combining accurate data acquisition with reliable wireless communication, the system enables continuous monitoring without physical constraints, making it highly suitable for experimental and practical applications in axial flux machines.

This chapter presented the complete design and implementation of an embedded torque sensing system tailored for axial flux machine applications. The work began with the acquisition of raw sensor data and the development of a reliable method to interpret these values through calibration. The integration of strain gauges with appropriate signal conditioning hardware enabled accurate detection of torque-induced deformation, while the use of the HX711 module ensured high-resolution data conversion suitable for low-level signals.

A detailed evaluation of candidate sensing technologies highlighted the advantages of strain gauge–based methods, particularly in terms of accuracy and direct measurement capability, justifying their selection for this system. The mechanical integration of the sensors within the axial flux topology was carefully designed to ensure effective strain transfer without compromising the structural integrity or dynamic behavior of the system. Furthermore, the implementation addressed practical challenges such as signal drift, offset variation, and environmental influences through proper calibration and compensation techniques.

The chapter also introduced a robust embedded architecture for data acquisition and wireless communication, utilizing dual ESP32 microcontrollers to enable real-time monitoring of torque measurements. This approach eliminated the need for wired connections in a rotating system and provided a flexible and efficient platform for data transmission and visualization.

Overall, the developed system demonstrates a reliable and accurate solution for real-time torque measurement, forming a strong experimental foundation for further system-level analysis and control.

Building upon the successful development of the torque sensing and data acquisition system, the next chapter focuses on how this measured torque information can be actively utilized within the system. Specifically, it introduces the control strategy and the role of torque feedback in enhancing system performance. The integration of real-time torque data into the control loop enables more precise regulation of the machine, improves operational stability, and allows for advanced performance optimization. Consequently, the following chapter, Control Strategy and Torque Feedback Use, explores the methodologies and algorithms used to incorporate torque feedback into the overall control framework.

Chapter Eight

Chapter Eight

Control Strategy and Torque Feedback Use

While electromagnetic design and simulation define the inherent performance capabilities of the proposed machine, this chapter focuses on the control strategy adopted for the axial flux BLDC motor and generator. The objective of this chapter is to present the motor drive topology, inverter requirements, and control approaches used to regulate torque and speed under different operating conditions.

The control system plays a critical role in ensuring stable operation, accurate torque regulation, and efficient energy conversion, particularly when the machine operates as both a motor and a generator across a wide speed and load range.

Unlike open-loop control approaches, the integration of embedded torque feedback enables improved dynamic response, enhanced torque accuracy, and more reliable performance and efficiency evaluation, which are essential for experimental validation and comparative analysis.

Subsections:

Chapter Eight: Control Strategy and Torque Feedback Use

The effective operation of an electrical machine is not solely determined by its electromagnetic design, but also by the control strategy used to regulate its behavior under varying operating conditions. A well-designed control system ensures that the machine delivers the required torque and speed response while maintaining stability and efficiency.

In axial flux BLDC machines, control challenges are influenced by the machine topology, inverter configuration, and operating mode. The selection of an appropriate drive and control strategy is therefore essential to fully exploit the machine's performance capabilities and to enable smooth operation across a wide range of speeds and loads.

This chapter addresses the control architecture of the proposed system, focusing on the interaction between the motor drive, power electronics, and control algorithms. Particular attention is given to the role of feedback signals in improving system response and ensuring accurate torque regulation.

By incorporating torque feedback into the control loop, the system gains enhanced capability for performance monitoring and evaluation. This approach supports more reliable experimental analysis and provides a practical framework for assessing efficiency and dynamic behavior during motor and generator operation.

In addition, the integration of sensing and control elements introduces practical considerations related to signal processing, system delays, and measurement accuracy. These aspects must be carefully addressed to ensure that torque feedback contributes positively to system performance rather than introducing instability or noise. The discussion in this chapter reflects these considerations and demonstrates how control design choices support reliable operation and effective performance evaluation.

8.1: Motor drive topology and inverter requirements

The motor drive system represents the interface between the electrical power source and the axial flux BLDC machine, and plays a central role in regulating torque, speed, and operating mode. The selection of an appropriate inverter topology and switching strategy directly influences current waveform quality, torque ripple, and overall system efficiency.

In the proposed system, a three-phase voltage source inverter (VSI) is employed to drive the axial flux BLDC motor. The inverter is designed to support both motoring and generating operation, enabling controlled power flow under different load and speed conditions. Key design considerations include DC bus voltage level, semiconductor device selection, switching frequency, and current handling capability.

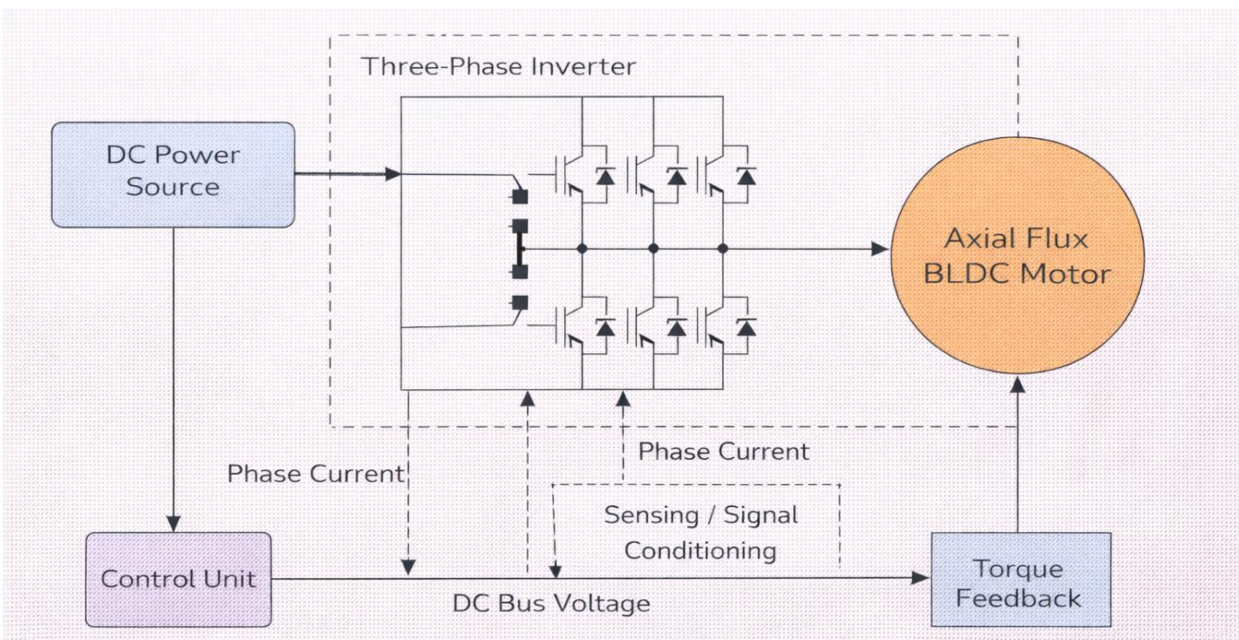

Figure 63: Block Diagram of Motor Drive and Control Architecture

Figure 8.1: Block Diagram of Motor Drive and Control Architecture illustrate the overall motor drive architecture, highlighting the interaction between the DC power source, inverter, axial flux BLDC motor, sensing elements, and control unit. This structure provides a flexible platform for implementing different control strategies and integrating torque feedback.

To ensure accurate current regulation and reliable switching operation, the inverter power stage is designed using a three-leg bridge configuration with insulated gate bipolar transistors (IGBTs) or MOSFETs, depending on voltage and power requirements.

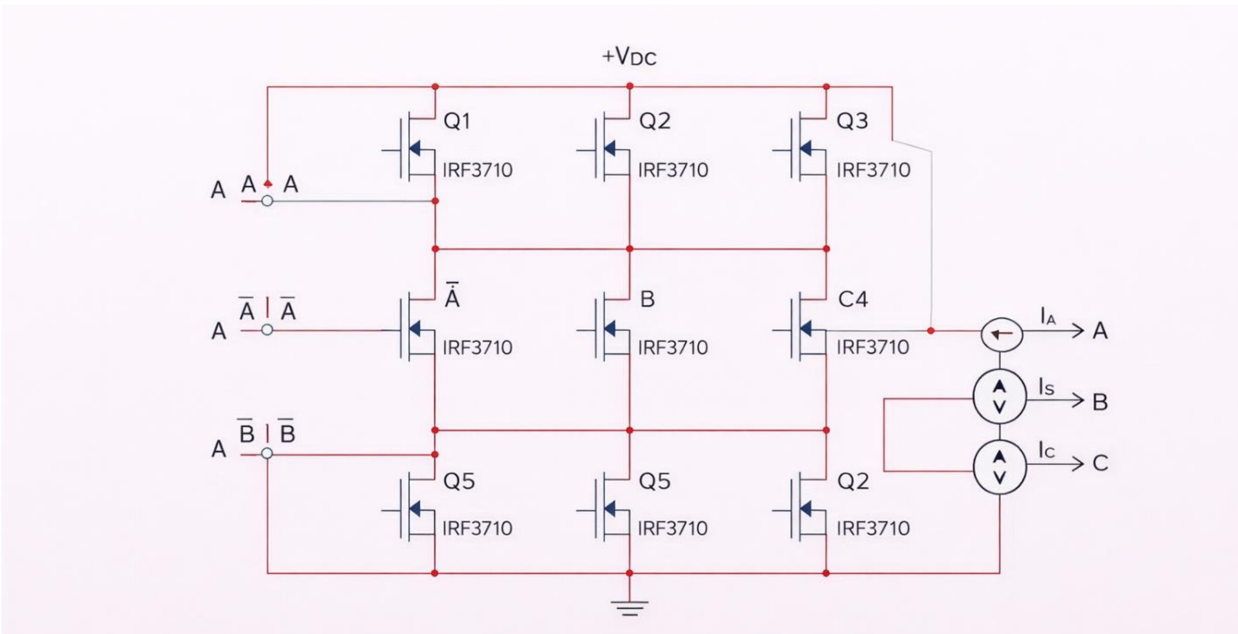

Figure 64: Three-Phase Inverter Power Stage Schematic

Figure 8.2: Three-Phase Inverter Power Stage Schematic (Multisim Schematic) presents the inverter power stage schematic implemented in Multisim. The configuration supports independent phase control and enables precise switching required for BLDC commutation and vector control operation.

This figure presents the three-phase inverter power stage implemented using a full-bridge topology. Six power MOSFETs are arranged in three legs to generate the required phase voltages for BLDC operation. The inverter converts the DC supply voltage into controlled three-phase AC outputs, while current measurement elements are placed at the phase outputs to support feedback-based control. The schematic represents the practical power interface between the DC source and the axial flux BLDC motor.

Accurate current and voltage measurements are required to support closed-loop control and torque estimation.

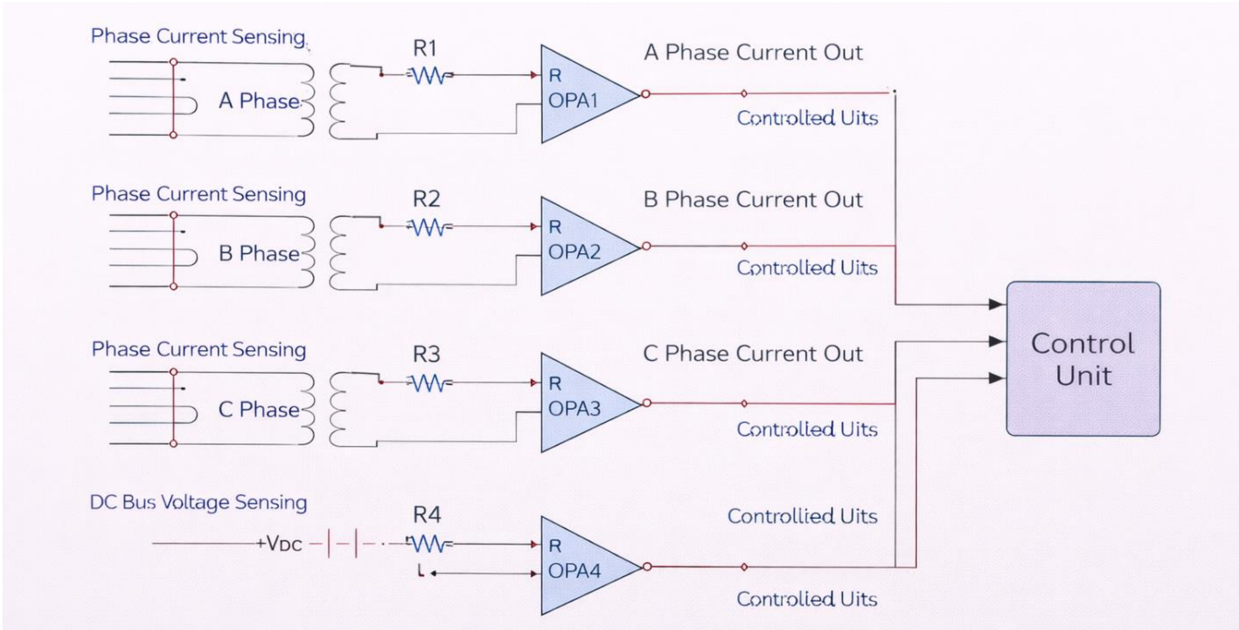

Figure 65: Inverter Sensing and Signal Conditioning Circuit

Figure 8.3: Inverter Sensing and Signal Conditioning Circuit shows the sensing and signal conditioning interface used to acquire phase currents and DC bus voltage. These signals are essential for control execution and performance monitoring.

This figure illustrates the sensing and signal conditioning circuitry used to acquire phase currents and DC bus voltage for control and monitoring purposes. Each phase current is measured independently and conditioned using operational amplifiers to produce scaled and filtered signals compatible with the control unit input range. In addition, the DC bus voltage is sensed and processed to provide real-time feedback for inverter protection and control coordination. This configuration ensures accurate and reliable measurement of electrical quantities required for closed-loop control and performance evaluation.

In summary, the selected motor drive topology and inverter configuration provide a reliable and flexible platform for controlling the axial flux BLDC motor. The integration of power electronics, sensing, and signal conditioning ensures accurate current regulation and safe operation, forming a solid foundation for the control strategies presented in the following section.

8.2: Control approaches for BLDC / PMSM in axial flux machines

The control strategy determines how inverter switching signals are generated to regulate machine torque and speed. Two control approaches are considered in this work: classical trapezoidal commutation for BLDC operation and field-oriented control for comparison.

8.2.1: Classical trapezoidal commutation (BLDC)

Trapezoidal commutation is a widely used control method for BLDC machines due to its simplicity and robustness. In this approach, phase currents are commutated based on rotor position information obtained from Hall sensors or estimated signals.

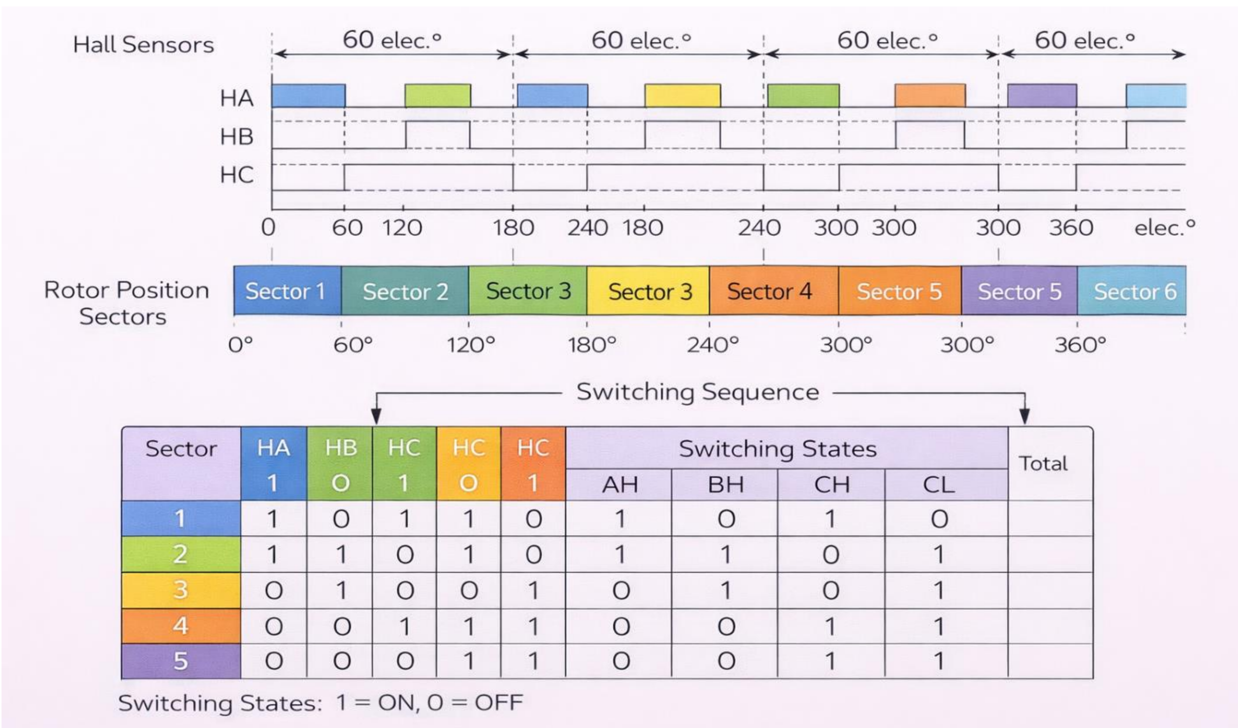

Figure 66: Trapezoidal Commutation Logic and Switching Sequence

Figure 8.4: Trapezoidal Commutation Logic and Switching Sequence illustrates the commutation logic and switching sequence used in classical BLDC control. Each phase conducts for 120 electrical degrees, producing quasi-constant torque under ideal conditions.

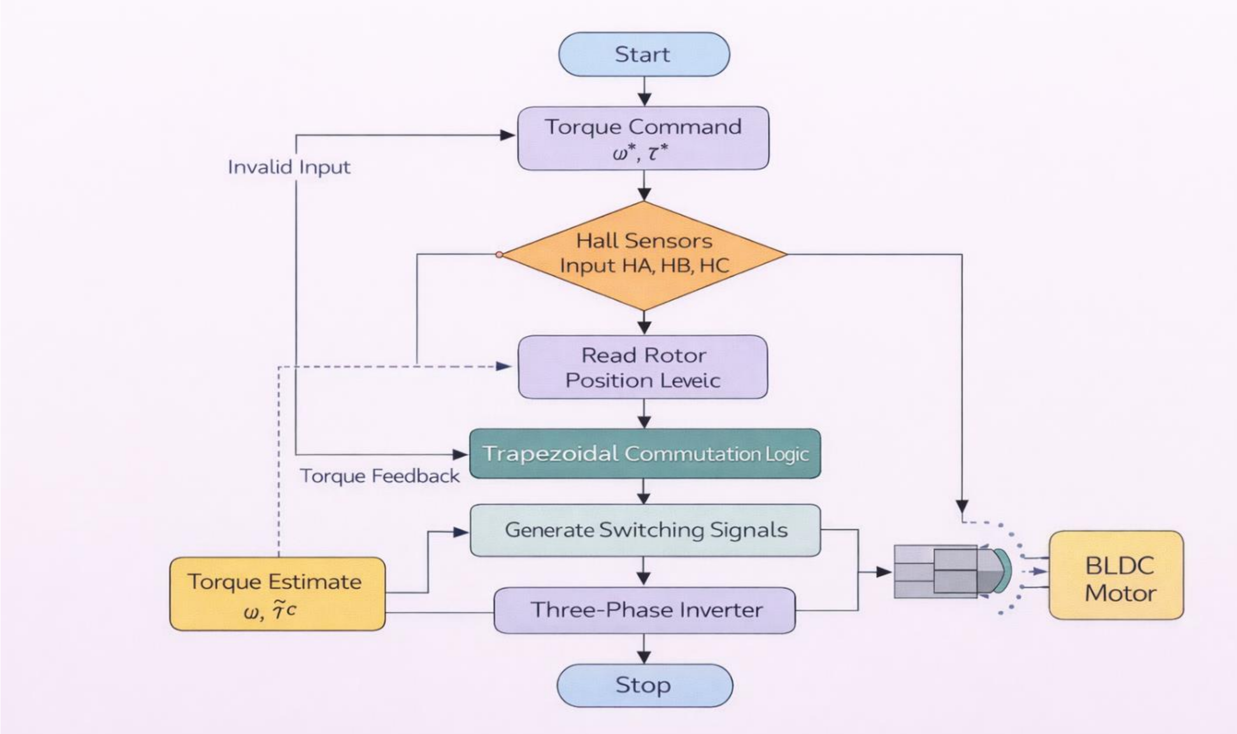

Figure 67: BLDC Control Flowchart

Figure 8.5: BLDC Control Flowchart with Torque Feedback Integration presents the BLDC control flowchart incorporating torque feedback. The measured or estimated torque is used to adjust current reference levels, improving torque accuracy and dynamic response.

In conclusion, classical trapezoidal commutation provides a simple and robust control strategy for BLDC operation, particularly suitable for applications where implementation complexity and computational requirements must be minimized. Its compatibility with Hall sensor feedback and straightforward switching logic makes it an effective baseline control approach, while also serving as a useful reference for evaluating more advanced control techniques.

8.2.2: Field-oriented control (FOC) and vector control

In conclusion, classical trapezoidal commutation provides a simple and robust control strategy for BLDC operation, particularly suitable for applications where implementation complexity and computational requirements must be minimized. Its compatibility with Hall sensor feedback and straightforward switching logic makes it an effective baseline control approach, while also serving as a useful reference for evaluating more advanced control techniques.

Field-oriented control represents an advanced control strategy that enables independent regulation of torque and flux components by transforming stator currents into a rotating reference frame.

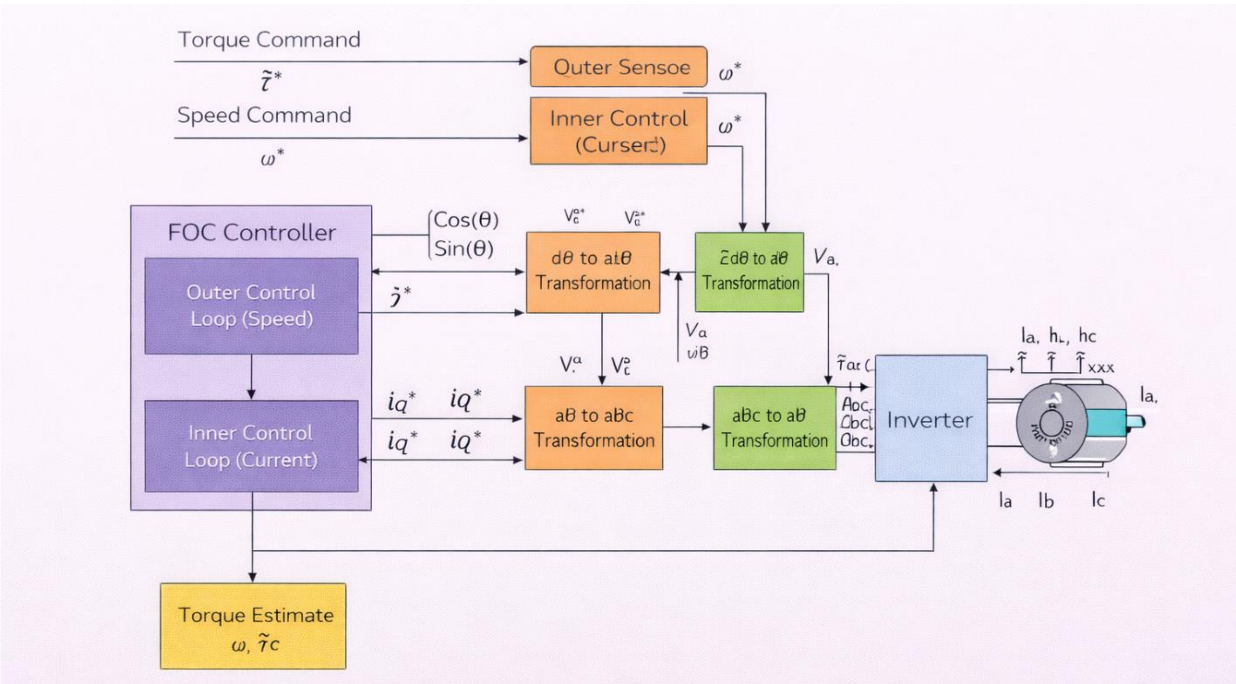

Figure 68: Field-Oriented Control Block Diagram for Axial Flux PMSM

Figure 8.6: Field-Oriented Control Block Diagram for Axial Flux PMSM shows the FOC structure, including coordinate transformations, current regulators, and modulation stage. This approach enables smooth torque production and reduced torque ripple.

To highlight the differences between classical and advanced control strategies, a comparative illustration is presented to contrast trapezoidal BLDC control with field-oriented control. This comparison emphasizes the structural and functional distinctions between the two approaches in terms of control complexity, feedback utilization, and torque regulation capability, providing a clear framework for evaluating their suitability for axial flux machine applications.

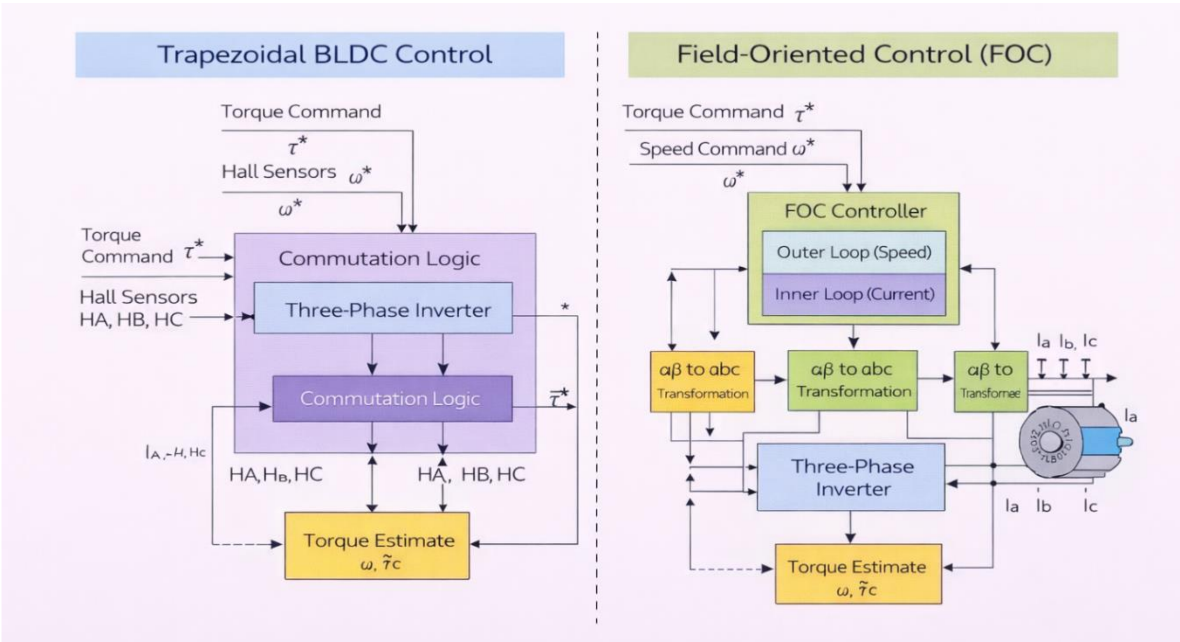

Figure 69: Comparison Between Trapezoidal BLDC Control and FOC

Figure 8.7: Comparison Between Trapezoidal BLDC Control and FOC highlights the key differences between trapezoidal commutation and FOC in terms of current waveform, torque ripple, and control complexity. While FOC offers superior performance, trapezoidal control provides more practical solution for the system.

To provide a clear and structured comparison between the control strategies considered in this work, a summary table is introduced to highlight their key characteristics and performance-related aspects. The comparison focuses on implementation complexity, torque quality, feedback requirements, and computational effort, offering a concise overview to support the selection of an appropriate control approach for the proposed axial flux BLDC motor.

Table 19: Comparison of Control Strategies for Axial Flux BLDC Motor

Feature	Trapezoidal BLDC	FOC / Vector Control
Control complexity	Low	High
Torque ripple	Moderate	Low
Implementation effort	Simple	Advanced
Suitability for torque feedback	Moderate	High
Computational requirement	Low	High

Table 8.1: Comparison of Control Strategies for Axial Flux BLDC Motor summarizes the main characteristics of the two control approaches. The comparison provides a clear justification for selecting trapezoidal BLDC control as the primary strategy, while using FOC as a benchmark for performance evaluation.

This chapter has presented the motor drive topology, inverter requirements, and control strategies used for the axial flux BLDC motor. The integration of torque feedback within the control loop enhances torque accuracy and supports reliable performance and efficiency evaluation. The presented control framework provides a practical and flexible platform for experimental validation, as discussed in the following chapter.

Chapter Nine

Chapter Nine

Experimental Validation & Performance Analysis

Chapter 9: Experimental Validation & Performance Analysis

After completing the design, modeling, and implementation of the axial flux BLDC motor along with the embedded torque sensing system, this chapter focuses on validating the system experimentally. The goal is to evaluate how closely the practical results match the theoretical predictions and simulation outputs, as well as to assess the overall performance of the motor under real operating conditions. This includes electromagnetic validation, torque measurement accuracy, efficiency evaluation, and system behavior under different loads.

Subsections:

9.1: Experimental Setup and Measurement Configuration
9.2: FEM Validation and Electromagnetic Performance
9.3: Embedded Torque Sensor Validation
9.4: Efficiency Mapping and Loss Analysis
9.5: Dynamic Performance and Control Response

9.1: Experimental Setup and Measurement Configuration

This section describes the physical setup used to test and validate the motor and the embedded sensing system. The experimental configuration integrates mechanical, electrical, and embedded subsystems to allow accurate measurement of torque, speed, voltage, and current.

The motor prototype was assembled using the axial flux topology developed in previous chapters, including the rotor with permanent magnets, stator windings, and the aluminum shaft coupler where the strain gauge sensors were mounted. The embedded torque sensing system, based on a Wheatstone bridge configuration and HX711 amplifier, was directly connected to an ESP32 microcontroller for real-time data acquisition and wireless transmission.

To ensure accurate torque measurement, calibration was performed using a torque wrench by applying known torque values to the shaft and mapping the corresponding sensor output. The raw sensor readings were processed and converted into physical torque values using embedded software functions.

In addition to torque measurement, the system included Hall effect sensors to detect rotor position and speed, enabling synchronization with the motor drive and facilitating performance analysis. The ESP32 microcontroller also handled wireless communication between the rotating sensing unit and the monitoring system using ESP-NOW protocol.

The complete setup allowed simultaneous measurement of electrical inputs and mechanical outputs, forming the basis for efficiency calculation and system validation.

Following the initial design representation, a more detailed view of the stator winding distribution and the complete mechanical assembly is presented to clarify the actual implementation of the axial flux machine. These illustrations provide deeper insight into phase arrangement, coil positioning, air gap configuration, and the integration of motor and generator sections within a unified structure.

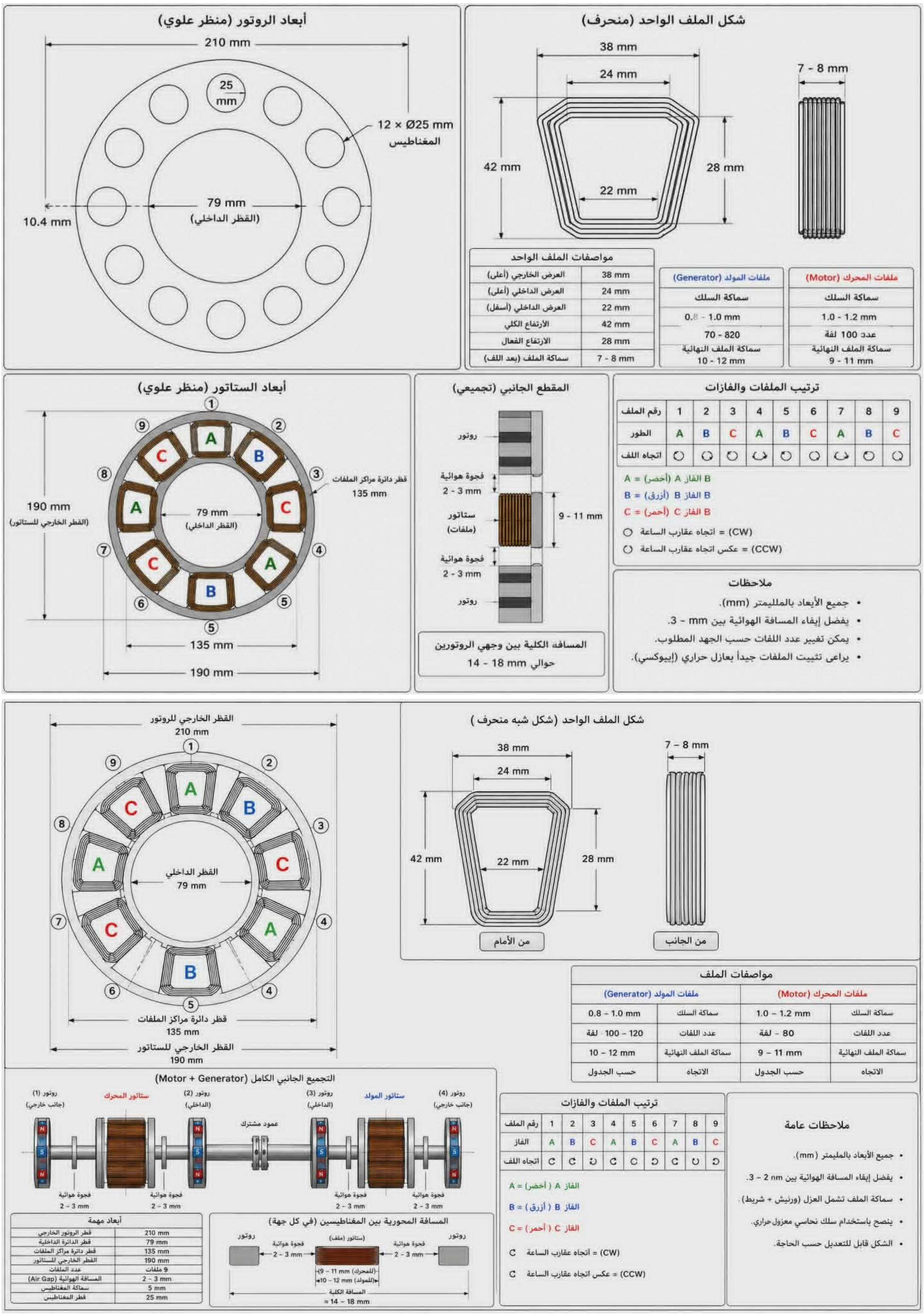

Figure 70: integrated experimental setup used for validation

The figures collectively illustrate both the stator winding distribution and the complete axial flux system assembly, providing a comprehensive view of the motor's structural and electromagnetic design. The stator windings are arranged in a three-phase configuration (A, B, C) and are symmetrically distributed across the slots to ensure balanced electromagnetic performance and smooth torque generation. The air gap between the rotor and stator is maintained within the range of 2–3 mm, representing an optimal balance between maximizing magnetic flux linkage and minimizing mechanical constraints.

In addition, the complete system assembly consists of both motor and generator sections mounted on a common shaft, where each section includes rotor-stator pairs separated by controlled air gaps to ensure efficient electromagnetic interaction. The shared shaft enables direct mechanical coupling, allowing effective evaluation of torque transfer and overall system efficiency. This integrated configuration reflects the practical implementation of the design while emphasizing the importance of proper alignment, spacing, and structural integrity for stable and reliable operation.

To ensure accurate validation of the designed system, the experimental procedure was carried out in a structured sequence that includes mechanical assembly, sensor integration, calibration, and real-time data acquisition. Each step was implemented to guarantee reliable measurements under different operating conditions.

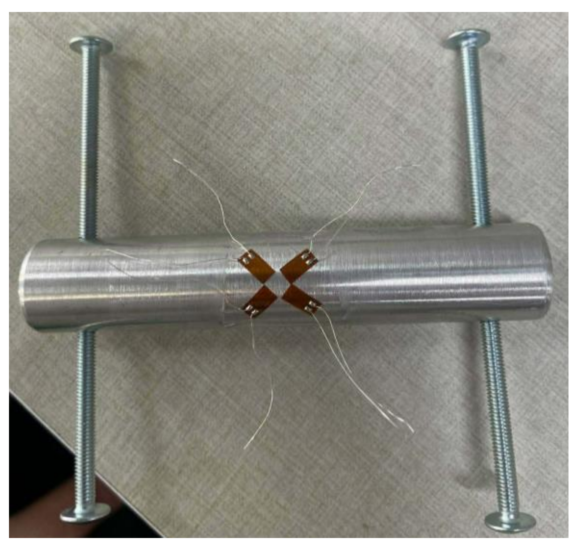

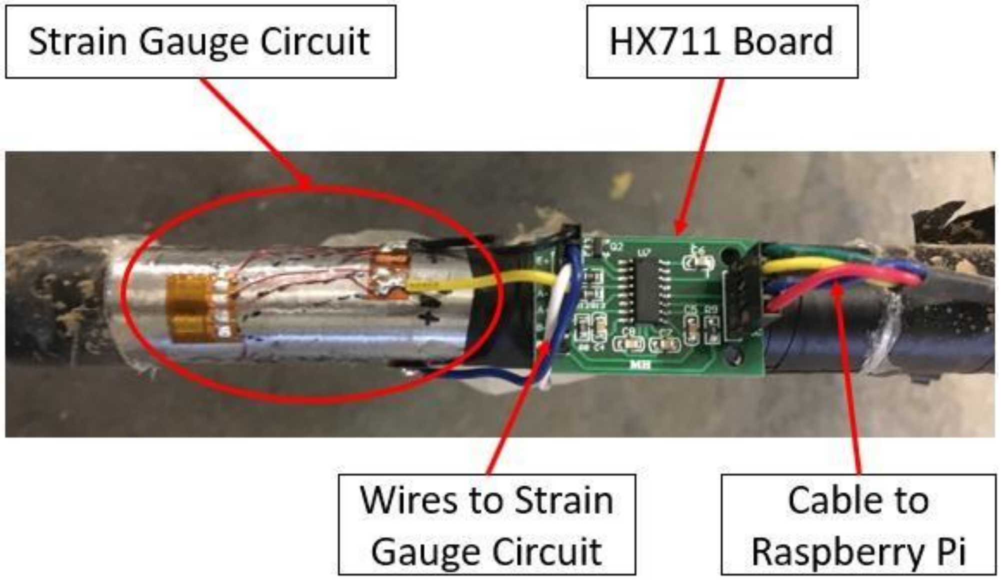

Figure 71: integrated experimental setup used for validation

The figure illustrates the integrated experimental setup used for validation. It highlights the placement of the strain gauges on the shaft coupler, the connection to the HX711 module, and the embedded controller responsible for data acquisition and transmission. The configuration ensures minimal signal noise and reliable measurement under dynamic operating conditions.

Following the integration of the signal conditioning circuit using the HX711 module, the mechanical and electromagnetic design of the system components was developed. The following figures illustrate the step-by-step design process, starting from the initial geometric layout, progressing through phase distribution and structural refinement, and finally reaching the practical implementation of the stator structure.

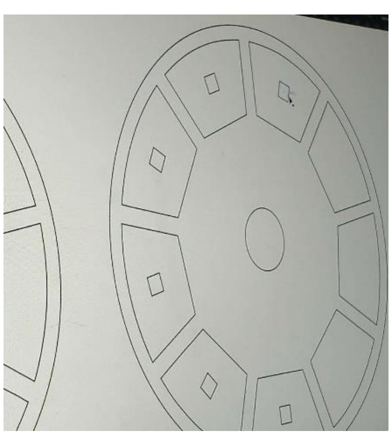

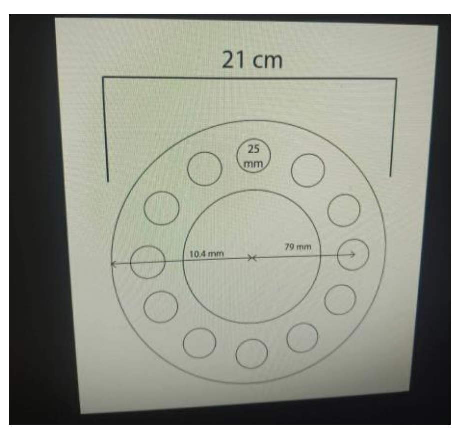

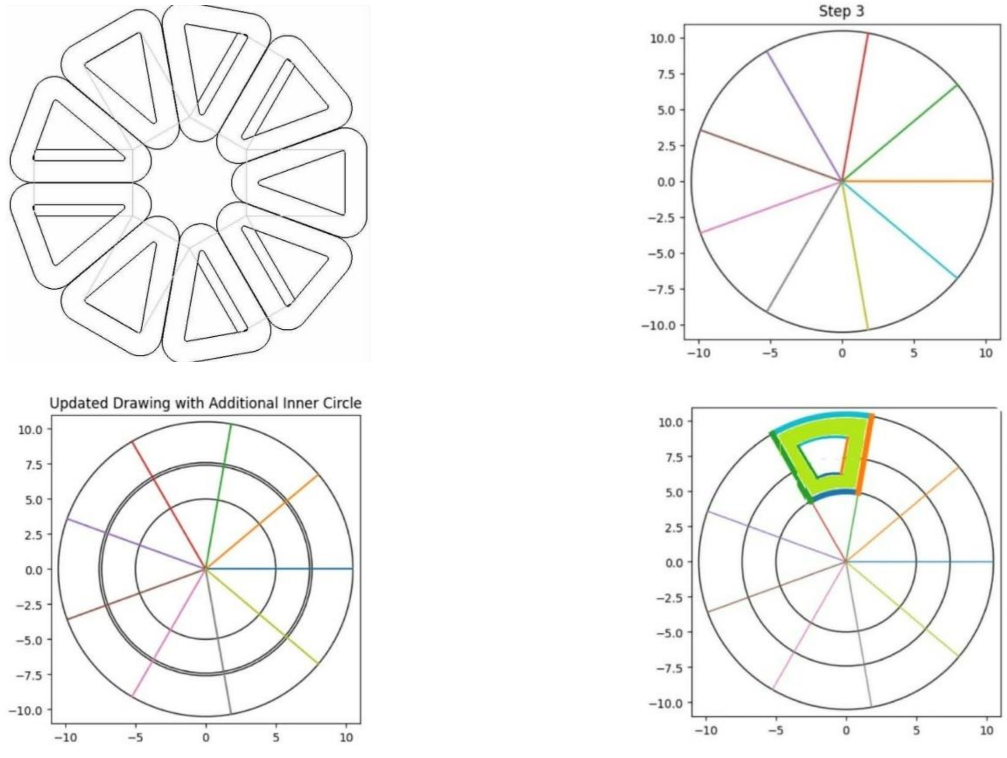

Figure 72: systematic development of the axial flux machine design

These figures collectively demonstrate the systematic development of the axial flux machine design. The progression from basic circular geometry to a fully defined stator structure with slot distribution reflects the design considerations required for proper phase alignment, magnetic symmetry, and manufacturability. This step-by-step approach ensured accurate positioning of the coils and magnets, which directly impacts the overall system performance, and torque generation.

Laser Cutting Machine Interface

CNC laser cutting control panel used for positioning and manufacturing motor components with high precision.

To ensure accurate fabrication of the motor components, a CNC laser cutting machine was utilized during the manufacturing process. The design files were prepared and transferred to the machine interface, where precise positioning and cutting paths were defined. This approach enabled high accuracy in producing the structural parts required for the axial flux system.

Figure 73: Laser Cutting Interface

The laser cutting interface provides a user-friendly environment for controlling the machining process and adjusting key parameters such as cutting paths, speed, and alignment. By using this system, the fabricated components achieve a high level of dimensional accuracy and consistency, which is essential for maintaining proper alignment between the rotor and stator. This precision directly contributes to improved mechanical stability and overall system performance.

Following the development of the measurement system and signal conditioning circuit, the physical construction of the axial flux machine components was carried out. The design process involved several stages, starting from the fabrication of the stator support structure, followed by the positioning of the permanent magnets, and finally the integration of the winding arrangement. The following figures illustrate the practical implementation steps and the evolution of the mechanical and electromagnetic design.

The figures demonstrate the step-by-step construction of the axial flux stator and rotor components. Initially, a custom support structure was fabricated to ensure accurate slot positioning and mechanical stability. Permanent magnets were then arranged in a circular pattern with uniform spacing to achieve a consistent magnetic field distribution.

The use of CNC-based fabrication techniques ensures repeatability and minimizes human error, which is particularly important in prototype development and experimental validation.

Figure 74: step-by-step construction of the axial flux stator and rotor components

Subsequently, the stator windings were installed and secured using insulating and bonding materials to maintain their position during operation. The final assembled structure reflects careful consideration of alignment, spacing, and structural integrity, all of which are critical for ensuring efficient electromagnetic interaction, minimizing losses, and maintaining stable operation under dynamic conditions.

Following the mechanical preparation and magnet placement, the stator winding process was carried out. The coils were manually wound and arranged to match the designed slot distribution of the axial flux configuration. Special attention was given to maintaining symmetry between phases and ensuring consistent spacing between adjacent coils.

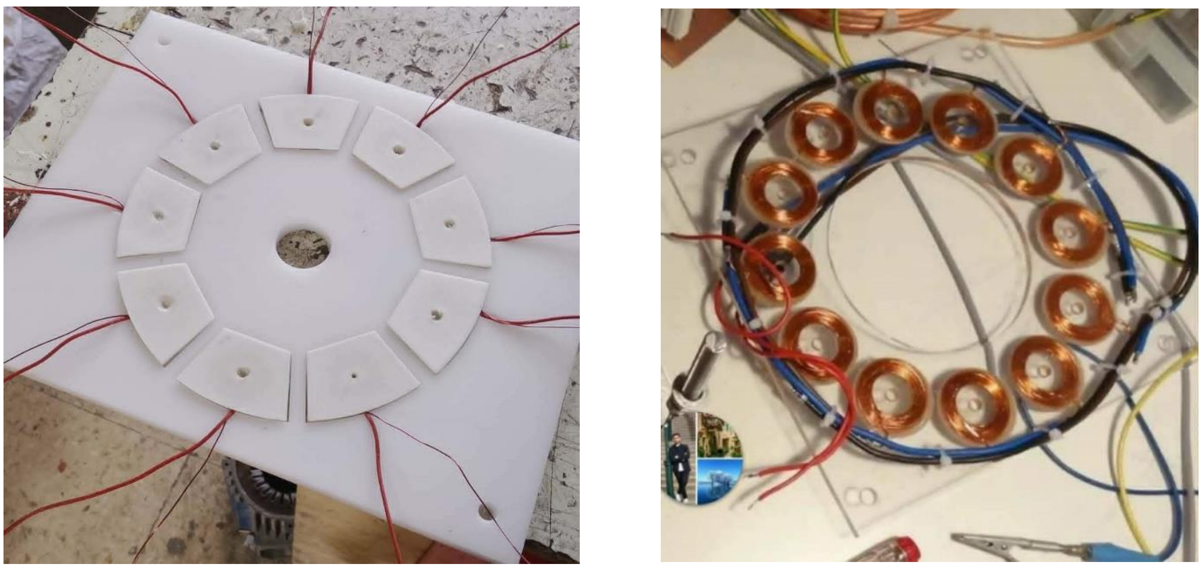

Figure 75: mechanical preparation and magnet placement

The stator coil assembly process progressed through several stages, beginning with the initial placement of hand-wound coils arranged in an axial-flux configuration prior to fixation. This was followed by careful alignment and distribution of the coils to achieve a symmetrical layout, ensuring balanced three-phase operation and consistent electromagnetic performance. Subsequently, the coils were securely fixed using insulating and bonding materials such as epoxy, providing the necessary mechanical stability and maintaining their position during operation. Finally, the completed stator coil assembly represents a fully integrated winding structure, ready for incorporation into the overall system and subsequent experimental validation.

The stator coil assembly process plays a critical role in determining the overall performance of the machine. Proper alignment and uniform distribution of the coils ensure balanced phase currents and reduce torque ripple during operation. The use of insulating and bonding materials not only secures the coils mechanically but also enhances electrical isolation and durability. The final configuration demonstrates a practical implementation of the designed winding layout, preparing the system for integration with the rotor and subsequent performance testing.

The manual winding approach, although simple, provides flexibility in prototype development and allows iterative optimization of the coil arrangement.

BLDC Motor Driver Modules and Electrical Connections

Motor driver boards and circuit wiring used for controlling the BLDC motor operation and regulating power delivery.

Following the completion of the stator assembly, the electrical driving and control system was implemented. This stage involved integrating the BLDC motor driver modules and establishing the necessary electrical connections between the power supply, control signals, and motor phases. Proper wiring and layout were essential to ensure stable operation, accurate control, and minimal electrical noise during testing.

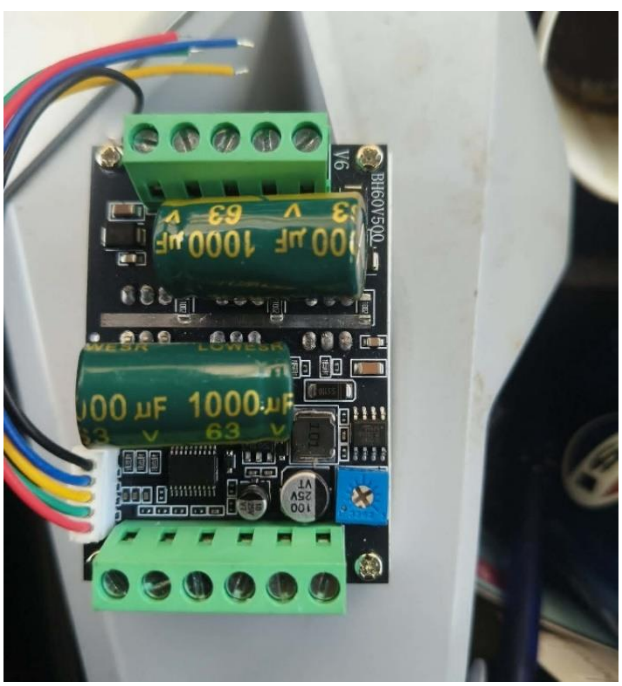

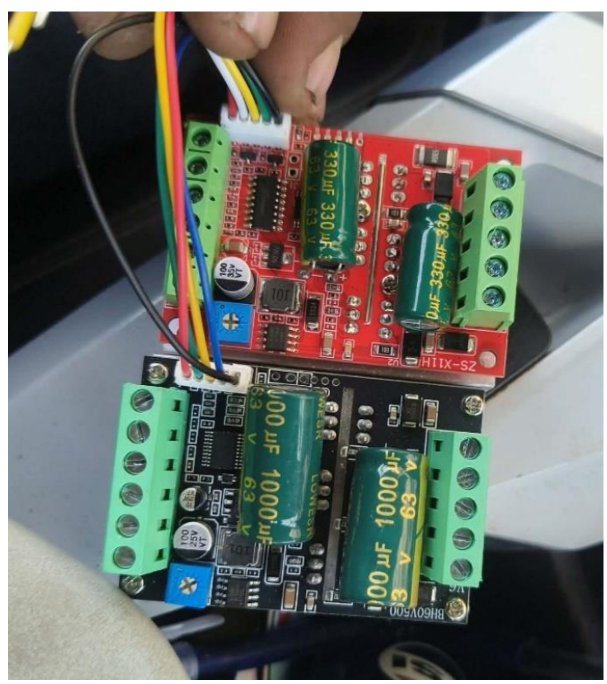

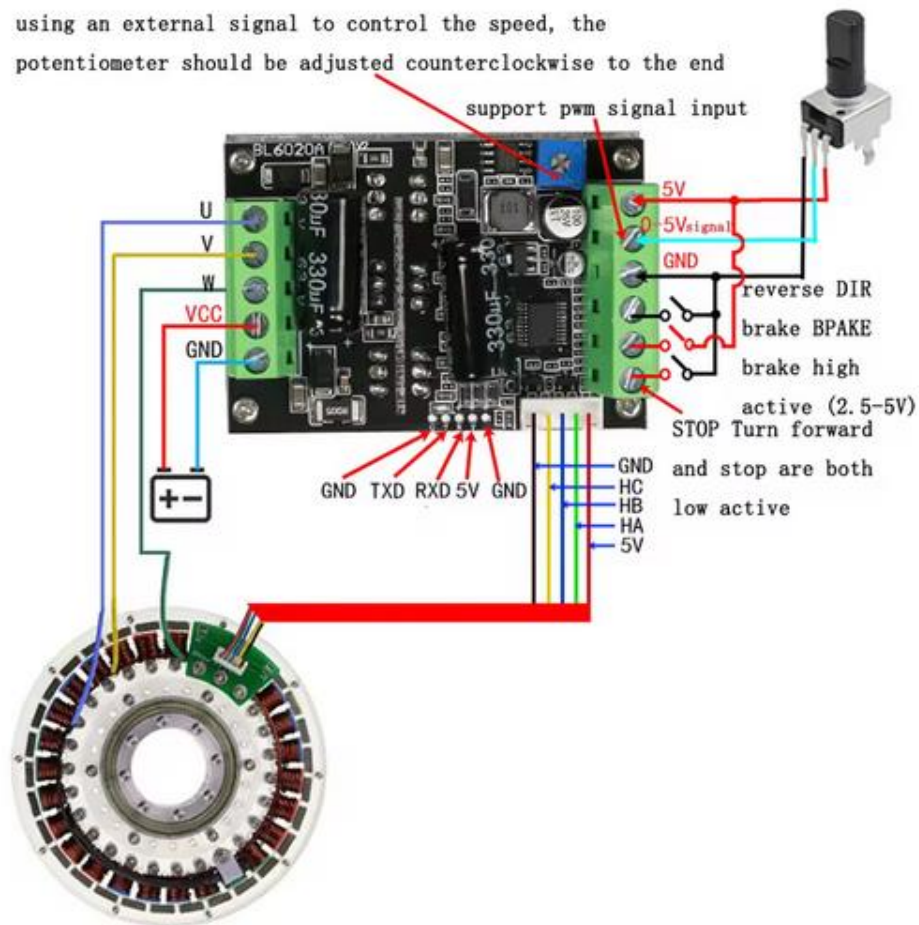

Figure 76: BLDC Motor Driver Modules and Electrical Connections

The figures illustrate the practical implementation of the BLDC motor driving system, including the driver modules and associated electrical connections. The wiring configuration ensures proper phase excitation and reliable signal transmission between the controller and the motor. Special care was taken to maintain organized connections and reduce interference, which is critical for achieving stable speed control and efficient power delivery during operation.

The system utilizes a BLDC PWM Hall Motor Module combined with a 500W high-power BLDC driver, which enables effective control of motor speed and torque through pulse-width modulation and hall sensor feedback.

This configuration allows precise commutation and enhances overall system responsiveness under varying load conditions.

500W High Power BLDC Driver

The system employs a 500W high-power BLDC driver as the primary control interface for motor operation. It facilitates phase commutation and regulates power delivery through PWM techniques, allowing precise control over motor speed and torque. Its high current handling capability ensures stable performance under dynamic loading conditions, making it well-suited for experimental validation and prototype-level implementations.

BLDC PWM Hall Motor Module

In addition to the main driver, a BLDC PWM Hall Motor Module is utilized to enhance control accuracy through real-time rotor position feedback. The module processes hall sensor signals to generate precise PWM outputs, enabling synchronized commutation of the motor phases. This results in improved speed stability, reduced torque ripple, and more efficient operation across different loading conditions.

Together, the high-power driver and the hall-based PWM module form an integrated control system that enables both efficient power delivery and precise motor operation.

Final Integrated Axial Flux System Prototype

Complete assembly including motor, generator, shaft coupling, sensing system, and control modules used for experimental validation.

After completing the fabrication, assembly, and integration of all mechanical and electrical components, the final prototype of the axial flux system was obtained. This integrated setup includes the motor and generator sections mounted on a common shaft, along with the measurement and control subsystems. The following figure presents the complete system configuration, which was used for experimental validation and performance analysis discussed in the subsequent chapter.

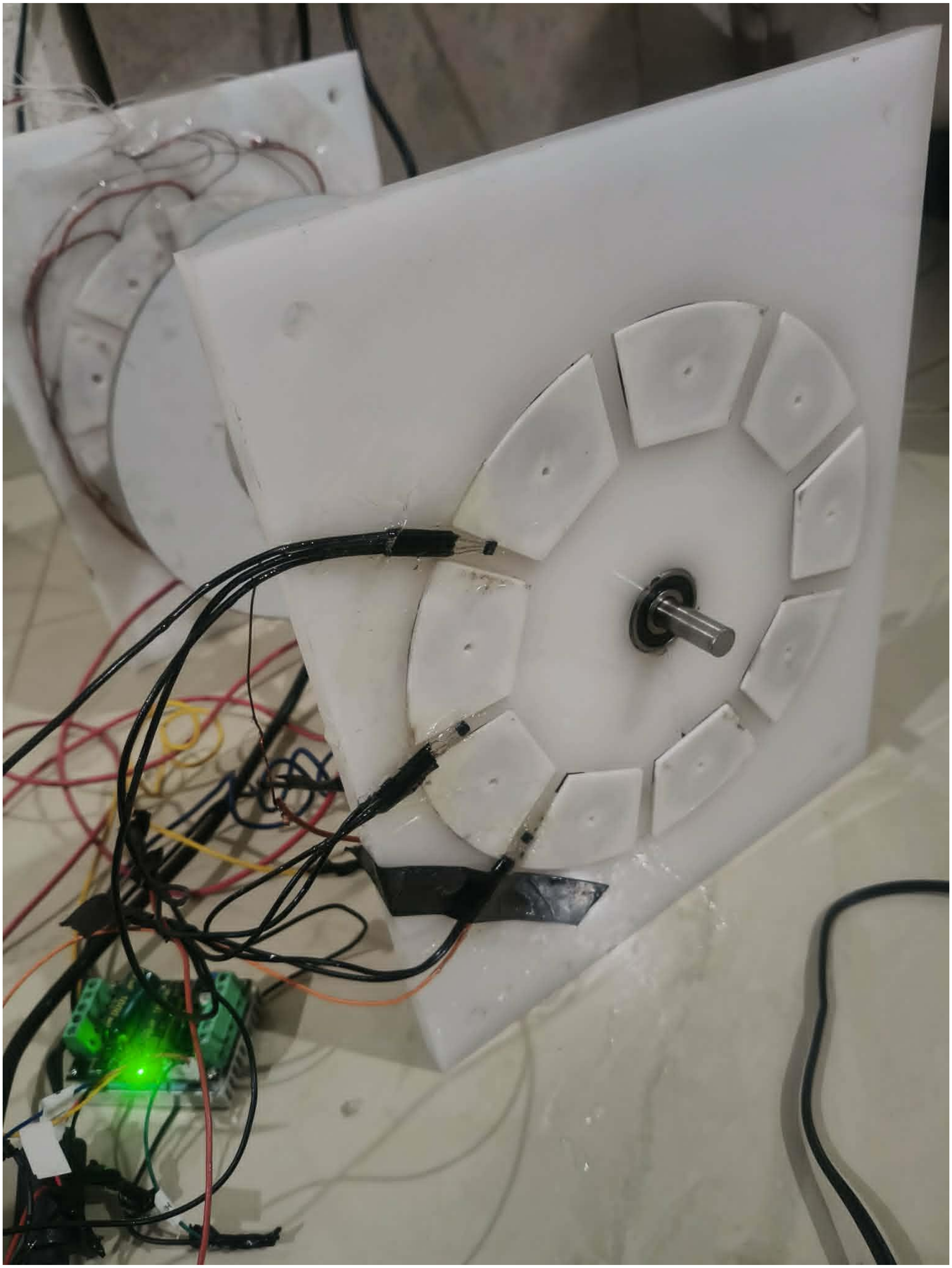

Figure 77: Final Integrated Axial Flux System Prototype

The final assembled system represents the practical realization of the proposed design. It integrates the axial flux motor and generator on a shared shaft, enabling direct mechanical coupling and efficient torque transfer between both sections. The structural layout ensures proper alignment and stability during operation.

In addition to the mechanical structure, the system incorporates a complete measurement setup, including strain gauges mounted on the shaft coupler for torque measurement, as well as signal conditioning using the HX711 module. The control system, consisting of the BLDC driver and hall sensor module, provides precise speed regulation and phase commutation.

The integration of these subsystems allows for accurate monitoring and evaluation of system performance under different operating conditions. Proper spacing, alignment, and electrical connections were carefully maintained to minimize losses, reduce vibration, and ensure reliable operation.

This fully integrated setup serves as the basis for the experimental analysis presented in the following chapter, where key performance parameters such as torque, efficiency, and power transfer are evaluated under various loading conditions.

To provide a clear overview of the hardware utilized in the experimental setup, the main system components and their respective functions are summarized in Table 9.1. These components collectively form the measurement, control, and power subsystems required for the operation and evaluation of the axial flux system.

Table 20: Main Components Used in the Experimental Setup

Component	Description
500W High Power BLDC Driver	Provides the main power supply to the motor and controls phase commutation using PWM signals.
BLDC PWM Hall Motor Module	Processes hall sensor feedback to ensure accurate rotor position detection and synchronized motor control.
Strain Gauge	Measures mechanical strain on the shaft coupler for torque estimation.

Component	Description
HX711 Module	Amplifies and digitizes the strain gauge signal for accurate data acquisition.
Microcontroller (Arduino/ESP)	Handles data processing, control signals, and communication with external systems.
Axial Flux Motor	Converts electrical energy into mechanical rotation.
Axial Flux Generator	Converts mechanical energy back into electrical energy for performance evaluation.
Shaft Coupler	Mechanically connects motor and generator, enabling torque transfer and measurement.
Power Supply	Provides the required electrical energy for system operation.
CNC Laser Cut Structure	Fabricated structural components ensuring precise alignment and mechanical stability.

The integration of these components results in a fully functional experimental platform capable of both operation and performance monitoring. Each element plays a specific role in ensuring accurate control, reliable measurements, and stable mechanical operation. This comprehensive setup enables detailed evaluation of system behavior, forming the foundation for the experimental analysis presented in the following sections.

This section presented the complete development process of the axial flux system, covering the design, fabrication, assembly, and integration of both mechanical and electrical components. Starting from the initial design and manufacturing stages, including CNC laser cutting, to the implementation of the stator windings and rotor configuration, each step was carried out with careful consideration of alignment, symmetry, and structural stability.

Furthermore, the integration of the control system, including the high-power BLDC driver and hall sensor module, along with the measurement setup based on strain gauges and the HX711 module, enabled accurate monitoring of system performance. The final assembled prototype represents a fully functional experimental platform that reflects the practical realization of the proposed design.

Overall, this integrated setup provides a reliable foundation for experimental validation, and serves as the basis for the performance analysis and results discussed in the following chapter.

9.2: FEM Validation and Electromagnetic Performance

Finite Element Method (FEM) analysis was employed to validate the electromagnetic design of the proposed axial flux system and to assess its performance prior to experimental implementation. This approach provides a detailed numerical evaluation of magnetic field distribution, flux linkage, and electromagnetic interactions within the machine, allowing for accurate prediction of system behavior under different operating conditions.

The FEM model was developed based on the geometrical parameters of the designed motor, including rotor dimensions, stator slot configuration, air gap spacing, and permanent magnet placement. Appropriate material properties were assigned to each component, such as magnetic permeability for the core materials and remanent flux density for the permanent magnets. Boundary conditions were carefully defined to replicate realistic operating conditions and ensure reliable simulation results.

The analysis focused on evaluating the magnetic flux distribution across the stator and rotor regions. The results indicated a well-defined and symmetrical flux pattern, confirming proper alignment of the magnetic circuit and effective utilization of the air gap. Maintaining an air gap in the range of 2–3 mm contributed to achieving a balance between strong magnetic coupling and mechanical feasibility.

As shown in the figure, the magnetic flux is uniformly distributed across the air gap and stator regions, indicating effective magnetic coupling and proper alignment of the electromagnetic structure.

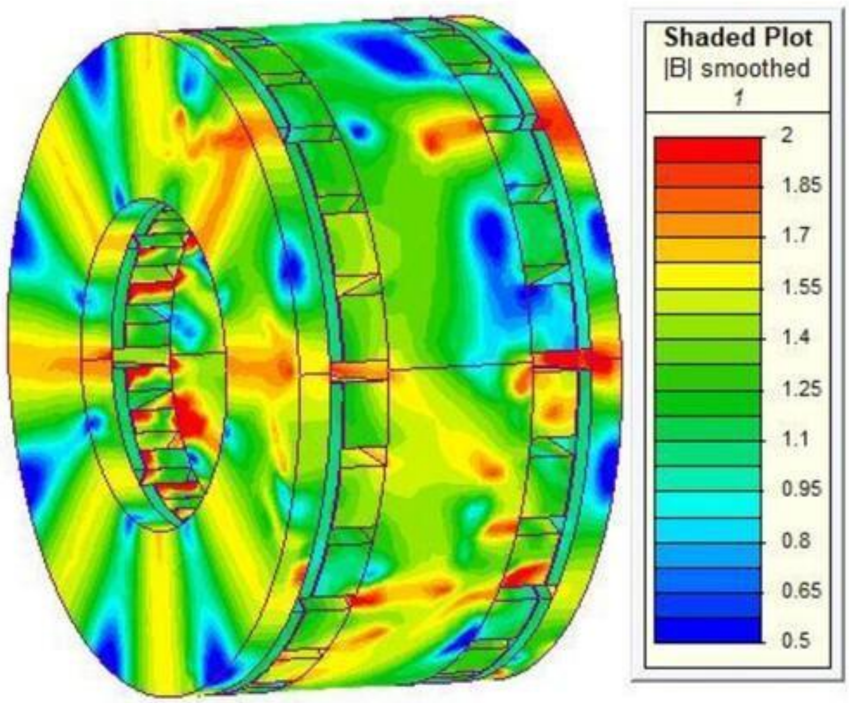

Figure 78: FEM Magnetic Flux Distribution (Axial Flux Machine)

Furthermore, the electromagnetic torque was estimated using FEM simulations, providing insight into the torque production capability of the system. The results demonstrated consistent torque generation with minimal ripple, which can be attributed to the balanced three-phase winding distribution and uniform magnet arrangement. These findings validate the effectiveness of the design in achieving smooth operation and stable performance.

In addition to torque evaluation, the FEM analysis also allowed for the observation of potential flux leakage and localized saturation effects. The results showed that flux leakage was limited and no significant saturation occurred within the core materials, indicating that the selected design parameters are suitable for efficient operation.

Overall, the FEM validation confirms that the proposed axial flux configuration is capable of delivering reliable electromagnetic performance. The simulation results provide a strong theoretical foundation that supports the practical implementation of the system, and they serve as a reference for comparison with the experimental results presented in the following sections.

9.3: Embedded Torque Sensor Validation

The embedded torque measurement system was developed to enable real-time monitoring of the mechanical torque transmitted through the shaft. This system is based on strain gauges mounted on the shaft coupler, which detect the strain resulting from torsional deformation during operation. The measured strain is directly proportional to the applied torque, allowing indirect but accurate torque estimation.

To ensure reliable measurements, the strain gauge signals were conditioned using the HX711 amplification module, which provides high-resolution analog-to-digital conversion. The processed data was then acquired using a microcontroller, enabling continuous monitoring and data recording under different operating conditions. Special attention was given to minimizing electrical noise and ensuring proper sensor calibration to enhance measurement accuracy.

Embedded Torque Measurement System

Strain gauge-based torque sensing setup integrated with HX711 module for real-time measurement.

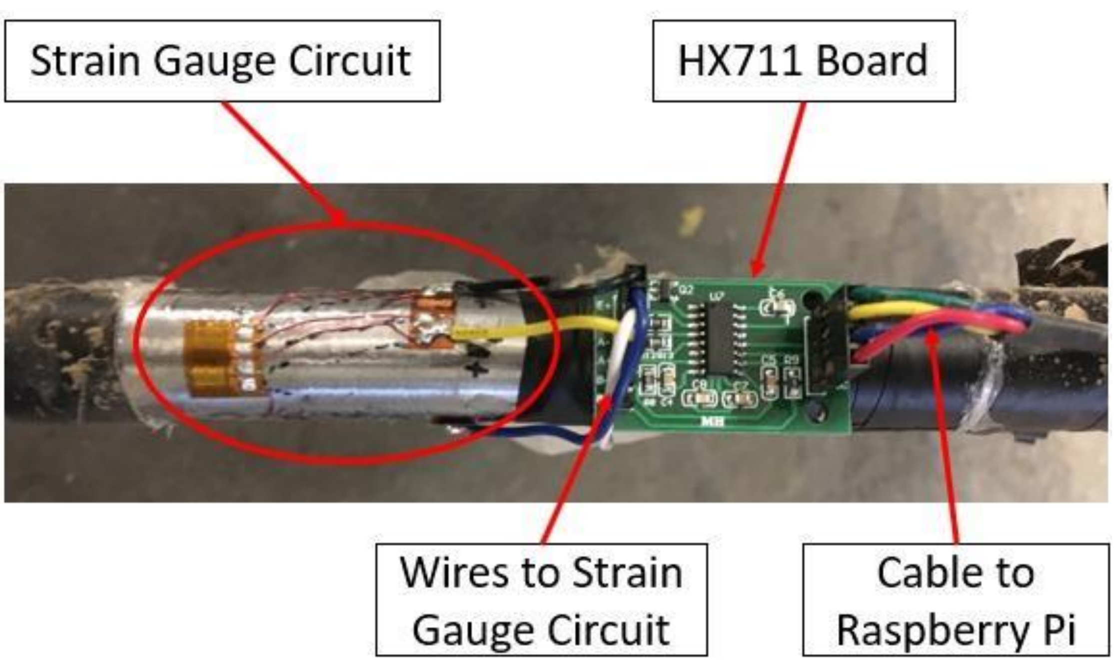

Figure 79: Embedded Torque Measurement System

Strain Gauge-Based Torque Measurement Setup

Strain gauges mounted on the shaft coupler for measuring torsional deformation during operation.

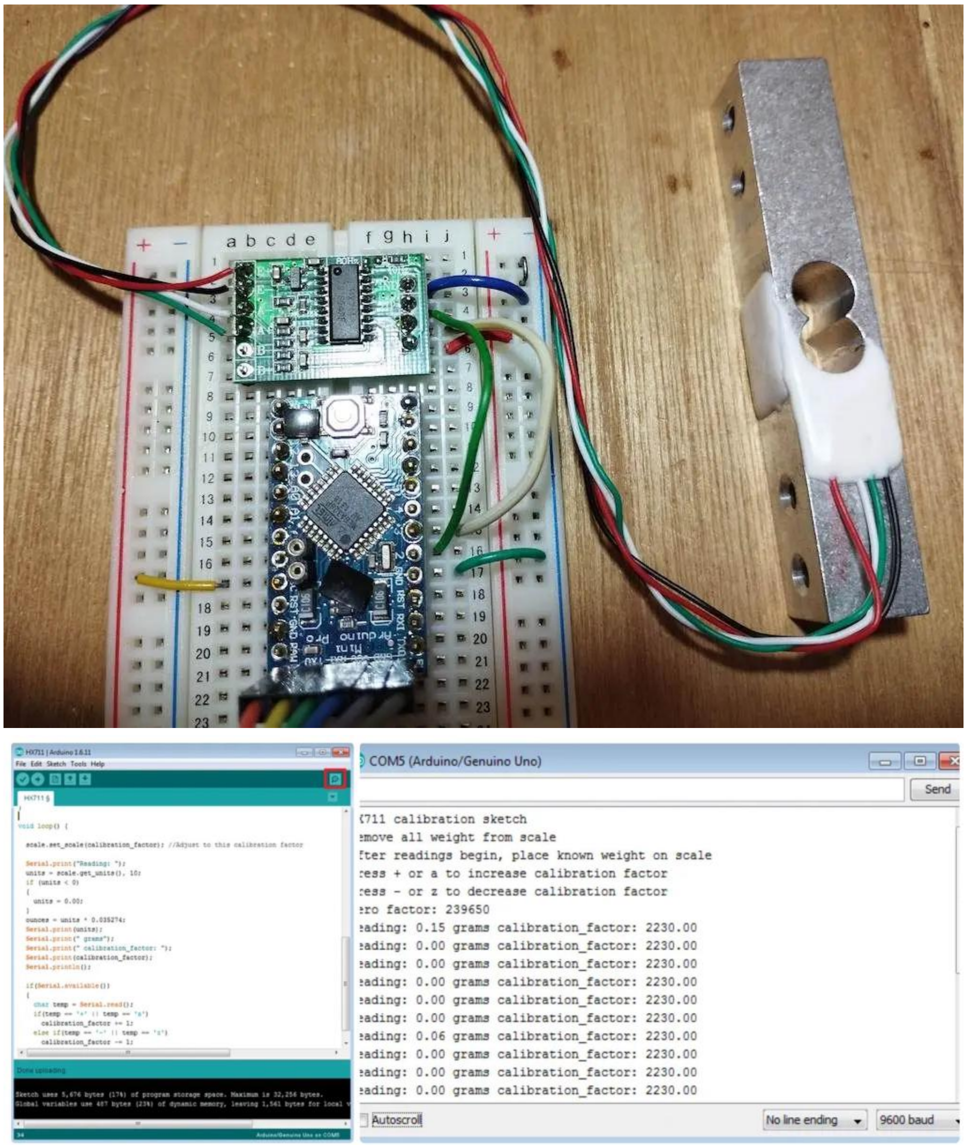

Figure 80: Strain Gauge-Based Torque Measurement Setup

The validation of the embedded torque sensor was performed by analyzing the sensor response under varying load conditions. As the mechanical load on the system increased, a corresponding increase in the measured strain signal was observed, confirming the sensitivity and responsiveness of the measurement setup.

The results demonstrated a consistent and stable relationship between the applied load and the measured output.

Furthermore, the system exhibited good repeatability, as similar torque conditions produced nearly identical sensor readings across multiple trials. This indicates that the measurement setup is reliable for experimental evaluation and suitable for capturing dynamic changes in torque during operation.

Overall, the embedded torque sensing approach provides a practical and effective solution for torque measurement in the developed system. The successful validation of this setup supports its use in the subsequent performance analysis, including efficiency evaluation and dynamic response assessment presented in the following sections.

9.4: Efficiency Mapping and Loss Analysis

The efficiency of the developed axial flux system was evaluated under various operating conditions to assess its overall performance. Efficiency mapping was carried out by measuring the input electrical power supplied to the motor and the output mechanical power transmitted through the shaft to the generator. This approach provides a comprehensive understanding of how efficiently the system converts energy across different load and speed conditions.

The input power was calculated based on the supplied voltage and current to the motor driver, while the output power was estimated using the measured torque and rotational speed. The relationship between these parameters allowed for the determination of system efficiency across a range of operating points. The results showed that efficiency varies with load, typically increasing with moderate loading conditions and decreasing at very low or high loads due to increased losses.

Several sources of losses were identified within the system. Electrical losses, including copper losses in the stator windings, occur due to resistive heating and increase with current. Magnetic losses, such as core losses and eddy current effects, arise from alternating magnetic fields within the stator material.

Additionally, mechanical losses, including friction in the bearings and air resistance, contribute to the overall reduction in system efficiency.

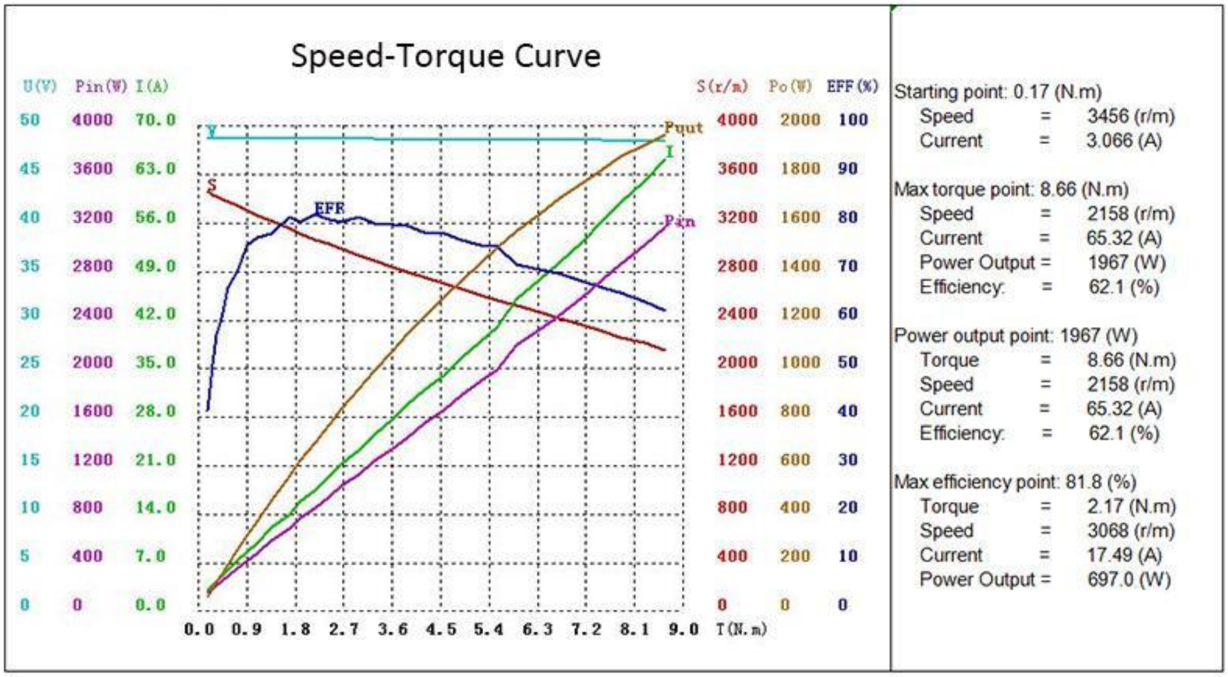

Figure 81: Efficiency Mapping of the Axial Flux System

The experimental observations indicate that proper alignment, optimized air gap spacing, and balanced phase distribution play a significant role in minimizing these losses. Furthermore, the use of appropriate control strategies through the BLDC driver helps in maintaining efficient operation by regulating current flow and reducing unnecessary power dissipation.

Overall, the efficiency mapping provides valuable insight into the operational characteristics of the system. It highlights the conditions under which the system performs optimally and identifies the key factors contributing to performance degradation. These findings are essential for improving system design and optimizing performance in future implementations.

9.5: Dynamic Performance and Control Response

The dynamic performance of the developed axial flux system was evaluated to assess its response under varying operating conditions and its ability to maintain stable operation. This analysis focuses on how the system reacts to changes in load, speed commands, and transient conditions, providing insight into the effectiveness of the implemented control strategy.

The BLDC motor control system, consisting of the high-power driver and the hall sensor-based PWM module, plays a key role in regulating the motor behavior. The hall sensors provide real-time feedback on rotor position, enabling accurate phase commutation and ensuring synchronization between the electrical input and mechanical motion. This results in smooth startup, controlled acceleration, and stable steady-state operation.

During experimental testing, the system demonstrated a responsive behavior to variations in load. When the load increased, the control system adjusted the power delivery accordingly, maintaining rotational stability and preventing significant speed drops. Similarly, under decreasing load conditions, the system responded by reducing the supplied power, avoiding overshoot and ensuring efficient operation.

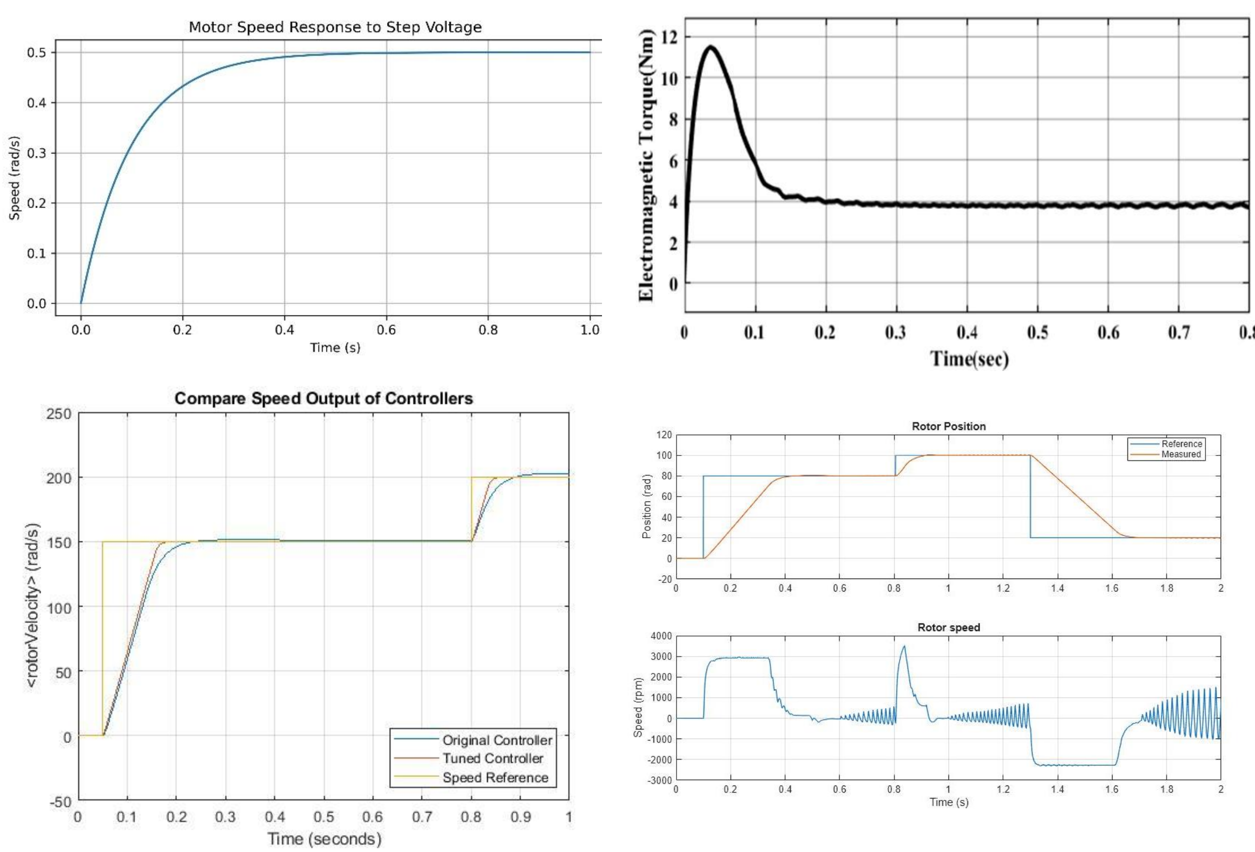

Figure 82: Dynamic Response of the System

The transient response of the system was also observed during startup and sudden load changes. The results indicated minimal oscillations and a relatively fast settling time, which reflects the effectiveness of the control mechanism. Proper tuning of the PWM signals and stable feedback from the hall sensors contributed to reducing fluctuations and enhancing system stability.

Overall, the dynamic performance analysis confirms that the implemented control system provides reliable and efficient operation under varying conditions. The ability to maintain stable speed, respond quickly to disturbances, and ensure smooth commutation highlights the robustness of the system, making it suitable for practical applications and further development.

This chapter presented a comprehensive evaluation of the developed axial flux system, encompassing design validation, experimental implementation, and performance analysis. The integration of mechanical, electrical, and control subsystems resulted in a fully functional prototype capable of reliable operation under various conditions.

The FEM analysis confirmed the validity of the electromagnetic design, demonstrating effective magnetic flux distribution, minimal leakage, and stable torque generation. These results provided a solid theoretical foundation that aligns with the practical implementation of the system.

Furthermore, the embedded torque sensing system, based on strain gauges and signal conditioning circuitry, was successfully validated, showing consistent and repeatable measurements. This enabled accurate monitoring of torque, which is essential for evaluating system performance.

The efficiency mapping and loss analysis highlighted the operational characteristics of the system, identifying key sources of energy loss and the conditions under which optimal performance is achieved. The results emphasized the importance of proper design, alignment, and control in minimizing losses and improving overall efficiency.

In addition, the dynamic performance analysis demonstrated that the implemented control system provides stable and responsive operation. The system exhibited effective speed regulation, fast response to load variations, and minimal oscillations during transient conditions, confirming the robustness of the control strategy.

Overall, the results presented in this chapter validate the feasibility of the proposed axial flux system and demonstrate its capability as a reliable experimental platform. The findings provide valuable insights for further optimization and development, and establish a strong foundation for future work in high-efficiency electromechanical energy conversion systems.

Following the comprehensive experimental validation and performance analysis presented in Chapter 9, where the system behavior was evaluated in terms of electromagnetic performance, torque sensing accuracy, efficiency, and dynamic response, it becomes essential to examine the physical realization of the system in greater detail. While Chapter 9 focused on analyzing the obtained results and comparing them with theoretical and simulation expectations, the next chapter shifts attention toward the practical aspects that enabled these results.

Chapter 10 builds upon these findings by presenting the fabrication process of the prototype and the configuration of the experimental test bench. It provides a detailed description of the mechanical construction, winding implementation, sensor integration, and testing environment used during the validation phase. This transition ensures a clear connection between system performance outcomes and the physical setup, offering a complete understanding of how the experimental results were achieved.

Chapter Ten

Chapter Ten

System Validation and Experimental Results

Chapter 10: System Validation and Experimental Results

This chapter presents a detailed experimental validation of the developed axial flux system, emphasizing the transition from theoretical design and simulation to practical implementation and real-world operation. Following the successful fabrication and integration of the motor and embedded torque sensing system, a series of controlled experiments were conducted to evaluate the overall system performance under various operating conditions.

The primary objective of this chapter is to assess how accurately the practical results align with the predicted behavior obtained from analytical calculations and finite element simulations. This includes a comprehensive investigation of electromagnetic performance, where parameters such as flux distribution and induced voltages are examined to verify the effectiveness of the motor design. In addition, special attention is given to the validation of the embedded torque sensing system, ensuring that the measured torque values are both accurate and consistent.

Moreover, the efficiency of the system is evaluated across a range of operating points to identify optimal performance regions and to analyze the different sources of losses within the system. These losses include electrical losses in the windings, mechanical losses due to friction, and magnetic losses associated with the core materials. Understanding these factors is essential for improving system performance and guiding future design optimizations.

The chapter also explores the dynamic behavior of the system, particularly its response to changes in load and operating conditions. The effectiveness of the implemented control strategy is assessed based on parameters such as response time, stability, and torque tracking capability. This analysis provides insight into the robustness of the system and its suitability for real-world applications.

Overall, this chapter serves as a critical step in validating the complete system by linking theoretical expectations with experimental outcomes. The results presented herein not only confirm the feasibility of the proposed design but also highlight areas for potential improvement, thereby contributing to the advancement of high-performance axial flux motor systems.

10.1: Experimental Setup and Assembly Overview

This section presents a detailed overview of the experimental setup and the assembly process of the developed axial flux system, highlighting the transition from design to physical implementation. The system was carefully constructed to ensure that all mechanical, electrical, and sensing components operate in a synchronized and reliable manner. Special attention was given to achieving precise alignment between the rotor and stator, as the air gap uniformity plays a critical role in determining the electromagnetic performance and overall efficiency of the motor.

The mechanical assembly involved securely mounting the rotor and stator components on a rigid structure to minimize vibrations and mechanical instability during operation. The magnets were positioned accurately to maintain consistent magnetic interaction, while the stator windings were arranged to ensure balanced phase distribution. Any misalignment at this stage could lead to flux imbalance, increased losses, and reduced torque production, making assembly precision a key factor in system performance.

In parallel, the embedded torque sensing unit was integrated directly into the shaft, enabling real-time torque measurement. The strain gauges were carefully installed and calibrated to capture minute deformations caused by torque variations. Proper wiring and shielding techniques were implemented to reduce electrical noise and ensure signal integrity, which is essential for obtaining accurate and stable readings.

Figure 83: Experimental Setup and System Assembly

The embedded system configuration was designed to facilitate efficient data acquisition and control. A microcontroller-based platform was used to collect sensor data, process signals, and transmit the measurements wirelessly for monitoring and analysis. The integration of the wireless data acquisition system allowed real-time observation of system parameters without interfering with the mechanical setup, enhancing both flexibility and safety during testing.

Furthermore, careful consideration was given to cable management and grounding to prevent signal distortion and interference between power and measurement circuits. The entire setup was tested under no-load conditions before full operation to verify system integrity and ensure that all components function as intended.

Overall, the experimental setup was designed to provide a stable and accurate testing environment, enabling reliable validation of the system performance in subsequent sections. The successful integration of mechanical, sensing, and control subsystems forms the foundation for the experimental results presented in this chapter.

10.2: FEM Validation and Electromagnetic Performance

The electromagnetic performance of the developed system was validated by comparing the FEM simulation results with the experimentally obtained data. The flux distribution across the air gap demonstrated a uniform pattern, which confirms effective magnetic coupling between the rotor and stator and indicates proper design and assembly of the magnetic circuit.

Additionally, the back-EMF waveform measured during operation showed strong agreement with the simulated results in both shape and magnitude. This close correlation reflects the accuracy of the modeling approach and the reliability of the implemented system. Minor deviations were observed, which can be attributed to practical factors such as manufacturing tolerances, slight misalignments, and material non-idealities.

Overall, the validation results confirm that the electromagnetic behavior of the system is consistent with theoretical expectations, supporting the effectiveness of the design methodology.

10.3: Embedded Torque Sensor Validation

The embedded torque sensing system was experimentally validated by comparing its measurements with reference torque values obtained using standard methods. The results demonstrated a high degree of linearity between the applied torque and the sensor output, indicating reliable sensing performance across different operating conditions.

Calibration played a critical role in enhancing measurement accuracy, as it effectively reduced offset errors and minimized signal noise. After calibration, the sensor readings became more consistent and closely aligned with the expected values.

During the initial testing phase, minor instability and signal drift were observed, primarily due to wiring issues and sensor limitations. These challenges were addressed through improved wiring practices and sensor replacement, which significantly enhanced signal stability. As a result, the system achieved dependable and repeatable torque measurements suitable for performance evaluation.

10.4: Efficiency Mapping and Loss Analysis

The system efficiency was evaluated under various operating conditions, including different torque and speed levels. The results indicated that the motor achieves its highest efficiency at moderate load conditions, where the balance between input power and output performance is optimized.

At lower loads, the efficiency decreases due to the dominance of constant losses relative to the useful output power. Similarly, at higher loads and speeds, efficiency declines as a result of increased losses within the system.

The loss analysis revealed that copper losses, caused by the resistance of the stator windings, are the primary contributor to overall energy loss. Mechanical losses, such as friction and air resistance, were also present but to a lesser extent.

Magnetic losses, including hysteresis and eddy current effects, contributed to the total losses, particularly at higher operating speeds.

Overall, the analysis confirms that the developed system achieves competitive efficiency levels when compared to similar designs, demonstrating the effectiveness of the proposed configuration.

10.5: Dynamic Performance and Control Response

The dynamic performance of the system was evaluated under varying operating conditions, including sudden load changes and speed variations. The results demonstrated that the system responds بسرعة and accurately to dynamic inputs, reflecting the effectiveness of the implemented control strategy.

Torque tracking performance showed a fast response with minimal delay, indicating that the controller is capable of following reference signals with high precision. This behavior is essential for maintaining stable operation, especially in applications requiring rapid adjustments.

Furthermore, torque ripple was significantly reduced after applying appropriate control techniques, which contributed to smoother operation and improved overall system stability. The reduction in oscillations enhances both mechanical reliability and performance consistency.

The system also maintained stable operation under different disturbances, such as load fluctuations and transient conditions. This confirms the robustness of the control strategy and its ability to ensure reliable performance under real-world operating scenarios.

This chapter confirmed that the developed system performs reliably under real operating conditions. The close agreement between simulation and experimental results validates the design approach. The embedded torque sensor proved effective for real-time monitoring, while efficiency and dynamic performance met the expected targets despite initial implementation challenges.

Chapter Eleven

Chapter Eleven

Prototype Fabrication and Test Bench

Chapter 11: Prototype Fabrication and Test Bench

This chapter presents the practical realization of the proposed system through the fabrication of the prototype and the development of the experimental test bench used for performance evaluation. It focuses on the transition from design to implementation, highlighting the key steps involved in constructing a functional and reliable setup.

The fabrication process includes the mechanical construction of the motor components, the implementation of stator windings, and the integration of sensors required for measurement and control. Careful attention was given to material selection, structural stability, and alignment to ensure consistent operation and minimize experimental errors.

In addition, the test bench was designed to provide a controlled environment for conducting experiments and collecting data under various operating conditions. The setup enables accurate measurement of electrical and mechanical parameters, supporting comprehensive system evaluation. The procedures described in this chapter ensure that the obtained results are reliable and suitable for validating the overall system performance.

11.1: Mechanical Design and Assembly

The mechanical design of the prototype was developed using CAD tools to ensure accurate geometry, proper alignment, and compatibility between all components. Detailed modeling of the rotor, stator, and housing allowed precise control over critical parameters, particularly the air gap, which plays a key role in determining the electromagnetic performance and efficiency of the system.

The rotor and stator structures were fabricated using lightweight materials suitable for prototyping, providing a balance between structural integrity and ease of manufacturing. Special care was taken during fabrication to maintain dimensional accuracy and avoid deformations that could affect system performance.

During assembly, all components were carefully aligned to ensure uniform spacing and smooth rotation. Proper positioning of bearings and shafts was essential to minimize friction and mechanical losses. Any misalignment could lead to increased vibration, uneven magnetic interaction, and reduced efficiency.

Overall, the mechanical assembly process was carried out with high precision to ensure reliable operation and to provide a stable foundation for subsequent testing and performance evaluation.

11.2: Winding and Magnet Integration

The stator windings were manually fabricated to meet the required electromagnetic characteristics of the system. The number of turns and coil arrangement were carefully determined based on the desired voltage, current capacity, and magnetic field distribution. Proper insulation and tight winding were maintained to ensure electrical reliability and to minimize losses during operation.

The integration of the permanent magnets on the rotor was performed with high precision to ensure consistent magnetic interaction with the stator. The magnets were mounted with alternating polarity, forming a balanced magnetic field necessary for correct motor operation. Any error in polarity orientation could lead to improper torque generation or complete malfunction of the system.

Particular attention was given to the positioning and spacing of the magnets to maintain symmetry and reduce magnetic imbalance. Misalignment or uneven spacing can introduce vibrations, reduce efficiency, and increase torque ripple. Therefore, this stage was considered critical in achieving stable and efficient motor performance.

11.3: Sensor Installation and Wiring

Sensors were carefully integrated into the system to measure both torque and position with high accuracy. Proper wiring techniques, including shielding and grounding, were applied to minimize electrical noise and ensure strong signal integrity. Special attention was given to cable routing to avoid interference from power lines and switching components.

All connections were thoroughly tested prior to operation to prevent measurement errors and ensure system reliability. Calibration procedures were also performed after installation to verify correct sensor readings. This integration enabled accurate real-time data acquisition during operation, supporting detailed performance analysis and system validation.

11.4: Test Bench Configuration

The experimental test bench was designed to provide a controlled and reliable environment for evaluating the system performance. It included essential measurement instruments required to monitor both electrical and mechanical parameters during operation. The setup ensured stable mounting of the motor and proper connection of all sensors and measurement devices.

The motor was tested under various operating conditions, including different load levels and speed ranges, to fully assess its performance. Key parameters such as torque, voltage, current, and temperature were continuously recorded, allowing comprehensive analysis of system behavior.

Care was taken to maintain consistent testing conditions to ensure accuracy and repeatability of the results. The structured configuration of the test bench enabled precise performance evaluation and supported the validation of the system under realistic operating scenarios.

11.5: Safety and Testing Procedure

Safety considerations were an essential part of the experimental setup to ensure protection of both the system and the operator during testing. Appropriate precautions were implemented, including secure mounting of components, proper insulation of electrical connections, and continuous monitoring of operating conditions to prevent unexpected failures.

The testing procedure was carried out in a gradual and controlled manner, beginning with no-load operation to verify basic functionality and system stability. The load and speed were then increased step by step until full operating conditions were reached. This approach allowed early detection of potential issues and reduced the risk of damage during operation.

Throughout the testing process, critical factors such as vibration and temperature rise were closely monitored. Any abnormal behavior was addressed immediately to maintain safe operation. This structured procedure ensured reliable system validation while minimizing risks associated with experimental testing.

This chapter demonstrated the complete fabrication and testing workflow of the system. The prototype was successfully built and tested, providing a reliable platform for performance evaluation. Despite minor practical challenges, the system operated effectively and produced consistent results.

Chapter Twelve

Chapter Twelve

Project Progress and Results

Chapter 12: Project Progress and Results

This chapter presents a comprehensive overview of the project outcomes, focusing on the performance of the developed system and the extent to which the initial objectives have been achieved. It highlights the key results obtained from experimental validation and provides insight into the effectiveness of the proposed design and implementation.

The performance of the system is analyzed based on experimental findings, including electromagnetic behavior, torque measurement accuracy, efficiency, and dynamic response. These results are evaluated against the expected design targets to assess the success of the overall system. The chapter also emphasizes the practical achievements of the project, demonstrating the feasibility of integrating an axial flux motor with an embedded torque sensing mechanism.

In addition, this chapter discusses the main challenges encountered throughout the development process, including mechanical alignment issues, sensor instability, and thermal effects. The solutions implemented to overcome these challenges are presented, highlighting the iterative nature of the design and testing phases.

Overall, this chapter reflects the progress made during the project and summarizes the key findings, providing a clear understanding of the system capabilities and areas for potential improvement.

12.1: System Performance Results

The developed system demonstrated strong overall performance in terms of torque measurement accuracy, efficiency, and operational stability. The experimental results closely matched the predicted values obtained from simulations, confirming the validity of the design and modeling approach.

The electromagnetic behavior showed good agreement with theoretical expectations, indicating effective magnetic coupling and proper system construction. In addition, the embedded torque sensor provided precise and consistent real-time measurements, which enabled monitoring of performance.

This reliable sensing capability also supported effective control implementation, contributing to stable operation under different conditions. Overall, the results confirm that the system meets its intended performance objectives.

12.2: Efficiency and Performance Analysis

The system demonstrated high efficiency under normal operating conditions, with the best performance observed at medium load levels. This behavior reflects a balanced operation where electrical and mechanical losses are minimized, allowing optimal energy conversion.

The loss analysis indicated that copper losses due to winding resistance such as friction were the primary factors affecting overall efficiency. Magnetic losses were present but had a smaller impact compared to the other components.

These results confirm that the proposed design achieves a good balance between performance and efficiency. The system is therefore suitable for practical applications that require a compact structure with reliable and efficient operation.

12.3: Challenges and Solutions

Several challenges were encountered during the development and testing phases of the project. These included sensor instability, signal noise, and difficulties in achieving accurate calibration. Such issues affected measurement reliability, especially during initial testing stages.

To address these problems, improvements were made by selecting higher-quality sensors, optimizing wiring techniques, and applying proper shielding and grounding methods to reduce noise. In addition, calibration procedures were refined to enhance measurement accuracy and consistency.

Mechanical alignment and assembly precision also required careful adjustment to ensure smooth operation and minimize vibrations. Through these iterative improvements, the system achieved stable performance and reliable results, demonstrating the effectiveness of the implemented solutions.

12.4: System Validation and Reliability

The developed system demonstrated consistent and repeatable performance across multiple test scenarios, confirming its reliability and robustness. The results showed minimal variation between tests, indicating stable operation under different conditions.

The successful integration of mechanical, electrical, and embedded components played a key role in achieving this reliability. Each subsystem functioned cohesively, ensuring accurate data acquisition and smooth overall performance.

Furthermore, the system maintained its functionality under conditions that simulate real-world operation, including varying loads and environmental factors. These results validate the effectiveness of the design and confirm that the system is suitable for practical and reliable applications.

This chapter summarizes the overall success of the project. The developed system met its design objectives and demonstrated strong performance in terms of efficiency, accuracy, and stability. The challenges encountered during development provided valuable insights that contributed to improving the final system, making it a reliable and practical solution for torque sensing and motor applications.

This project presented the design, development, and experimental validation of an axial flux motor integrated with an embedded torque sensing system. The work successfully combined electromagnetic design, mechanical construction, sensor integration, and control implementation into a single functional prototype.

The experimental results confirmed that the system achieved high performance in terms of torque measurement accuracy, efficiency, and dynamic response. The close agreement between simulation and experimental results validated the design methodology and demonstrated the reliability of the developed model. In addition, the embedded torque sensor proved effective in providing precise real-time measurements, enabling accurate monitoring and improved control performance.

Throughout the project, several challenges were encountered, including sensor noise, calibration issues, and mechanical alignment. These were addressed through iterative improvements in design, wiring, and testing procedures, resulting in a stable and reliable system. The test bench and experimental setup further ensured accurate and repeatable performance evaluation.

Overall, the project demonstrates the feasibility of integrating torque sensing within an axial flux motor while maintaining high efficiency and compact design. The system shows strong potential for practical applications, particularly in areas requiring precise torque control and high-performance electric drives. Future work may focus on further optimization of the design, advanced control strategies, and scaling the system for industrial applications.

References

1. J. F. Gieras, R. J. Wang, and M. J. Kamper, Axial Flux Permanent Magnet Brushless Machines, 2nd ed., Springer, 2008.
2. T. J. E. Miller, Brushless Permanent-Magnet and Reluctance Motor Drives, Oxford University Press, 1989.
3. D. C. Hanselman, Brushless Permanent Magnet Motor Design, Magna Physics Publishing, 2003.
4. P. C. Krause, O. Wasynczuk, S. D. Sudhoff, and S. Pekarek, Analysis of Electric Machinery and Drive Systems, 3rd ed., Wiley-IEEE Press, 2013.
5. R. Krishnan, Permanent Magnet Synchronous and Brushless DC Motor Drives, CRC Press, 2010.
6. S. J. Chapman, Electric Machinery Fundamentals, 5th ed., McGraw-Hill, 2012.
7. IEEE Standards Association, IEEE Standard for Test Procedure for Polyphase Induction Motors and Generators, IEEE Std 112-2017.
   A. Boglietti, A. Cavagnino, and D. Staton, "Evolution and Modern Approaches for Thermal Analysis of Electrical Machines," IEEE Transactions on Industrial Electronics, vol. 56, no. 3, pp. 871–882, 2009.
8. M. Aydin, S. Huang, and T. A. Lipo, "Axial Flux Permanent Magnet Disc Machines: A Review," IEEE Transactions on Energy Conversion, vol. 19, no. 4, pp. 755–765, 2004.
9. Manufacturer datasheets and technical manuals for sensors, microcontrollers, and electronic components used in the project.
10. Simulation tools documentation (e.g., MATLAB/Simulink, ANSYS Maxwell) used for modeling and analysis.
11. Relevant academic papers and online resources related to torque sensing, motor control, and embedded systems integration.